

**EXPANDING THE UTILITY OF AMINE DEHYDROGENASES
THROUGH PROTEIN AND REACTION ENGINEERING FOR THE
BIOCATALYTIC PRODUCTION OF CHIRAL AMINES**

A Dissertation
Presented to
The Academic Faculty

by

Robert Donald Franklin

In Partial Fulfillment
of the Requirements for the Degree
Doctor of Philosophy in the
School of Chemical and Biomolecular Engineering

Georgia Institute of Technology
August 2020

COPYRIGHT © 2020 BY ROBERT D. FRANKLIN

**EXPANDING THE UTILITY OF AMINE DEHYDROGENASES
THROUGH PROTEIN AND REACTION ENGINEERING FOR THE
BIOCATALYTIC PRODUCTION OF CHIRAL AMINES**

Approved by:

Dr. Andreas S. Bommarius, Advisor
School of Chemical and Biomolecular
Engineering
School of Chemistry and Biochemistry
Georgia Institute of Technology

Dr. Corey J. Wilson
School of Chemical and Biomolecular
Engineering
Georgia Institute of Technology

Dr. Julie A. Champion
School of Chemical and Biomolecular
Engineering
Georgia Institute of Technology

Dr. Brent D. Feske
Department of Chemistry and
Biochemistry
Georgia Southern University

Dr. Anant K. Paravastu
School of Chemical and Biomolecular
Engineering
Georgia Institute of Technology

Date Approved: May 14th, 2020

[To Ladd and Jean Franklin, whose encouragement and support have never wavered]

ACKNOWLEDGEMENTS

There is a famous quote from 1675 letter from Isaac Newton to Robert Hooke which scientists the worldwide hold dear. It reads “If I have seen further it is by standing on the shoulders of giants.”¹ It refers to the inescapable fact that all scientific advances are built upon the accomplishments of those who came before. While this is certainly true, the contributions of a scientist’s mentors and peers are just as important, if not more. I owe my success to many people who have been with me for many years.

Thank you to Dr. Andy Bommarius for your guidance and support over these past five years. You have helped me grow to be a better scientist and engineer.

Another special thanks to the four other members of the thesis committee, Julie Champion, Bent Feske, Anant Paravastu, and Corey Wilson for their input and suggestions along the way.

I would also like to acknowledge generous funding from the National Science Foundation NSF I/UCRC grant IIP-1540017 to the Center for Pharmaceutical Development and through CBET grant 1512848, and financial support from the School of Chemical and Biomolecular Engineering at the Georgia Institute of Technology.

Additionally, I would like to acknowledge the Biopolymer Characterization (BPC) core facility at the Parker H. Petit Institute for Bioengineering and Bioscience at the Georgia Institute of Technology for the use of its shared equipment, services and expertise.

I would like to thank Dr. Bettina Bommarius for teaching me almost everything I know about working in a microbiology lab and Dr. Mick Robbins for teaching me everything I know about enzyme kinetics.

The members of the Bommarius research group, both current and former, have been a fantastic source of advice, humor, and support. More specifically, of the former members I would like to thank Dr. Thomas Kwok for his relentlessly positive attitude and good spirits, Dr. Harrison Rose for his insights and advice on science, career, and life concerns, and Dr. Mick Robbins for teaching me everything I know about enzyme kinetics.

Dr. Adam Caparco, my compatriot on Amine Dehydrogenases, has been my closest collaborator. Thank you for working with me all these years, when things were going well, and when things were a bit harder. I am excited to see where your career takes you. Matt McDonald and Dr. Alex Tsoras have also been with me since the beginning of this journey. The four of us have learned about, discussed, and joked about countless topics over the past five years and I hope we can continue to do so as we go our separate ways.

To Conner Mount and Joshua Whitley, my two undergraduate co-authors, thank you for the truly massive contributions you both made to the project. Your dedication, insights, and ideas were above and beyond what I ever expected and made the work much better. I was glad I got the chance to get to know both of you.

To my wonderful parents, Ladd and Jean Franklin, and my amazing sister and brother, Alison and Bryan Buenavista, the four of you are my foundation. Thank you for always being there for me.

And finally, thank you to Pebbles for keeping me sane while writing this thesis under quarantine.

TABLE OF CONTENTS

ACKNOWLEDGEMENTS	iv
LIST OF TABLES	xi
LIST OF FIGURES	xii
LIST OF SYMBOLS AND ABBREVIATIONS	xv
SUMMARY	xxi
CHAPTER 1. Introduction	1
1.1 Motivation	1
1.1.1 Chiral Centers in Small Molecule Drugs	1
1.1.2 Prevalence of Chiral Amines in API Manufacturing	2
1.2 Asymmetric Synthesis of Chiral Amines	2
1.3 Enzymatic Routes to Chiral Amines	4
1.3.1 Advantages of Biocatalysis Over Traditional Chemical Catalysis	4
1.3.2 ω -Transaminases (ω -TAs)	4
1.3.3 Imine Reductases (IREDs)	7
1.3.4 Amine Dehydrogenases (AmDHs)	9
1.4 Generating Chirality from a Racemic Mixture of Amines	10
1.4.1 Diastereomeric Salt Separation	11
1.4.2 Kinetic Resolution	11
1.4.3 Chemoenzymatic Dynamic Kinetic Resolution	12
1.5 Development, Enhancement, and Utilization of Amine Dehydrogenases	12
1.5.1 Generation of L-AmDH from Leucine Dehydrogenase	12
1.5.2 Building a Family of Amine Dehydrogenases	14
1.5.3 Modifications to Improve Activity and Stability	15
1.5.4 Cofactor Regeneration	16
1.5.5 Utilization in Multi-Enzyme Cascades	17
1.5.6 Immobilization	19
CHAPTER 2. Expanding the Binding Pocket of L-AmDH to Accommodate Larger Substrates	21
2.1 Introduction	21
2.2 Plan for Mutations	22
2.3 Materials and Methods	24
2.3.1 Materials Used	24
2.3.2 DNA and Amino Acid Sequences	26
2.3.3 Overlap Extension Mutagenesis	28
2.3.4 Enzyme Expression	29
2.3.5 Enzyme Purification	30
2.3.6 Activity Assays	31
2.3.7 Melting Temperature Estimation with Differential Scanning Fluorimetry	32

2.3.8	50 mL Scale Conversions	33
2.3.9	Derivatization with Benzoyl Chloride	34
2.3.10	Diastereomeric Derivatization with FDAA	34
2.3.11	Analytics	35
2.4	Results	41
2.5	Conclusion	46
CHAPTER 3. Mechanistic Insight into Amine Dehydrogenase Kinetics		48
3.1	Introduction	48
3.2	Materials and Methods	50
3.2.1	Materials Used	50
3.2.2	Enzyme Expression	51
3.2.3	Spectrophotometer Assays	51
3.2.4	Plate Reader Assays	52
3.2.5	Nonlinear Fitting to Find Rate Equation	52
3.2.6	Kinetic Solvent Viscosity Effect Determination	53
3.2.7	Product Inhibition	54
3.3	Results	55
3.3.1	Global Fit for the Reductive Amination Rate Law	55
3.3.2	Global Fit for the Oxidative Deamination Rate Law	56
3.3.3	First- and Second-Order Rate Constants	57
3.3.4	Product Inhibition	58
3.3.5	Kinetic Solvent Viscosity Effects	59
3.4	Discussion	60
3.5	Conclusion	67
CHAPTER 4. The Journey toward continuous manufacturing of chiral amines		68
4.1	Motivation and Introduction	68
4.2	The Enzyme Membrane Reactor	68
4.2.1	Overview and Initial Setup	68
4.2.2	Results and Challenges	70
4.3	Immobilization Onto Immobeads in a Packed Bed Reactor	70
4.3.1	Rationale	70
4.3.2	Initial Immobilization Screening	72
4.3.3	Continuous amine Production Results	74
4.4	Immobilization onto Immobeads® Modified with Leucine Zippers	77
4.4.1	Leucine Zipper Binding Scheme	77
4.4.2	Immobilization Results	78
4.4.3	Continuous Amine Production Results	79
4.5	The Packed Bed Recycle Reactor (PBRR)	79
4.5.1	System Setup	80
4.5.2	Residence Time Distributions in the PBRR	81
4.5.3	Conversion Results and Why it Would Not Have Worked	82
CHAPTER 5. Continuous production of chiral amines in a packed bed reactor		86
5.1	Introduction	86
5.2	Enzyme immobilization	89

5.3	Materials and Methods	90
5.3.1	Sources of Raw Materials	90
5.3.2	Buffers Used for Expression, Immobilization and Reaction	91
5.3.3	Enzyme Expression	91
5.3.4	Enzyme Purification	92
5.3.5	Enzyme Immobilization	92
5.3.6	Binding Capacity Determination	93
5.3.7	AmDH to FDH Binding Ratio Optimization	94
5.3.8	Continuous Flow Reactor System Setup	94
5.3.9	Flow Meter Calibration	95
5.3.10	Residence Time Distributions	96
5.3.11	Conversion Determination With HPLC	97
5.4	Results	98
5.4.1	Enzyme Leaching Under Reaction Conditions	98
5.4.2	Enzymatic Activity and Stability in Reaction Conditions	98
5.4.3	Binding Capacity	99
5.4.4	AmDH to FDH Binding Ratio	102
5.4.5	Flow Characteristics of the Reactor System	102
5.4.6	Continuous Amine Production: Initial Tests	105
5.4.7	Improved Reaction Conditions	108
5.5	Estimation of Limitations to Conversion	111
5.5.1	Damköhler Numbers	111
5.5.2	Enzyme Kinetics	113
5.5.3	Internal Mass Transfer	120
5.5.4	External Mass Transfer	121
5.6	Discussion	124
CHAPTER 6.	Future Perspectives	127
6.1	Protein Engineering	127
6.1.1	Motivation for Protein Engineering Work	127
6.1.2	Directed Evolution for AmDH Engineering	129
6.2	Understanding the Kinetics of Amine Dehydrogenases	133
6.2.1	Motivation: Binding of Ammonia	133
6.2.2	Ammonia Does Not Bind to the Enzyme	134
6.2.3	Further Exploration of AmDH Kinetics	135
6.3	Reaction Engineering for the Production of Chiral Amines	137
6.3.1	Obtaining Improved Physical Parameters	137
6.3.2	Other Assumptions That Need to be Tested	140
6.3.3	Is Predictive Modelling of the Reactor System Useful?	141
6.3.4	Repeatability of Reactor Characterization Measurements	142
6.3.5	Empirical Approach to Reactor Characterization	143
6.3.6	Scale-Up of Enzyme Production and Immobilization	143
APPENDIX A.	Licenses to republish copyrighted works	145
A.1	Chemical Engineering Journal 2019 paper	145
A.2	ChemCatChem 2020 paper	145

REFERENCES

150

VITA

167

LIST OF TABLES

Table 2-1	Activity enhancement of L-AmDH toward aliphatic ketones and the generation of L-AmDH-TV	42
Table 2-2	Effects of A112G and T133G on activity toward n-ketones	44
Table 2-3	Activity of L-AmDH variants toward long branched ketones	45
Table 2-4	Conversion values for preparative-scale reactions	46
Table 3-1	Global rate law fit parameters for reductive amination by L-AmDH and LeuDh	56
Table 3-2	Global rate law fit parameters for oxidative deamination by L-AmDH and LeuDh	57
Table 3-3	Comparison of first and second order rate constants between L-AmDH and LeuDh	57
Table 3-4	Summary of product inhibition patterns for LeuDh and L-AmDH	59
Table 4-1	Degree of binding of cFL1-AmDH and FDH to various enzyme immobilization beads	42
Table 5-1	Comparison of enzyme binding ratios and the effect on batch conversion	102

LIST OF FIGURES

Figure 1-1	Representative reaction scheme for an ω -transaminase	5
Figure 1-2	Representative reaction schemes for imine reductases.	7
Figure 1-3	Representative reaction scheme for reductive amination of a ketone by an amine dehydrogenase	9
Figure 1-4	Residues in the active site of <i>Rhodococcus sp.</i> phenylalanine dehydrogenase identified as important for substrate binding (PDB ID: 1C1D)	13
Figure 1-5	Example AmDH reaction with cofactor regeneration by formate dehydrogenase	16
Figure 2-1	Reaction scheme for the reductive amination of amines with AmDH and list of relevant ketones	22
Figure 2-2	A homology model of the engineered L-AmDH sequence mapped onto a published LeuDh structure	23
Figure 2-3	Representative SDS-PAGE gel showing the steps to the purification of an AmDH	31
Figure 2-4	Melting profiles of L-AmDH and L-AmDH TV.	33
Figure 2-5	Representative chromatogram of the HPLC quantification of 2-aminononane after derivatization with benzoyl chloride	36
Figure 2-6	Comparison of HPLC chromatograms of 2-aminononane derivatized with FDAA.	37
Figure 2-7	Representative chromatogram of the HPLC quantification of 2-aminoheptane	38
Figure 2-8	Comparison of HPLC chromatograms of 2-aminoheptane derivatized with FDAA.	39
Figure 2-9	Representative chromatogram of the HPLC quantification of 2-aminopentane derivatized with benzoyl chloride	40

Figure 2-10	Comparison of HPLC chromatograms of 2-aminopentane derivatized with FDAA.	41
Figure 2-11	Expansion of the L-AmDH binding pocket to accommodate ketones of larger sizes due to mutations at position L39	43
Figure 3-1	Balanced reactions for the leucine dehydrogenase (LeuDH) from <i>Bacillus stearothermophilus</i> and the engineered leucine amine dehydrogenase (L-AmDH)	49
Figure 3-2	Kinetic Solvent Viscosity Effects on L-AmDH and LeuDH	60
Figure 3-3	Effect of increasing ionic strength on the kinetic parameters for reductive amination of 2-pentanone by L-AmDH.	62
Figure 4-1	Photo of the continuous enzyme membrane reactor setup	69
Figure 4-2	Promotional image from ChiralVision outlining their available enzyme binding chemistries	72
Figure 4-3	Reactor cartridge packed with Immobeads	75
Figure 4-4	Photo of the first packed bed reactor setup with AmDH and FDH	76
Figure 4-5	Covalent binding of $Z_R C_{10} Z_R$ to Immobeads® followed by noncovalent binding of AmDH-ZE <i>via</i> leucine zipper interactions	77
Figure 4-6	Photo of the final packed bed recycle reactor setup	80
Figure 4-7	Residence time distributions in the PBRR for various recycle ratios.	82
Figure 4-8	Flow diagram of a recycle reactor from Rippin, 1967	83
Figure 5-1	Reductive amination of 5-methyl-2-hexanone with cofactor regeneration	87
Figure 5-2	Block flow diagram of the continuous flow packed bed reactor system	95

Figure 5-3	Batch conversions of 5-methyl-2-aminohexane by AmDH and FDH immobilized on Nuvia IMAC before and after 30 days of storage in NH ₄ COOH buffer	99
Figure 5-4	Experimental binding curves of AmDH and FDH to Nuvia IMAC resin.	101
Figure 5-5	Residence time distribution at 0.574 mL/min	103
Figure 5-6	Dependence of mean residence time on flow rate in the packed bed reactor	104
Figure 5-7	Effect of temperature on reaction conversion	106
Figure 5-8	Arrhenius plot of the observed relationship between conversion and temperature in the packed bed reactor	107
Figure 5-9	Apparent deactivation kinetics of immobilized FDH and AmDH under continuous flow conditions.	108
Figure 5-10	Impact of flow rate on conversion and productivity in the AmDH/FDH packed bed reactor.	110
Figure 5-11	Relative percent error in the Michaelis Menten equation at various enzyme and substrate concentrations	116
Figure 5-12	Relationship between conversion and reaction rate for AmDH amination of 5-methyl-2-hexanone	118
Figure 6-1	Obtaining (<i>R</i>)-chloroquine with the help of L-AmDH	127
Figure 6-2	Steps in the substrate walk toward 5DAP	128
Figure 6-3	Potential sites for site-saturation libraries in L-AmDH/TV/L39A	132

LIST OF SYMBOLS AND ABBREVIATIONS

ε_{340}	Molar extinction coefficient at 340 nm [$\text{mM}^{-1}\text{cm}^{-1}$]
ϕ_m	Thiele modulus [-]
E_a^{app}	Apparent activation energy [kcal mol^{-1}]
\hat{K}	Dimensionless Michaelis constant
$K_{M,eff}$	Effective Michaelis constant with product inhibition incorporated
[E]	Enzyme concentration [mol m^{-3}]
1X PBS	Standard phosphate-buffered saline solution
5M2H	5-methyl-2-hexanone
6xHis	Metal affinity protein tag with six sequential histidine residues
a	Volume averaged external surface area of a packed bed [$\text{m}^2 \text{m}^{-3}$]
A_0	Preexponential factor in the Arrhenius equation
AADH	Amino acid dehydrogenase
ACN	Acetonitrile
AlaDH	Alanine dehydrogenase
AmDH	Amine dehydrogenase
AmDH-ZE	cFL1-AmDH with a Z_E tag added to the amino acid sequence
An-GluDH	Glutamate dehydrogenase from <i>Aspergillus niger</i>
API	Active pharmaceutical ingredient
$^{app}k_{cat}$	Apparent or observed k_{cat} value [s^{-1}]
$^{app}K_M$	Apparent K_M value [mM]
AspRedAm	Reductive aminase derived from <i>Aspergillus oryzae</i>
BzCl	Benzoyl chloride

C_A	Concentration of species A [mol m^{-3}]
$C_{A,0}$	Inlet concentration of component A [mol m^{-3}]
CALB	Lipase B from <i>Candida antarctica</i>
C_{As}	Surface concentration of species A [mol m^{-3}]
<i>cb</i> -FDH	Formate dehydrogenase from <i>candida boidinii</i>
cFL1-AmDH	Chimeric phenylalanine-leucine amine dehydrogenase
Coeff _x	Term in a ternary enzyme rate law corresponding to the binary complex of the enzyme and component x
CSTR	Continuously stirred tank reactor
C_{W-P}	Weisz-Prater criterion [-]
Da	Damköhler Number [-]
D_A	Diffusion coefficient or diffusivity [$\text{m}^2 \text{s}^{-1}$]
$Da_{(I)}$	First Damköhler number [-]
$Da_{(II),ex}$	Second Damköhler number for external mass transfer [-]
$Da_{(II),i}$	Second Damköhler number for internal mass transfer [-]
$D_{A,eff}$	Effective diffusivity inside a catalyst pore [$\text{m}^2 \text{s}^{-1}$]
DI	deionized
DMSO	Dimethyl sulfoxide
d_p	Particle diameter [m]
d_r	Reactor internal diameter [m]
DSF	Differential scanning fluorimetry
<i>ee</i>	Enantiomeric excess [%]
EMR	Enzyme membrane reactor
FDAA	Marfey's reagent, 1-fluoro-2-4-dinitrophenyl-5-L-alanine amide
FDH	Formate dehydrogenase

FDH-ZE	<i>cb</i> -FDH with a Z _E tag added to the amino acid sequence
f_i	Fraction of a tracer leaving a recycle stream after pass i [-]
GDH	Glucose dehydrogenase
GluDH	Glutamate dehydrogenase
HPLC	High-performance liquid chromatography
IB-COV2	Covalent enzyme immobilization support offered by ChiralVision
IMAC	Immobilized metal affinity chromatography
IRED	Imine reductase
k	First-order rate constant [s ⁻¹]
k_{cat}	Enzyme turnover number [s ⁻¹]
k_{cat}/K_M	catalytic efficiency, or second order rate constant [mM s ⁻¹]
K_I	Inhibitor constant [mM]
K_{iq}	Dissociation constant for substrate q [mM]
k_L	Mass transfer coefficient in the liquid phase [m s ⁻¹]
k_L	External mass transfer coefficient [m s ⁻¹]
$k_L a$	Volumetric mass transfer coefficient [s ⁻¹]
KLeu	Ketoleucine
K_M	General symbol for the Michaelis constant for a substrate [mM]
K_M/K_I	Inhibitor ratio [-]
KSVE	Kinetic solvent viscosity effect
K_x	Michaelis constant for component x [mM]
l	Characteristic length [m]
L-AmDH	Leucine amine dehydrogenase
L-AmDH-TV	L-AmDH mutant containing D32A/F202S/C290V mutations
LB	Luria-Bertani broth

Leu	(<i>S</i>)-leucine
LeuDH	Leucine dehydrogenase
MIBK	Methyl isobutyl ketone
NAD(H)	Nicotinamide adenine dinucleotide, either the oxidized or reduced form
NADP(H)	Nicotinamide adenine dinucleotide phosphate, either the oxidized or reduced form
Ni-NTA	Nickel chelated nitrilotriacetic acid
NOX	NADH oxidase
O.D.	Outside diameter [mm]
PBR	Packed bed reactor
PBRR	Packed bed recycle reactor
PCR	Polymerase chain reaction
<i>Pe</i>	Peclet number
Pent	2-pentanone
PFR	Plug flow reactor
PheDH	Phenylalanine dehydrogenase
Q or v or v_f	Volumetric flow rate [$\text{m}^3 \text{s}^{-1}$]
R	Recycle ratio [-] or the gas constant [$\text{kcal mol}^{-1} \text{K}^{-1}$]
$-r_A$	Reaction rate per unit volume [$\text{mol m}^{-3} \text{s}^{-1}$]
Re	Reynolds number [-]
RedAm	Reductive aminase
RPM	Rotations per minute
RTD	Residence time distribution
Sc	Schmidt number [-]
SDS-PAGE	Sodium dodecyl sulfate polyacrylamide gel electrophoresis

Sh	Sherwood number [-]
T	Temperature [°C] or [K]
U/mg or mU/mg	Specific activity per milligram of enzyme, 1 U, or unit, is the amount of enzyme required to react one micromole of substrate in one minute
U_{SF}	Superficial or free stream velocity in a packed bed [m s^{-1}]
UV/Vis	Ultraviolet/visible spectroscopy
V	Reactor volume [m^3]
v/v %	Percent volume of a compound based on volume of solution
ValDH	Valine dehydrogenase
V_{max}	Maximum velocity of an enzymatic reaction [$\text{mol m}^{-3} \text{s}^{-1}$]
$V_{max,app}$	Apparent maximum velocity of an enzymatic reaction [$\text{mol m}^{-3} \text{s}^{-1}$]
v_o	Specific activity [U mg^{-1}]
X	Conversion [%]
Z_E	Glutamate rich leucine zipper
Z_R	Arginine rich leucine zipper
$Z_R C_{10} Z_R$	Peptide containing two Z_R motifs joined by an unstructured linker
ΔA_{340}	Change in absorbance of light at 340 nm [arbitrary units]
ϵ_{bead}	Porosity of a macroporous bead [-]
η	Dynamic viscosity [Pa s^{-1}]
η_E	External effectiveness factor [-]
η_I	Internal effectiveness factor [-]
η_{rel}	Relative dynamic viscosity [Pa s^{-1}]
θ	Dimensionless time (in a residence time distribution, t/τ_{sys})
λ	Wavelength of light [nm]
ν	(Greek letter nu) Kinematic viscosity [$\text{m}^2 \text{s}^{-1}$]

τ	Residence time [s]
τ_{bead}	Tortuosity of a macroporous bead [-]
τ_{bed}	Residence time of the reactor alone in a reactor system [s]
τ_{sys}	Residence time of an entire reactor system [s]
ϕ_{bed}	Void fraction of a packed bed
ω -TA	ω -transaminase

SUMMARY

The purpose of this project was to expand the understanding and utility of a pre-existing family of engineered amine dehydrogenases (AmDHs) which catalyze the reductive amination of prochiral ketones to chiral amines. Work toward this goal was focused in three generally independent directions, enzyme improvement through site-directed mutagenesis, understanding of the kinetic mechanism, and reaction engineering toward scalable continuous amine production. Through a combination of mutations shown to have positive effects in other related amine and amino acid dehydrogenases, new AmDH variants were produced with multiple-fold higher activity, 8 °C higher melting temperature, and new activity for large substrates not found for the base case. A detailed series of initial rate experiments allowed us to propose a kinetic mechanism for L-AmDH and showed that the mutations which produced the amine dehydrogenase from the parent amino acid dehydrogenase also caused changes in the kinetic mechanism. After investigations of multiple reactor platforms, enzyme immobilization strategies, and analytical methods, a robust packed bed reactor platform was characterized. The accessible design space of the reactor was explored. Impacts of flow rate, temperature, substrate concentration, rapid recycle, and bed height on conversion, productivity, and enzyme stability were examined. The reported work, especially aim 3, fills an important gap in the field. Detailed discussions of the impact of physical process parameters on productivity allow for concrete engineering decisions. The growing importance of enzymes in pharmaceutical and fine chemical production requires an increased focus on biocatalysis from an engineering prospective.

CHAPTER 1. INTRODUCTION

1.1 Motivation

1.1.1 Chiral Centers in Small Molecule Drugs

The presence of a chiral center often imposes significant complications and expense to the production of an active pharmaceutical ingredient (API), but failure to achieve enantiomeric purity can have dire consequences. For molecules with a single chiral center, most of physical and chemical properties of the two enantiomers will be identical. However, the biological activity of the two compounds can be vastly different. The (*R*)- and (*S*)- enantiomers of carvone for example smell to humans like spearmint and caraway seeds, respectively, due to differences in how the molecules interact with our olfactory receptors.³ Just like olfactory receptors, other proteins and enzymes in the body have interactions with small molecules that are specific to one enantiomer or the other. For example, even though the ubiquitous over the counter analgesic ibuprofen is sold as a racemate, it has been shown that only (*S*)-ibuprofen has the desired pain blocking effects.⁴ The metabolic pathways the two enantiomers of ibuprofen become involved in are very different, though both forms of the drug are safe. Some chiral drugs, however, not only have a single effective enantiomer, but a single safe one. The popular 1950s sleep aid thalidomide, sold as a racemic mixture, was found to be responsible for thousands of birth defects by the early 1960s.⁵ Subsequent research over the past 50 years has shown that only (*S*)-thalidomide causes the defects.⁶ Of the 200 top selling (by total revenue) small molecule drugs in 2018, 121 contain at least one chiral center which is not prepared as a

racemate.⁷ For all of the enantiopure drugs on the market today, significant effort in the manufacturing process is put into ensuring their chiral purity.

1.1.2 Prevalence of Chiral Amines in API Manufacturing

The focus of the work reported in this doctoral thesis is the production of chiral amines. Of the top small molecule drugs with nonracemic chiral centers, 27% contain a chiral amine functional group such as sitagliptin (Januvia®), clopidogrel (Plavix®), and dolutegravir (Tivicay®). A further 25% contain chiral amide groups which have published synthetic pathways with intermediates which contain a chiral amine group such as tadalafil (Cialis®), ezetimibe (Zetia®), and levetiracetam (Keppra®).⁸⁻³² The retail sales revenue for each of the six drugs named above was over \$1 billion USD in 2018. In total, the manufacturing processes of 31.5% of the 200 top selling small molecule drugs, representing over \$86 billion in sales, required the production of at least one chiral amine.⁷ With this large of an existing market, and many more in drug pipelines across the world, developments toward more of efficient production strategies for chiral amines create impacts on global pharmaceutical manufacturing.

1.2 Asymmetric Synthesis of Chiral Amines

When a chiral amine is incorporated into an API, the chiral purity, which is generally discussed in terms of enantiomeric excess (% *ee*), must be greater than 98%, as per FDA guidelines (or else a separate toxicology must be presented). Percent enantiomeric excess is defined as the absolute percentage difference between the concentrations of the two enantiomers in solution, as shown in (1).

$$\% ee = \frac{|[R] - [S]|}{|[R] + [S]|} \times 100\% \quad (1)$$

A racemate (50:50 mixture of *R* and *S*) has 0% *ee*, a 60:40 mixture of *R* and *S* has 20% *ee*, and a 99:1 mixture of *R* and *S* has 98% *ee*. Generally, in a classic amination reaction from an achiral starting material, the product will be a racemic mixture of *R* and *S* at the chiral center. However, if the catalysts or substrates in the reaction are chiral, then asymmetric synthesis of a single amine enantiomer can be accomplished. For the purposes of this discussion, chiral catalysts will be split into two categories: chemical catalysts and enzyme biocatalysts.

Chemical catalysis toward asymmetric amination often utilizes chiral organometallic compounds which contain a transition metal like iron, palladium, or iridium. While a detailed discussion of chemical amination is outside the scope of this work, the first 13 chapters of the 2010 book *Chiral Amine Synthesis* contain hundreds of diverse examples which utilize a wide variety of chemistries.³³

Across the natural world, there are countless varieties of enzyme biocatalysts which catalyze millions of different biochemical reactions. Because each amino acid residue (other than glycine) in a protein is chiral and present as the enantiomerically pure (*S*)-isomer, the active sites of enzymes are naturally chiral and bind to ligands and substrates in very specific orientations. Enzymes will typically only bind productively to a single enantiomer of a chiral substrate. Likewise, if a chiral center is generated in an enzymatic reaction, just one enantiomer is typically produced with >99.9% *ee*. The naturally high

enantioselectivity of enzymes is their primary selling point for pharmaceutical production, but other advantages are discussed in 1.3.1.

1.3 Enzymatic Routes to Chiral Amines

1.3.1 *Advantages of Biocatalysis Over Traditional Chemical Catalysis*

The primary advantage of a biocatalytic approach to a reaction over chemical catalysis is often specificity and regioselectivity.³⁴ The effects of target reactions resulting from an enzyme reaction are typically orders of magnitude less severe compared to other catalysts. This can allow for reactions on complex molecules with multiple similar functional groups without the need for extensive protection and deprotection steps. The operating conditions for biocatalysis can offer significant advantages in terms of safety and capital costs as enzymes often operate near ambient temperatures and pressures, with moderate pH values in aqueous solutions. Additionally, enzymes are produced from living microorganisms which feed on renewable materials and are readily biodegradable.

1.3.2 *ω -Transaminases (ω -TAs)*

1.3.2.1 Reaction

Thus far, the most widely utilised family of enzymes for the production of chiral amines has been the ω -transaminases (ω -TAs).³⁵⁻³⁶ Key examples APIs whose manufacturing processes made use of ω -TAs include UCB's epilepsy drug levetiracetam (Keppra®),³⁷ Merck's type 2 diabetes drug Sitagliptin (Januvia®),³⁸⁻⁴⁰ and suvorexant (Belsomra®),⁴¹ an insomnia drug also from Merck. As shown in the simple example reaction in Figure 1-1, a prochiral ketone is transformed into an enantiomerically pure

primary (*S*) amine with the transfer of the nitrogen from an amine donor and simultaneous transfer of the carbonyl between ketone substrate and amine donor. Common amine donors used for ω -transaminase reactions include alanine,⁴² isopropylamine,⁴³⁻⁴⁴ and methylbenzylamine. ω -transaminases can also be used in kinetic resolution applications by operating in the reverse direction compared to Figure 1-1.

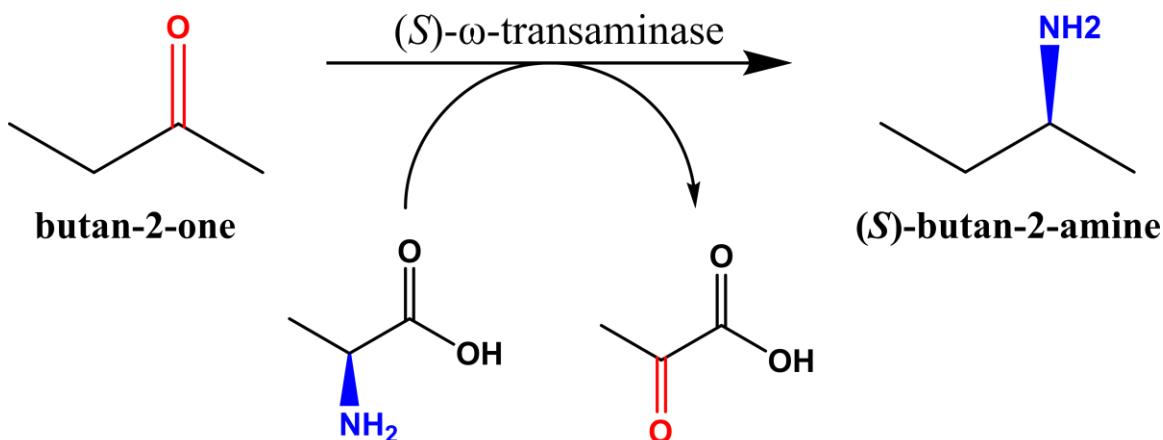


Figure 1-1 Representative reaction scheme for an ω -transaminase

1.3.2.2 Advantages

ω -TAs are a highly versatile family of enzymes.⁴⁵ Both (*R*)-selective (from *Aspergillus terreus* and *Arthrobacter sp.* for example) and (*S*)-selective (from *Arthrobacter citreus* and *Geobacillus thermodenitrificans* for example) ω -TAs are available. Primary amines anywhere in the structure are accessible. Because of their use in blockbuster drugs, some ω -TAs have been heavily engineered to increase their activity, stability, and solvent tolerance. To produce an enzyme which was active on their substrate of interest, and was stable in 50% dimethyl sulfoxide (DMSO), Merck employed 11 successive rounds of directed evolution on the (*R*)-selective transaminase from *Arthrobacter sp.* to produce sitagliptin.³⁸ Another advantage of ω -TAs over some other enzymes in this list is the lack of a requirement for an expensive consumable cofactor. Amine dehydrogenase (1.3.4),

reductive aminase (1.3.3.3), and imine reductase (1.3.3) reactions all require a hydride transfer from NADH or NADPH, while ω -TA reactions do not.

1.3.2.3 Limitations

The primary limitation to asymmetric amine production with ω -transaminases is the often significant thermodynamic limitations in the direction of the desired reaction.⁴⁶ Additionally, ω -TA reactions suffer from severe product inhibition limitations.⁴⁷ To combat these limitations, some form of product removal is required to drive equilibrium toward chiral amine products. Additionally, the amino donor must be present in the reaction in great excess to further drive equilibrium and overcome inhibitions. At small scales, multi-enzyme cascades have been employed. In one such scheme, alanine acts as the amino donor for the ω -TA and is transformed into pyruvate. Lactate dehydrogenase is then used to recycle pyruvate back into lactate. However, because lactate dehydrogenase uses NADH, a very expensive cofactor, a third enzyme, glucose dehydrogenase, must be used to regenerate NADH from NAD⁺.⁴² The addition of two enzymes to the process greatly increases complexity and cost, making this approach difficult to scale. In the large-scale manufacturing process for sitagliptin, isopropylamine was selected as the amine donor. The resulting 2-propanone was evaporated out of the solution as the reaction proceeded, thus driving the equilibrium toward product.³⁸ Other groups have used so-called “smart” amine donors such as *ortho*-xylenediamine.⁴² After the donation of one of its amine groups to the reaction substrate, the amine donor forms a transient cyclic imine with the remaining nitrogen. This imine spontaneously and nearly irreversibly converts to an aromatic isoindole. The isoindole further polymerizes in solution to form a colored precipitate,

which can be used as a rapid colorimetric assay to screen large numbers of mutant enzyme variants.

1.3.3 Imine Reductases (IREDs)

1.3.3.1 Reaction

Imine reductases (IREDs), as their name suggests, catalyse the reduction of prochiral imines to chiral amines. To accomplish this transformation, all natural IREDs require a hydride transfer from NADPH (see Figure 1-2A). Recently, multiple groups have been able to engineer an IRED to accept the much cheaper NADH instead of NADPH.⁴⁸⁻⁴⁹ Most substrates for IRED reactions are secondary cyclic imines which are stable in solution. The ability to generate chiral cyclic amines, which are common in APIs is the primary advantage of IREDs over the other enzymes described in this section. However,

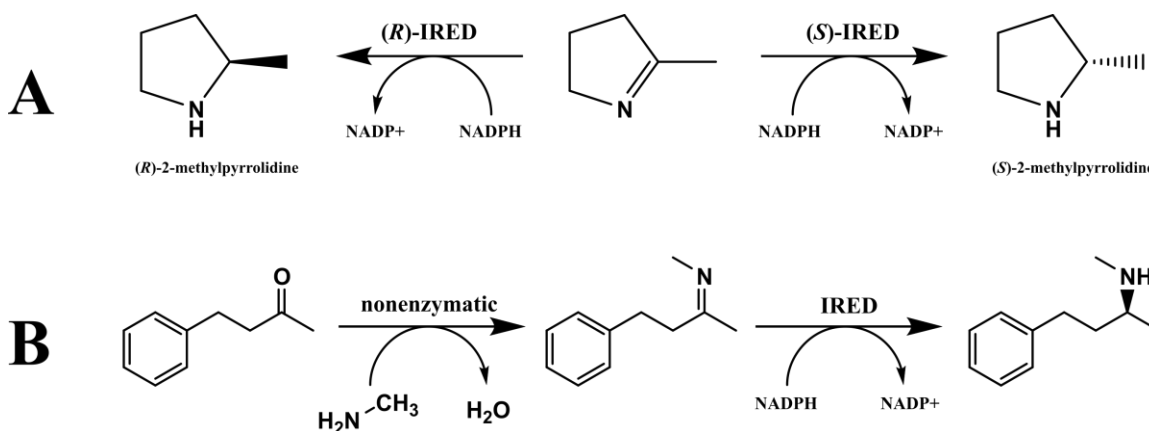


Figure 1-2 Representative reaction schemes for imine reductases. Scheme A denotes the availability of both (*R*)- and (*S*)-selective IREDs. Scheme B shows the reaction scheme for the direct amination of ketones with an alkylamine.

amination of ketones with imine reductases to form secondary amines has also been reported, though with usually limited conversion (see Figure 1-2B).^{36, 50} Amination of

ketones is accomplished by taking advantage of the unstable imines which form in free solution when ketones are exposed to alkyl amines. The resulting imines can act as substrates in the IRED, and their conversion to amines drives the equilibrium nonenzymatic imine formation reaction toward the imine direction. More than 1000 putative imine reductases have been collected in an imine reductase engineering database.³⁶

1.3.3.2 Limitations

While they offer access to unique chemistries compared to oxidoreductases, there are significant limitations which must be addressed to make use of IREDs. First, except for a couple of recent engineered enzymes, all IREDs require NADPH, which is at least an order of magnitude more expensive than NADH. Additionally, the accessible *ee* values vary widely between enzymes and substrates.⁵¹ Overall, activity is low for IREDs, which requires high loads of enzyme to achieve high conversions. For most IREDs capable of reductive amination of ketones, specific activity is low, and ratios of amine to ketone required for conversion can be as high as 50:1, which leads to a poor atom economy for the chemical process.³⁶

1.3.3.3 Reductive Aminases (RedAms)

Recently, a group of fungal enzymes homologous to IREDs have been discovered and given the name reductive aminase (RedAm). The first of these enzymes is derived from *Aspergillus oryzae* (*AspRedAm*).⁵² What sets RedAms apart from IREDs is their greatly enhanced ability to perform reductive amination at much lower ratios of amine to ketone, and their broad substrate scope. Alkeu *et al.* reported the successful production of 37 different chiral amines including aliphatic, aromatic, and cyclic amines.⁵² In a study

focused on two additional RedAms from *Aspergillus terreus* and *Ajellomyces dermatitidis*, it was discovered that the fungal RedAms, unlike IREDS, are able to directly bind to ketones and facilitate imine formation.⁵³ This is likely why RedAms are so much more effective than IREDS at reductive amination.

1.3.4 Amine Dehydrogenases (AmDHs)

Amine dehydrogenases are the focus of the work reported in this thesis and are briefly discussed here.

1.3.4.1 Reaction

Amine dehydrogenases (AmDHs) catalyze the reductive amination of prochiral ketones to form chiral amines.⁵⁴ AmDHs require aqueous ammonia as the nitrogen source and a simultaneous hydride transfer from NADH. Typically, AmDH reactions are run between pH values of 8.5 and 10, with between 2 M and 4 M of an ammonium salt, usually either NH_4COOH or NH_4Cl . The reaction scheme for the reductive amination of 5-methyl-2-hexanone to (*R*)-5-methyl-2-aminohexane is shown in Figure 1-3.

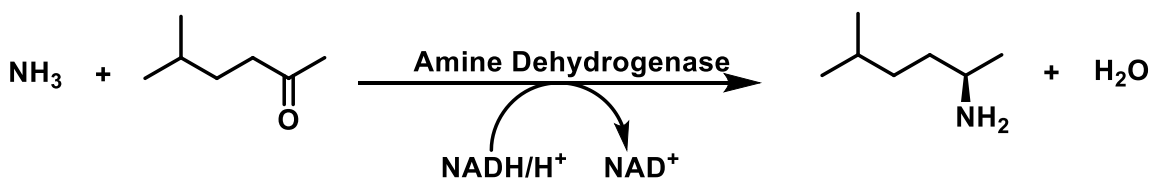


Figure 1-3 Representative reaction scheme for reductive amination of a ketone by an amine dehydrogenase

1.3.4.2 Advantages

Compared to ω -transaminases, amine dehydrogenases feature a more favorable atom economy, due to the direct incorporation of ammonia, rather than taking a nitrogen

group from a sacrificial alkyl amine donor. Additionally, AmDHs are not subject to the severe equilibrium limitations of ω -TAs, meaning product through evaporation is not required to drive catalysis. The acceptance of NADH by AmDHs serves as a distinct advantage over IREDs and AmReds, which both require the more expensive NADPH.

1.3.4.3 Limitations

Compared to reductive aminases and transaminases, the range of substrates accessible to AmDHs is limited. AmDHs are only capable of producing primary amines and are active only on methyl ketones and cyclic ketones. Like reductive amination with IREDs and ω -TAs, a great excess of the nitrogen donor is required to drive catalysis. Mechanistic studies of the L-AmDH found that the apparent K_M value for ammonium chloride was higher than the solubility limit for ammonium chloride.⁵⁵ High concentrations of ammonium salts can cause issues for further processing and separations after the amination reaction is complete.

1.4 **Generating Chirality from a Racemic Mixture of Amines**

Isolation of a single enantiomer of an amine from a racemic mixture, also known as deracemization, provides an alternative to asymmetric synthesis. This can be useful when the starting material in a process contains a racemic amine, or when asymmetric amination is infeasible or prohibitively expensive. The clear disadvantage of most deracemization is that the theoretical yield is limited to 50% which can greatly reduce the overall yield of a multi-step API manufacturing process. As the number of steps in a chemical process grows, each with their own yield values, so too does the penalty for having a single step with a

50% yield. The two main methods of deracemization are kinetic resolution and diastereomeric salt separation.

1.4.1 Diastereomeric Salt Separation

While most of the physical properties, including solubilities, of the two enantiomers of a molecule with a single chiral center are identical, this is not true for diastereomers. Though not impossible, the crystallization of a single pure enantiomer from a racemic mixture is rare, so separation of racemates by simple crystallization is also rare. However, the two different salts formed by the addition of an enantiomerically pure carboxylic acid to a racemic amine tend to crystallize separately and have different solubilities. Once the pure diastereomer salt is isolated, the resolving agent can be removed with the addition of a strong acid. Mandelic acid derivatives are often used to resolve racemic amines.⁵⁶ However, the *ee* of a diastereomer salt separation is not always perfect,⁵⁷⁻⁵⁸ which is not acceptable for API manufacturing.

1.4.2 Kinetic Resolution

Resolution of a racemic amine can also be accomplished through a reactive process where a catalyst is introduced to the racemate which reacts with only one of the enantiomers. This is most frequently accomplished enzymatically but can also be done chemically. Many of the enzymes described in 1.3 are useful for kinetic resolution in addition to asymmetric synthesis. When AmDHs are used for kinetic resolution, a separate cofactor regeneration system is required to efficiently oxidize the NADH produced by the AmDH back to NAD⁺,⁵⁹ a task usually carried out by an NADH oxidase (NOX).⁶⁰ Recent work in the Bommarius group showed higher reaction rates could be achieved for NOX

cofactor regeneration if the reaction is carried out under a constant stream of oxygen or air bubbles.⁶¹ Another class of oxidoreductase enzymes that has shown to be useful for kinetic resolution are the monoamine oxidases, which catalyze the oxidative deamination of chiral amines.³⁶

1.4.3 Chemoenzymatic Dynamic Kinetic Resolution

Chemoenzymatic dynamic kinetic resolution has the capability to get around the 50% yield limitation mentioned in 1.4.⁶² Paetzold and Bäckvall described a process by which an enzymatic kinetic resolution with Lipase B from *Candida antarctica* (CALB) is paired with a ruthenium-containing organometallic racemization catalyst.⁶³ The process is given the label “dynamic kinetic resolution” rather than just kinetic resolution because the substrate is constantly racemized by the metal catalyst *in situ* while CALB only reacts with one of the enantiomers to form the corresponding chiral amide. The theoretical yield of this process is 100% with >99% *ee*. If needed, the chiral amide can be converted back to the amine chemically⁶⁴ or enzymatically⁶⁵ without sacrificing *ee*. Purely chemical dynamic kinetic resolution of amines has also been reported⁶⁶ but will not be discussed here in detail.

1.5 Development, Enhancement, and Utilization of Amine Dehydrogenases

1.5.1 Generation of L-AmDH from Leucine Dehydrogenase

The starting point for all engineered amine dehydrogenases is an amino acid dehydrogenase (AADH). AADHs catalyze the reductive amination of α -keto acids with ammonia to produce α -amino acids. These enzymes are key players in amino acid metabolism in all virtually all organisms. Abrahamson started with the crystal structure of

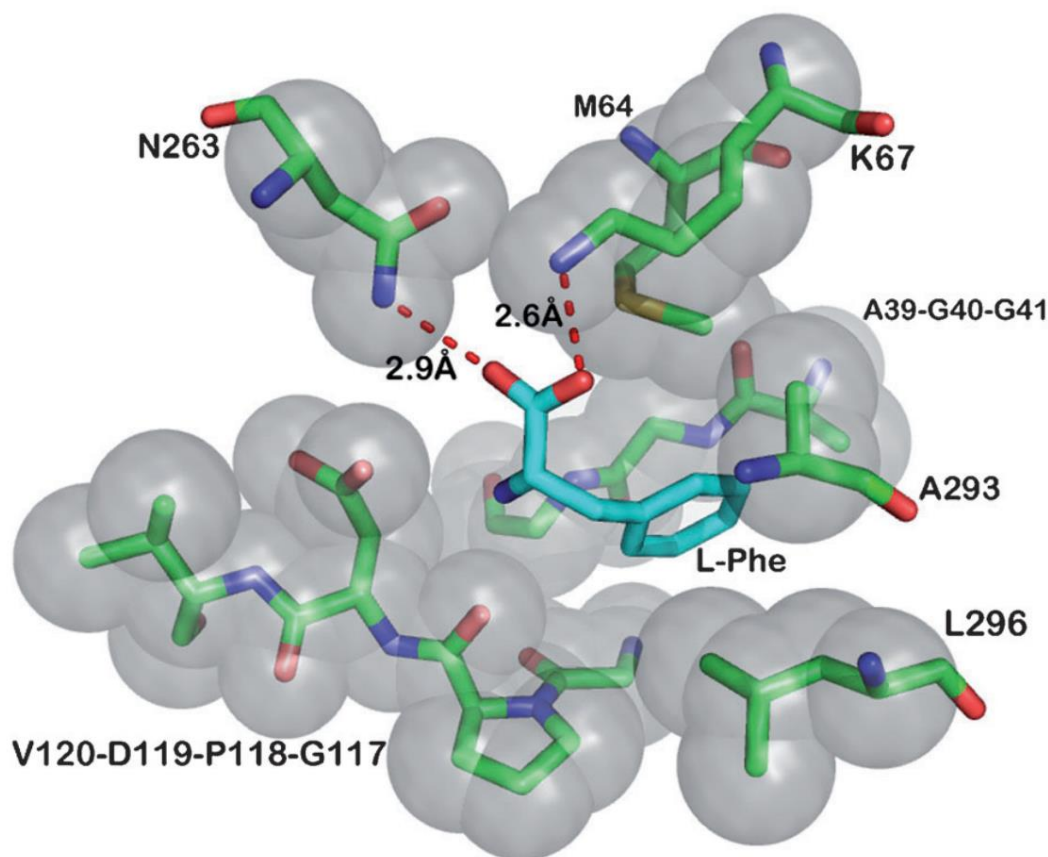


Figure 1-4 Residues in the active site of *Rhodococcus sp.* phenylalanine dehydrogenase identified as important for substrate binding (PDB ID: 1C1D). This figure was originally printed in Abrahamson's 2012 article on the L-AmDH.²

the phenylalanine dehydrogenase (PheDH) from *Rhodococcus sp.* M4 in the holo-form with NADH and phenylalanine bound in the active site (PDB ID: 1C1D).⁶⁷ From this crystal structure, key residues responsible for interacting with the substrate in the active site were located. Because the goal was to move from activity on keto-acids to ketones, special attention was paid to residues which interacted with the carboxylic acid. Because of the structural similarity among the family of amino acid dehydrogenases, the key residues found in the PheDH could be mapped to similarly located residues on the scaffold for the leucine amine dehydrogenase (L-AmDH), a leucine dehydrogenase (LeuDH) from

Geobacillus stearothermophilus. The locations of these important residues can be seen in Figure 1-4, from Abrahamson's 2012 paper.² The first key residue identified was PheDH K67, homologous to K68 in the LeuDH. The side chain of this lysine interacts closely with the phenylalanine acid group. A site saturation mutagenesis library was constructed at this location. The K68M mutant was found to catalyze the reductive amination of methyl isobutyl ketone (MIBK) with very low (0.2 mU/mg) but unprecedented activity.

Once the first small amount of activity was obtained, a lot of protein engineering work was done to enhance that activity to level that could be of use in larger-scale reactions. A broader library was created with targeted mutations at each of the marked locations in Figure 1-4 using the CASTing approach and the resulting mutants were screened for their deamination activity toward 4-methyl-2-aminopentane.⁶⁸ A quadruple mutant, K68S/E114V/N261L/V291C, was produced with significant activity towards MIBK (0.69 U/mg) and a few other prochiral ketones.

1.5.2 Building a Family of Amine Dehydrogenases

Once the first AmDH was created, work in the Bommarius group and around the world has been done to generate additional AmDHs with different properties. Two residues were identified as being key to L-AmDH binding to ketones, K68 and N261. Residues homologous to these in other AADHs have been similarly mutated to produce new amine dehydrogenases. To date, amine dehydrogenases have been produced from PheDHs,⁶⁹⁻⁷¹ LeuDH,⁷²⁻⁷⁴ and a valine dehydrogenase (ValDH) (unpublished). In the Bommarius group, the PheDH from *Bacillus badius* was used as the starting point for the published phenylalanine amine dehydrogenase (F-AmDH).⁶⁹ Additionally, a chimeric AmDH (cFL1-

AmDH) has been produced in the Bommarius lab by combining the substrate binding domain of F-AmDH and the cofactor binding domain of L-AmDH which resulted in an enzyme with much greater thermal stability, and a substrate profile different from the parent enzymes.⁷⁵ Recently, Tseliou *et al.* generated a novel L-AmDH (Le-AmDH) through homology modeling of the active site of the ϵ -deaminating L-lysine dehydrogenase from *Geobacillus stearothermophilus*, which is significantly different in sequence and structure from the AADHs which formed the scaffolds for the other engineered AmDHs.⁷⁶ Additionally, the wild-type parent enzyme of this AmDH was not capable of asymmetric amino acid synthesis, unlike previous AmDH scaffolds. The authors found that this Le-AmDH showed significantly reduced product inhibition compared to existing AmDHs. Finally, Carine Vergne-Vaxelaire's group has used metagenomic mining to uncover a variety of wild-type AmDHs for the first time.⁷⁷⁻⁷⁸

1.5.3 Modifications to Improve Activity and Stability

On top of generation of new AmDHs, work has been done in the Bommarius group and by others to improve the stability and activity of existing AmDHs. Work toward improving the L-AmDH engineered from *Geobacillus stearothermophilus* LeuDH was done by the Bommarius group⁷⁹ and is reported in CHAPTER 2. Pushpanath *et al.* introduced mutations to the Abrahamson F-AmDH⁶⁹ in addition to generating an AmDH from *Caldalkalibacillus thermarum* PheDH, with the goal of increasing activity, thermal stability, and solvent tolerance. Finally, Chen *et al.* introduced mutations into the active site of an AmDH derived from *Lysinibacillus fusiformis* LeuDH which reshaped the enzyme binding pocket, allowing activity towards aliphatic ketone substrates which were too large to bind to the original enzyme.⁸⁰

1.5.4 Cofactor Regeneration

For all the AmDH reactions studied by the Bommarius and reported in the literature, NADH more expensive by far than any other substrate or product. At the time of writing, 1 kilogram of the disodium salt of NADH can be purchased from VWR for \$17,225 USD, which amounts to \$12,219 USD per mole. At the same time, 500 mL of 5-methyl-2-hexanone, the ketone used extensively in CHAPTER 5, can be purchased from VWR for \$30 USD, which amounts to \$3.55 USD per mole. Because of the high cost of the cofactor, and because its oxidized form, NAD^+ is not a valuable product of the reaction, steps must be taken to greatly reduce how much cofactor is needed per mole of amine product produced.

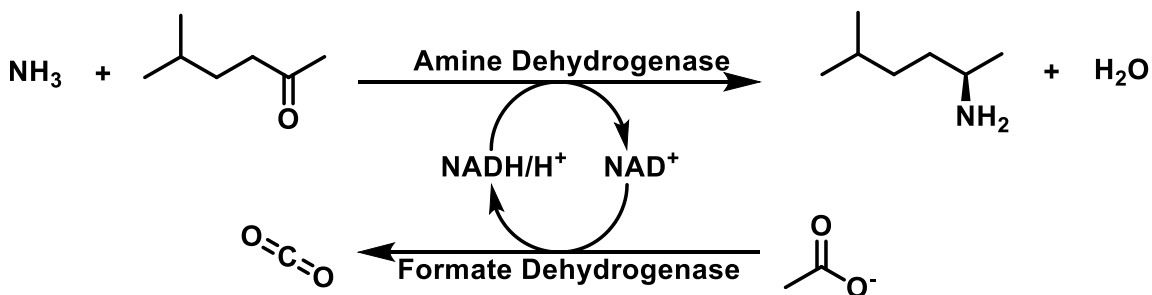


Figure 1-5 Example AmDH reaction with cofactor regeneration by formate dehydrogenase

To solve the NADH problem, an additional enzyme is added to the reaction which converts NAD^+ back to NADH at the expense of some substrate which is much cheaper than the cofactor. The two most common enzymes for this purpose are formate dehydrogenases (FDH), which convert formate to CO_2 and glucose dehydrogenases (GDH), which convert glucose to gluconic acid. FDH is generally preferred for AmDH reactions due to its more favourable atom economy. Additionally, the reaction of formate

to CO₂ is irreversible, which can help to drive the AmDH reaction toward completion, potentially overcoming any equilibrium limitations.⁸¹ The use of cofactor regeneration is ubiquitous in the literature for any enzymatic reaction which requires an NADH or NADPH cofactor.⁸²

In a growing body of work on a variety of enzyme platforms, enzymes which require redox cofactors are co-expressed as fusion proteins with a cofactor regeneration enzyme. Additionally, the cofactor itself is often covalently attached to the fusion construct with a flexible linker, such that the entire enzyme/cofactor system is a single macromolecular structure which can be immobilized in a flow reactor setup without the need to feed the cofactor.⁸³ Rather than generation of a genetic fusion between the two enzymes of interest, other work utilized the SpyTag/SpyCatcher system to generate covalent conjugation of the two proteins after enzyme expression.⁸⁴ The effects of fusion on enzymatic activity varies among enzymes, with some seeing improvement, and others seeing loss of activity.⁸⁵

1.5.5 Utilization in Multi-Enzyme Cascades

The deamination reactions performed by amine dehydrogenases can be paired with other enzymes in series to form multi-enzyme cascade reactions. The first application of AmDHs in a cascade reaction was reported by Mutti *et al.* in 2015.⁸⁶ In that study, the authors coupled an either an (*R*)-selective or (*S*) selective alcohol dehydrogenase (ADH) with cFL1-AmDH to generate a chiral amine from a chiral alcohol in a one-pot synthesis. This work was later expanded upon by Mutti⁸⁷⁻⁸⁸ and others.^{74, 89} One advantage of the ADH-AmDH cascade is that it is redox neutral, because the NADH produced by the ADH

reaction is converted back into NAD⁺ by the AmDH reaction. In 2020, Wang *et al.* added a step to the beginning of the alcohol to amine cascade by utilizing a cytochrome p450 monooxygenase to produce the racemic alcohols from ethyl benzene.⁹⁰ AmDHs have also been used to regenerate amine donors in ω -transaminase reactions.⁹¹

1.5.5.1 Whole Cell Biocatalysis

While most of the work on AmDHs has utilized purified enzymes in the solution phase, some groups have incorporated whole cell biocatalysis into their multi-enzyme cascade schemes. The use of whole cells removes the need for potentially costly and time-consuming purification protocols. Additionally, cells produce their own cofactors, potentially eliminating the need to add exogenous NADH.⁹² Jeon *et al.* co-expressed cFL1-AmDH and the NADH oxidase from *Lactobacillus brevis* in *E. coli* BL21 (DE3) cells to enable the kinetic resolution of racemic amines, with the best activity seen toward 2-aminoheptane and methylbenzylamine where 99% *ee* was achieved after five hours for both substrates.⁶⁰ Liu and Li demonstrated the use of whole cell biocatalysis in an ADH-AmDH system to enable separate cofactor regeneration systems for each enzyme, with the ADH and NADH oxidases inside *E. coli* cells and AmDH and glucose dehydrogenase in free solution.⁸⁹ In a rather exotic experiment, an L-AmDH produced by Chen *et al.* was paired with a formate dehydrogenase for the amination of ketones and aldehydes. What made the study exotic is that formate for the FDH was produced by photosynthetic algae rather than feeding it exogenously.⁹³ While interesting, this study is of dubious utility, as the resources needed to produce, isolate, and dispose of the algae are likely more expensive than just purchasing ammonium formate.

1.5.6 Immobilization

In addition to the work on directly improving existing AmDHs and generating new ones, the Bommarius group and others have worked toward increasing their usefulness in real-world applications through immobilization of the enzymes on to a wide variety of solid supports. Immobilization can offer important benefits over homogenous soluble biocatalysis,⁹⁴ key among them being the ease of separating the enzyme from the reaction mixture once the reaction is complete. In homogenous biocatalysis, steps must be taken to remove the enzyme from solution prior to further processing. For an immobilized enzyme, this separation can be achieved by a simple filtration. A related benefit is that because the biocatalyst is easy to separate without damaging the enzymes, it is also much easier to reuse over multiple batches or in a continuous reactor. Additionally, immobilized enzymes tend to be more stable and less prone to aggregation compared to their free-solution forms.⁹⁵

Many different immobilization platforms have been applied to co-immobilized amine dehydrogenases and cofactor regeneration enzymes. The Bommarius group and others have utilized the 6xHis tag generally used for purification to immobilize the enzyme onto solid supports with immobilized transition metal ions. Towards this aim, Liu *et al.* used Ni-NTA functionalized magnetic nanoparticles. Controlled porosity glass with immobilized Fe(III) ions have been used for AmDH immobilization in combination with formate dehydrogenase and alternatively an alcohol dehydrogenase by the Mutti⁸⁸ and Turner⁹⁶ groups. Additionally, work presented in CHAPTER 5 outlines the use of a polyacrylamide resin functionalized with Ni-NTA for the immobilization of cFL1-AmDH and FDH. Other immobilization strategies include encapsulation into titania

nanoparticles,⁹⁷ commercial hydrophobic and covalent supports,⁷³ and noncovalent immobilization onto calcium phosphate microparticles using leucine zippers.⁹⁸⁻⁹⁹

CHAPTER 2. EXPANDING THE BINDING POCKET OF L-AMDH TO ACCOMMODATE LARGER SUBSTRATES

The first portion of this chapter (up to and including section 2.5) was adapted from “Separate sets of mutations enhance activity and substrate scope of amine dehydrogenase” which was authored by R.D. Franklin *et al.* and published in *ChemCatChem* in 2020.⁷⁹

2.1 Introduction

For decades, chiral amine compounds have proven to be key intermediates for blockbuster drugs. Many of the top selling small molecule drugs today contain chiral amine groups.¹⁰⁰ Recently, there has been a growing interest in utilizing biocatalytic reductive amination of prochiral ketones to produce chiral amines. Biocatalytic production of chiral amines offers distinct advantages over classical heterogeneous catalysis. Key enzyme families in the field include ω -transaminases,⁴⁵ imine reductases,¹⁰¹ reductive aminases,^{52, 102} and amine dehydrogenases.³⁶ Amine dehydrogenases (AmDHs), first developed in 2012², catalyze the reductive amination of prochiral ketones to form chiral primary amines with the addition of aqueous ammonia. The reaction is dependent on a hydride transfer from NADH to form NAD⁺ (Figure 2-1). To-date, all the AmDHs engineered from amino acid dehydrogenases produce (*R*)-amines. The first AmDH, called leucine amine dehydrogenase (L-AmDH) was developed through targeted libraries of mutations in the active site of the leucine dehydrogenase (LeuDH) from *Geobacillus stearothermophilus*. After multiple rounds of mutations, activity toward keto acids was removed, and new activity toward ketones was obtained. Since 2012, multiple groups have produced similar

amine dehydrogenases from other amino acid dehydrogenase scaffolds^{69-70, 73, 76, 80, 103-105} or have identified AmDHs from natural sources.^{77-78, 106} Others have introduced new mutations to increase activity for new substrates by altering the size of the ketone binding pocket.⁸⁰ Still more work has been performed on enzyme immobilization,^{73, 88, 97-99, 107} rate law determination,⁵⁵ whole-cell biocatalysis,^{89, 104} and multi-enzyme cascades^{86, 88, 90-91, 108} to enable the use of amine dehydrogenases in the large-scale synthesis of chiral amines.

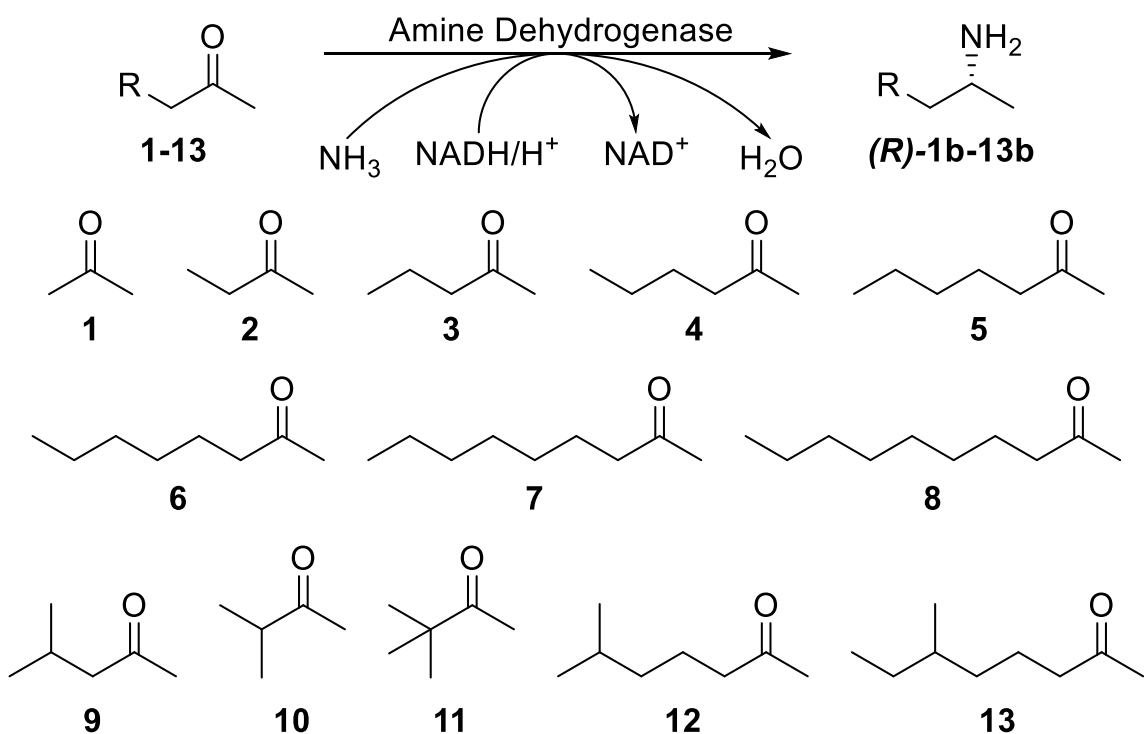


Figure 2-1 Reaction scheme for the reductive amination of amines with AmDH and list of relevant ketones

2.2 Plan for Mutations

In the present work, we sought to improve the published L-AmDH (referred to here as the base case) through two separate sets of mutations. The first group was selected to increase activity and stability without necessarily impacting substrate specificity. Position

V291 was shown to be important for substrate binding in LeuDH.¹⁰⁹ In the base case enzyme, this residue was mutated from valine to cysteine. It was speculated that mutating back to valine (Figure 2-2A) could positively impact activity. Two residues farther away from the active site were also shown to be promising candidates in a 2004 patent on mutations in LeuDHs.¹¹⁰ Based on the reported results, F101S and D32A were incorporated into the L-AmDH base case.

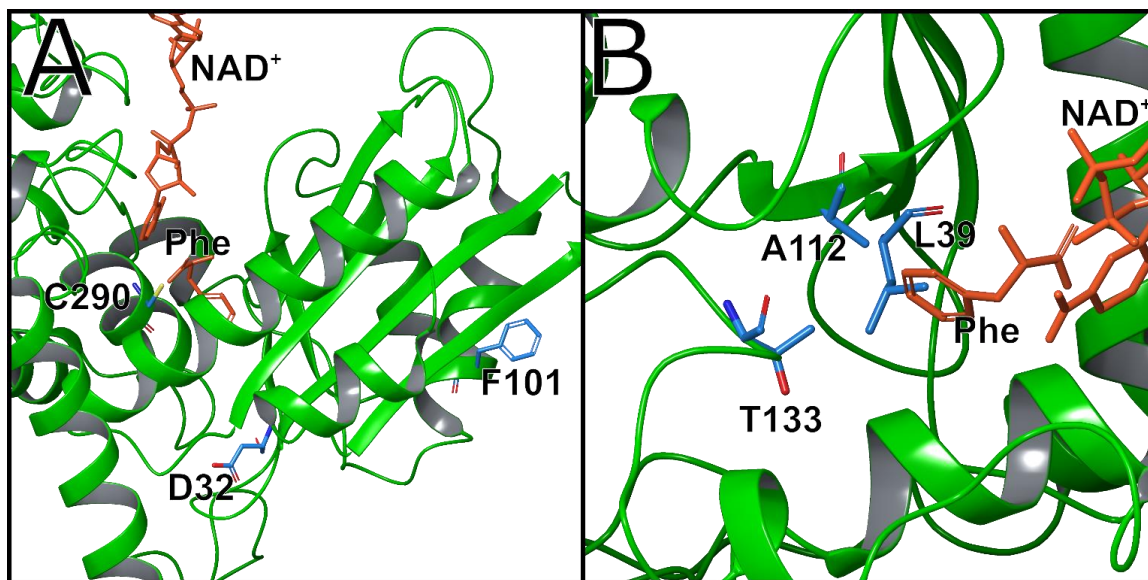


Figure 2-2 A homology model of the engineered L-AmDH sequence mapped onto a published LeuDH structure.

The homology model of L-AmDH was constructed with SWISS-MODEL¹¹¹⁻¹¹² and mapped the sequence of the engineered L-AmDH base case (2.3.2.1) onto the published cryo-EM structure of the LeuDH from *Geobacillus stearothermophilus* in the apo form (PDB ID: 6ACF).¹¹³ Because this structure is in the apo form, the holo-structure the PheDH from *Rhodococcus sp.* (PDB ID: 1C1D)¹¹⁴ was aligned to the homology model, the phenylalanine substrate and NAD⁺ cofactor position from this alignment can give a good idea of how the substrate and cofactor would be positioned in L-AmDH. Figure 2-2A

shows the positions of D32, F101, and C290 relative to the active site. Figure 2-2B shows the positions of L39, A112, and T133 in the active site.

In the second group of mutations, three residues close to the substrate side chain were identified as potential targets for altering the L-AmDH substrate scope. Kataoka and Tanizawa found that for *G. stearothermophilus* LeuDH, L39K and A112G mutations both caused major changes in the relative specific activities for different amino acid and keto acid substrates.⁸⁰ Recently, Chen *et al.* showed mutations homologous to A112G and T133G enhanced activity toward larger and bulkier ketones in multiple engineered L-AmDHs.⁸⁰ Replacing the residues at positions L39, A112, and T133 with smaller residues was hypothesized to enable activity toward larger ketones in our L-AmDH as well. The positions of the proposed mutations relative to the substrate binding pocket can be seen in Figure 2-2B.

Combinations of the six proposed mutations were introduced into L-AmDH and the resulting variants were screened for activity on a variety of straight and branched methyl ketones of different sizes. Other mutations were tested but showed poor results.

2.3 Materials and Methods

2.3.1 Materials Used

Overnight Express™ Instant TB Medium (MilliporeSigma, Burlington, MA, USA), sodium chloride 99% (BDH VWR Analytical, Radnor, PA, USA), potassium chloride >99% (VWR BDH Chemicals, West Chester, PA, USA), sodium phosphate dibasic anhydrous >99% (VWR BDH Chemicals, West Chester, PA, USA), potassium phosphate

monobasic >99% (Acros Organics, NJ, USA), imidazole 99% (Alfa Aesar, Heysham, England), Ni-NTA agarose resin (MCLAB, South San Francisco, CA, USA), dimethyl sulfoxide 99.9% (Fisher Chemical, Fair Lawn, NJ, USA), LB broth (US Biological, Salem, MA, USA), agar (VWR Life Science AMRESCO, Solon, OH, USA), kanamycin monosulfate (GoldBio, St Louis, MO, USA), NADH disodium salt trihydrate 99.6% (VWR Life Science AMRESCO, Solon, OH, USA), ammonium chloride 99.5% (VWR Life Science AMRESCO, Solon, OH, USA), ammonium hydroxide 28%-30% (Ricca Chemical, Arlington TX, USA), QIAprep spin miniprep kit (Qiagen, Hilden, Germany), agarose (Fisher Scientific, Hampton, NH, USA), QIAquick gel extraction kit (Qiagen, Hilden, Germany), midori green (Nippon Genetics Europe GmbH, Dueren, Germany), tris base 99.8% (Fisher BioReagents, Fair Lawn, NJ, USA), ethanol 95% (Decon Laboratories, King of Prussia, PA, USA), acetic acid 99.7% (Fisher Chemical, Fair Lawn, NJ, USA), FastLink DNA Ligase kit (Lucigen, Middleton, WI, USA), CutSmart® buffer (New England BioLabs inc., Ipswich, MA, USA), NdeI restriction endonuclease (New England BioLabs inc., Ipswich, MA, USA), XhoI restriction endonuclease (New England BioLabs inc., Ipswich, MA, USA), 1 kbp DNA ladder (New England Biolabs, Ipswich, MA, USA), Q5 DNA polymerase (New England Biolabs, Ipswich, MA, USA), Deoxynucleotide (dNTP) Solution Mix (New England Biolabs, Ipswich, MA, USA), acetone 99.9% (Fisher Chemical, Fair Lawn, NJ, USA), 2-butanone >99% (Sigma-Aldrich, St. Louis, MO, USA), 2-pentanone 99% (Alfa Aesar, Heysham, England), 2-hexanone >98% (TCI Chemical, Tokyo, Japan), 2-heptanone 99% (BeanTown Chemical, Hudson, NH, USA), 2-octanone >98% (TCI Chemical, Tokyo, Japan), 2-nonanone >98% (Alfa Aesar, Tewksbury, MA, USA), 2-decanone 97% (Alfa Aesar, Heysham, England), methyl isopropyl ketone 99%

(Sigma-Aldrich, St. Louis, MO, USA), methyl isobutyl ketone >99% (Sigma-Aldrich, St. Louis, MO, USA), pinacolone 98% (Sigma-Aldrich, St. Louis, MO, USA), 5-methyl-2-octanone >80% (TCI Chemical, Tokyo, Japan), 6-methyl-2-heptanone >98% (TCI Chemical, Tokyo, Japan), Marfey's Reagent >95% (TCI Chemical, Tokyo, Japan), Acetonitrile HPLC grade (Fischer Chemical, Fair Lawn, NJ, USA), Acetone HPLC grade (Fischer Chemical, Fair Lawn, NJ, USA), racemic 2-aminopentane >97% (TCI Chemical, Tokyo, Japan), racemic 2-aminoheptane >98% (Alfa Aesar, Haverhill, MA, USA), (R)-(-)-2-aminononane >99% (Alfa Aesar, Haverhill, MA, USA), (S)-(+)-2-aminononane >99% (Alfa Aesar, Haverhill, MA, USA), benzoyl chloride >99% (Alfa Aesar, Haverhill, MA, USA)

2.3.2 DNA and Amino Acid Sequences

2.3.2.1 L-AmDH Base Case Amino Acid Sequence

MGSSHHHHHSSGLVPRGSHMELFQYMEKYDYEQVLFCQDKESGLKAIIVIHDT
TLGPALGGTRMWMYNSEEEALEDALRLARGSTYSNAAAGLNLGGGKTVIIGDP
RKDKNEAMFRAFGRFIQGLNGRYITAVDVGTTVADMDIYQETDYVTGISPEFGS
SGNPSPATAYGVYRGMKAAAKEAFGSDSLEGKVVAVQGVGNVAYHLCRHLHE
EGAKLIVTDINKEAVARAVEEFGAKAVDPNDIYGVECDIFAPCALGGIINDQTIPQ
LKAKVIAGSALNQLKEPRHGDMIHEMGIVYAPDYVINAGGCINVADELYGYNRE
RAMKKIEQIYDNIEKVFAIAKRDNIPTYVAADRMAEERIETMRKARSQFLQNGHH
ILSRRRAR

Note, the numbering convention used in the reported work does not include the His-Tag sequence (marked in red) or the N-terminal methionine (marked in green). The exclusion

of the starting methionine in numbering is because in *E. coli*, this residue is cleaved from translated proteins by methionyl-aminopeptidase, and thus is not present in the expressed protein.

2.3.2.2 L-AmDH Base Case DNA Sequence

Atggaactgtttcaatatatggaaaaatac gattatgaacaagtgttgttttccaagacaaagaatccggattgaaggcgatcatt
gtcattcatgacacgacgctcgcccggcgctcggcgggacgcgcatgtggatgtacaattcggagaagaggcgcttgaag
acgccttgccctcgcccggcatgacgtacgtaacgcggcccgcccttaatttaggcgggggcaagacggcatcatc
ggcgatccgcgcaaagataaaaacgaggcgatgttccgcgcttcggccggtcattcaagggtgaacggccgctacattac
ggctgttgacgttggcagaccgtgccgatatggatatcatctatcaagaaaccgactatgcaccggcatttcgccggaattcg
gctcatccggcaaccgctcgccggccacggcttacggcgatatcgtgggatgaaagcggcggcgaaggaagcatttggcag
tgattcgcttgaaggaaaagtgtcgccgtccaaggagtcggcaatgtcgctaccatttatgccgccatttgcacgaagaagga
gcgaaactcatcgttaccgacatcaacaaggaagcgggtggcgcgcggctcagggaatttggggcgaaagcagtcgaccg
aacgacatttacggcgtggagtgcgacattttgctccatgcgcgctcggcggcatcatcaacgaccaaacgattccgcagctga
aagcgaagtgatcgccggctcggcgttgaatcagctgaaagagccgcgccatggcgacatgatccatgaaatgggcatcgtc
tatgcaccagattatgtgatcaacgccggcggtgcatcaacgtcgccgatgagctgtacggctacaaccgtgaacggcgat
gaaaaaatcgagcaaatttatgacaacatcgaaaaagtgttccatcgccaagcgtgacaacattccaacgtatgtggccgct
gaccgatggccgaagaacgaattgaaacgatgcgcaaagcgcgagccaattttgcaaacggccatcatatttaagccgc
cgccgcgcccgctaa

2.3.2.3 Primers Used

T7 promoter: TAATACGACTCACTATAGGG

T7 Terminator: GCTAGTTATTGCTCAGCGG

D32A Forward: GTCATTCATGCGACGACGCTCGGC
D32A Reverse: GCCGAGCGTCGTCGCATGAATGAC
L39A Forward: CTCGGCCCCGGCGGCCGGCGGGACGCGC
L39A Reverse: GCGCGTCCCGCCGGCCGCCGGGCCGAG
L39G Forward: CTCGGCCCCGGCGGGCGGC GGGACGCGC
L39G Reverse: GCGCGTCCCGCCGCCCGCCGGGCCGAG
F101S Forward: CTTTCGGCCGGAGCATTCAAGGGCTG
F101S Reverse: CAGCCCTTGAATGCTCCGGCCGAAAG
A112G Forward: CGCTACATTACGGGCGTTGACGTTGG
A112G Reverse: CCAACGTCAACGCCCGTAATGTAGCG
T133G Forward: GAAACCGACTATGTTCGGCGGCATTTGCGCCGG
T133G Reverse: CCGGCGAAATGCCGCCGACATAGTCGGTTTC
C290V Forward: GATCAACGCCGGCGGCATCAACGTCGCCGATG
C290V Reverse: CATCGGCGACGTTGATGACGCCGCCGGCGTTGATC

2.3.3 *Overlap Extension Mutagenesis*

Genes containing desired mutations were generated *via* overlap extension PCR using the primers above. For the first step, parallel PCR reactions were conducted using

the T7 promotor and mutagenic reverse primers in one reaction, and the mutagenic forward primer and T7 terminator primer in the other reaction. PCR products were purified using gel extraction, and then combined in a second PCR with T7 promotor and terminator primers. For the second PCR, 5 cycles are completed prior to adding primers in order to extend the overlaps in the two gene fragments to form whole a whole gene. The single product from the second PCR was purified *via* gel extraction. Purified gene fragment and empty pet28a vector were both restricted with NdeI and XhoI enzymes. Following a third gel extraction, gene fragment and cut vector were ligated using the FastLink DNA ligase kit from Lucigen and then transformed into chemically competent BL21(DE3) cells. The resulting colonies were screened for the successfully inserted gene by colony PCR. Validated colonies were grown overnight in 5 mL LB-Kanamycin broth and an aliquot was frozen at -80 °C in 10% DMSO. The pet28a plasmid containing the mutant L-AmDH gene was extracted from the remainder of the culture using the Qiagen QIAquick spin miniprep kit for sequencing and storage.

2.3.4 *Enzyme Expression*

Genes encoding L-AmDH variants were cloned into the pet28a vector and transformed into BL21(DE3) competent cells for expression. Frozen cell stocks were stored at -80 °C in 10% DMSO. For enzyme expression, a starter culture (5 mL LB with 25 µg/mL kanamycin) was seeded from the frozen stock and incubated at 37 °C, 250 RPM overnight. 500 µL of the starter culture was used to seed 50 mL of sterile Overnight Express™ Instant TB Medium with 25 µg/mL kanamycin in a 250 mL baffled flask. The full-scale culture was incubated in an orbital shaking incubator at room temperature for 24 hours. Cells were then isolated by centrifugation at 4000 RPM for 35 minutes. After

decanting the supernatant, cell pellets were either harvested immediately for protein purification or stored at -80 °C until needed.

2.3.5 *Enzyme Purification*

His-tagged L-AmDH binds tightly and specifically to Ni-NTA IMAC resins, which allows for simple purification of the enzyme from other host-cell proteins. Cell pellets were resuspended in 10 mL Lysis Buffer (1X PBS, 300 mM NaCl, 10 mM imidazole, pH 7.4) and lysed on ice using a probe sonicator for ten cycles of 1 minute/1 minute off. The insoluble fraction was removed by centrifugation (10,000 RPM, 4 °C, 40 minutes) and the supernatant applied to 2 mL of Ni-NTA agarose resin (MCLAB) which had been pre-equilibrated with lysis buffer. The His-tagged L-AmDH was incubated with the resin on ice for 15 minutes, with gentle resuspension every 3 minutes. The supernatant was drained in a small gravity column to waste. The resin is then washed twice, first with 10 mL of Wash 1 Buffer (1X PBS, 300 mM NaCl, 20mM imidazole, pH 7.4), followed by 10 mL of Wash 2 Buffer (1X PBS, 300 mM NaCl, 40 mM imidazole, pH 7.4). The washing is done to remove any non-specifically bound proteins. Finally, the resin was incubated for 5 minutes at room temperature in the Elution Buffer (1X PBS, 300 mM NaCl, 250 mM imidazole, pH 7.4) to recover the desired protein. Enzyme concentration was quantified using the Bradford Assay,¹¹⁵ and purity of each step was examined using SDS-PAGE. An example gel from the purification of L-AmDH/D32A can be seen in Figure 2-3.

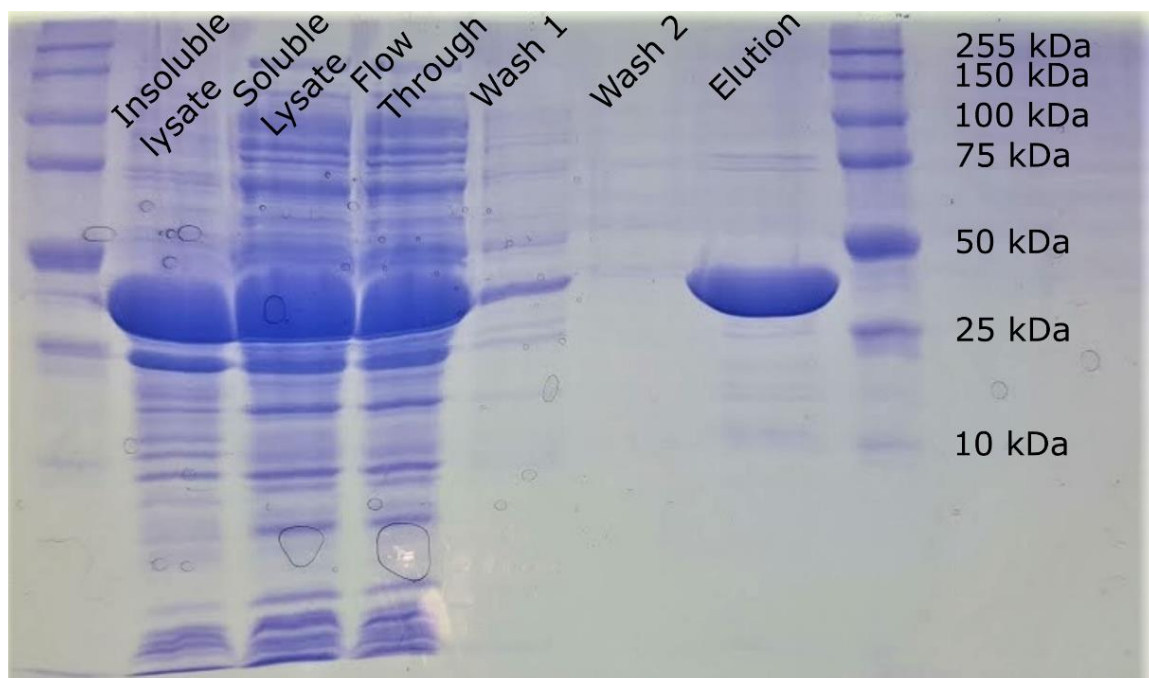


Figure 2-3 Representative SDS-PAGE gel showing the steps to the purification of an AmDH. Specifically, this was a gel collected after the purification of L-AmDH/D32A. The dark band at around 40 kDa is the protein of interest.

2.3.6 Activity Assays

Specific activity for various ketones was measured with UV-Visible spectroscopy (Beckman Coulter DU 800 Spectrometer). Reaction volume was fixed at 1 mL and temperature at 1 mL. All reactions were carried out in 4M NH₄Cl at pH 9.6, with 200 μM NADH, and 20 mM ketone. Stock solutions of 20 mM NADH in deionized water, 4M NH₄Cl/NH₄OH in deionized water, and 1M ketone in DMSO, and enzyme in the elution buffer were prepared ahead of time. 6 reactions were prepared in parallel with the addition of 20 μL NADH, 10-30 μL enzyme solution, and 20 μL of ketone solution. Reactions were initiated by the rapid addition and mixing of enough NH₄Cl solution to bring the final volume to 1 mL. Reaction rate was determined by the decrease of absorbance of NADH at 340 nm ($\epsilon_{340} = 6.22 \text{ mM}^{-1}\text{cm}^{-1}$) for at least 3 minutes. Enzyme concentrations in the

reactions were adjusted to ensure a linear reaction profile over the measurement period. To validate the repeatability of the activity assays, selected reactions were performed in triplicate. Standard deviations of the initial rate ranged from 2% to 10% of the average value, with the larger percent standard deviations found for the low activity substrates.

2.3.7 Melting Temperature Estimation with Differential Scanning Fluorimetry

Denaturation temperatures of L-AMDH and L-AMDH-TV were estimated using the Prometheus™ NT.48 differential scanning fluorimetry (nanoDSF) instrument from NanoTemper. Small samples (10 μ L) of protein solutions (~1 mg/mL in elution buffer) were heated in the instrument and the difference in fluorescence at 330 nm and 350 nm was measured to follow changes in the number of tryptophan residues exposed to solvent. The inflection point of the temperature vs fluorescence curve is the estimated melting temperature of the enzyme (see Figure 2-4).

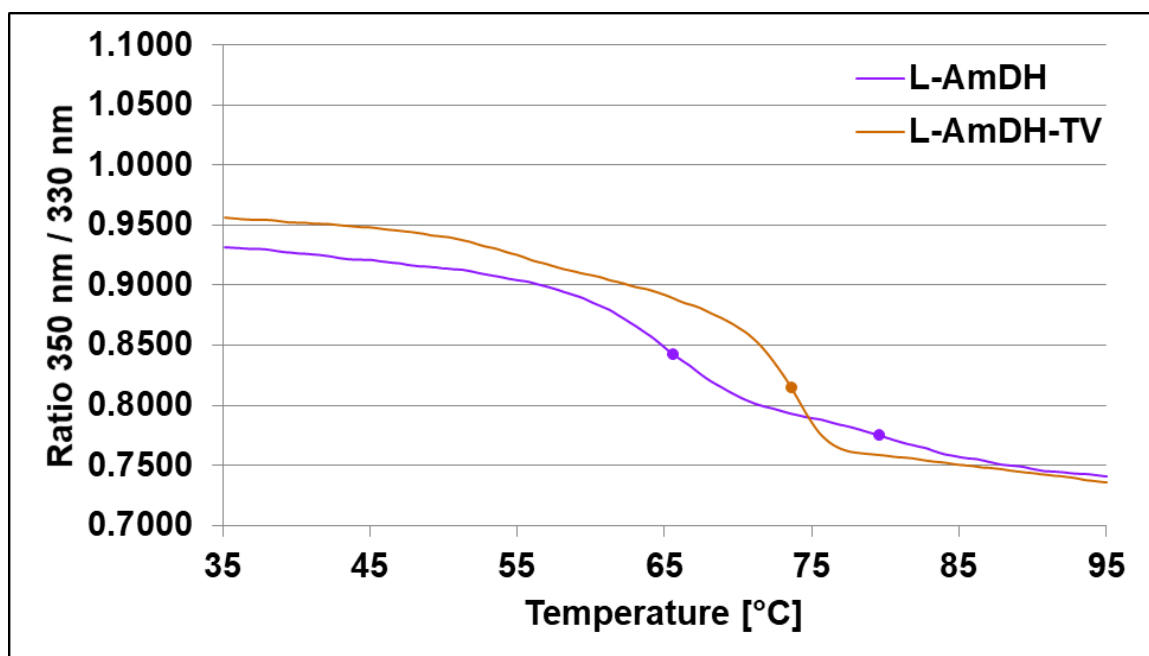


Figure 2-4 Melting profiles of L-AmDH and L-AmDH TV. Curves were collected by differential scanning fluorimetry with the ~1 mg/mL enzyme samples prepared in 250 mM imidazole elution buffer. Points on the curves indicate the measured apparent melting temperatures of the enzymes.

2.3.8 50 mL Scale Conversions

Selected reactions were carried out at the 50 mL scale to demonstrate the improvements in activity towards larger substrates granted by L-AmDH-TV/L39A compared to L-AmDH. Substrates selected were 2-pentanone, 2-heptanone, and 2-nonanone. Substrates **3** and **5** were present at 10 mM, while substrate **7** was present at 2 mM due to solubility limitations. The reaction buffer also contained 2 M $\text{NH}_4\text{COOH}/\text{NH}_4\text{OH}$ buffer at pH 8.5, and 1 mM NAD^+ . The formate dehydrogenase from *Candida boidinii* (cbFDH) was used to recycle the cofactor. Amine dehydrogenase and cbFDH were each expressed and purified as described above and desalted into 1X PBS using PD-10 desalting columns from GE Healthcare. Each reaction contained 2 mg of cbFDH and 2 mg of either L-AmDH or L-AmDH-TV/L39A. Conversions were carried out

in 50 mL conical tubes at room temperature (~21 °C) for 24 hours while spinning at 20 rpm in a tube rotator. After 24 hours, conversion was measured via HPLC UV/Vis after derivatization with benzoyl chloride, and chiral purity was observed via HPLC UV/Vis after derivatization with Marfey's reagent.

2.3.9 *Derivatization with Benzoyl Chloride*

Derivatization with benzoyl chloride (BzCl) was performed to add a chromophore to the amine products and make them detectable via HPLC UV/Vis. To 20 μL of AmDH reaction mixture, 10 μL of $\text{Na}_2\text{CO}_3/\text{NaHCO}_3$ (1M, pH 10.5), 40 μL H_2O , and 30 μL BzCl stock (50 mM in acetonitrile) were added. The mixture was vortexed for 10 seconds followed by a brief spin down to remove any liquid from the tube cap. The derivatization reaction was then quenched with 20 μL of HCl (1M) and diluted with 90 μL acetonitrile solution (83.33 v/v% in H_2O) to bring the final acetonitrile concentration to 50%. Samples were centrifuged at 14,500 rpm for 10 minutes to remove any protein in solution. Finally, 150 μL of each supernatant was transferred to an HPLC vial. Samples were analyzed by reversed-phase HPLC as described in the analytics section.

2.3.10 *Diastereomeric Derivatization with FDAA*

Chiral purity of the amine products was determined by reversed-phase HPLC UV/Vis after derivatization with FDAA (1-fluoro-2-4-dinitrophenyl-5-L-alanine amide), also known as Marfey's reagent. Reaction of a chiral amine with the chiral FDAA results in one of two diastereomers which can be separated without a chiral column. To 40 μL of AmDH reaction mixture, 16 μL of $\text{Na}_2\text{CO}_3/\text{NaHCO}_3$ (1M, pH 10.5) and 40 μL of FDAA solution (15 mM in acetone) were added. After mixing by vortexing, samples were

incubated at 50 °C and shaking at 600 rpm for 1 hour. Derivatization reactions were then quenched with the addition of 8 μ L HCl (4 M) and centrifuged at 14,500 rpm for 10 minutes to remove protein. 50 μ L of the supernatant was diluted first with 50 μ L pure acetonitrile, then an additional 100 μ L of 50 v/v% acetonitrile in water was added. After filtration through a 0.22 μ m syringe filter, samples were transferred to HPLC vials and analyzed as described in the analytics section.

2.3.11 Analytics

All HPLC chromatograms were collected using a YMC® ODS-AQTM column (100 x 3.0 mm, 5 μ m). With a mixture of ACN and H₂O as the eluent. Specific conditions for each amine are listed separately.

2.3.11.1 2-aminononane

BzCl derivative:

Eluent ACN/H₂O (50/50 isocratic); flow 0.5 mL min⁻¹; temperature 29 °C; injection volume 4 μ L; UV detection at λ = 215 nm. Peak at 15.682 minutes was integrated and the peak area of the reaction samples was divided by the peak area obtained from the derivatization of a 2 mM (*R*)-2-aminononane standard solution to calculate conversion.

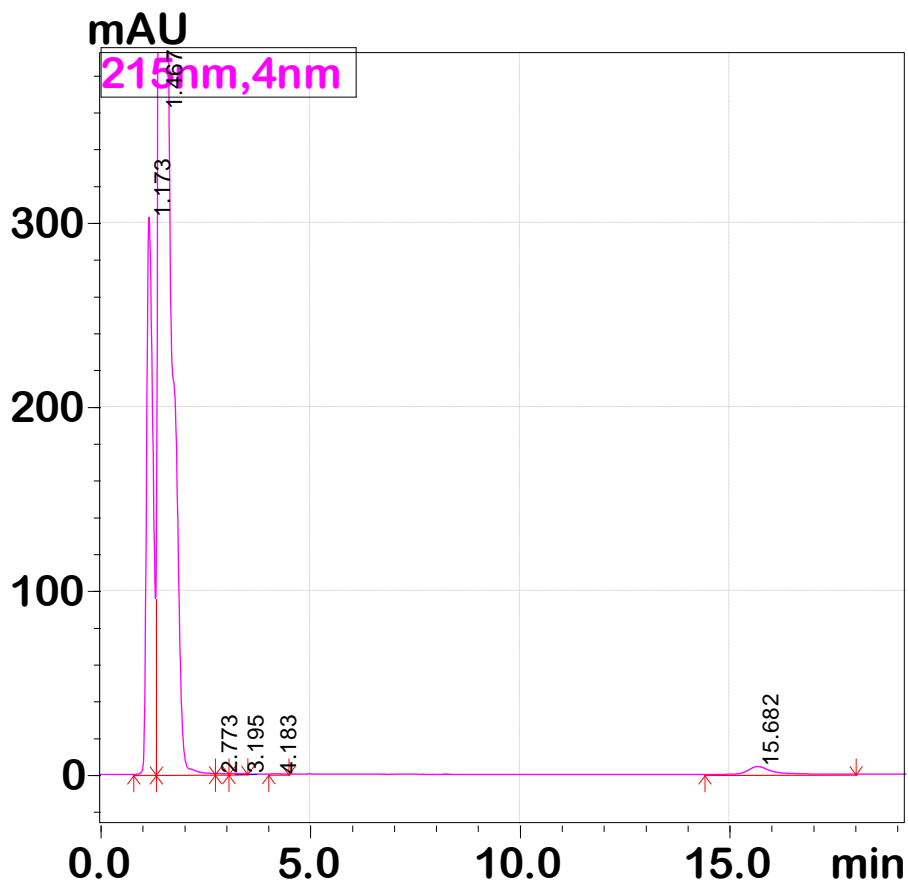


Figure 2-5 Representative chromatogram of the HPLC quantification of 2-aminononane after derivatization with benzoyl chloride

FDAA derivative:

Eluent ACN/H₂O (50/50 isocratic); flow 0.75 mL min⁻¹; temperature 40 °C; injection volume 10 μL; UV detection at λ = 340 nm. Enantiomerically pure standards were used for (R)- and (S)-2-aminononane. The product of the TV/L39A preparative-scale reaction can be positively identified as (R)-2-aminononane with an ee% greater than 99%.

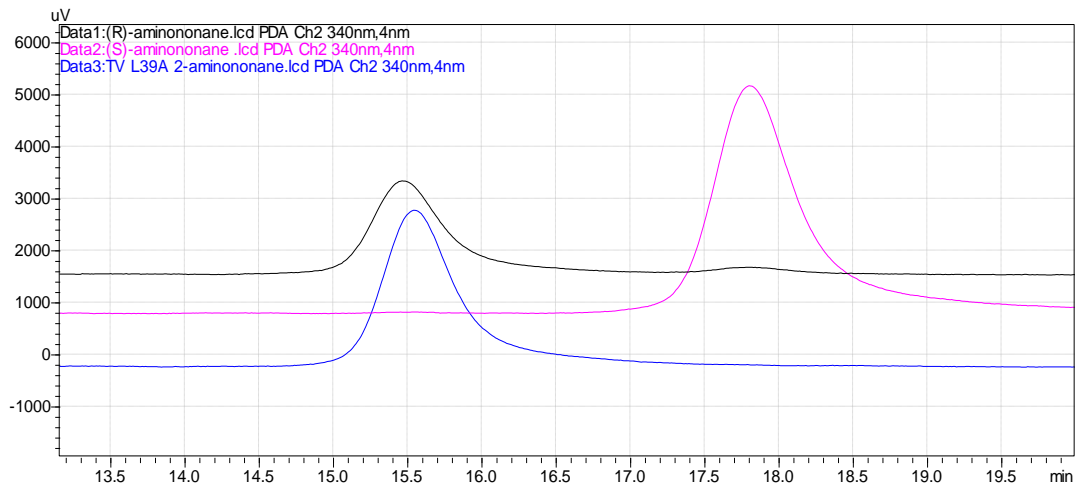


Figure 2-6 Comparison of HPLC chromatograms of 2-aminononane derivatized with FDAA.

2.3.11.2 2-aminoheptane

BzCl derivative:

Eluent ACN/H₂O (50/50 isocratic); flow 0.5 mL min⁻¹; temperature 29 °C; injection volume 4 μL; UV detection at $\lambda = 215$ nm. Peak at 7.544 minutes was integrated and the peak area of the reaction samples was divided by the peak area obtained from the derivatization of a 10 mM racemic 2-aminoheptane standard solution to calculate conversion.

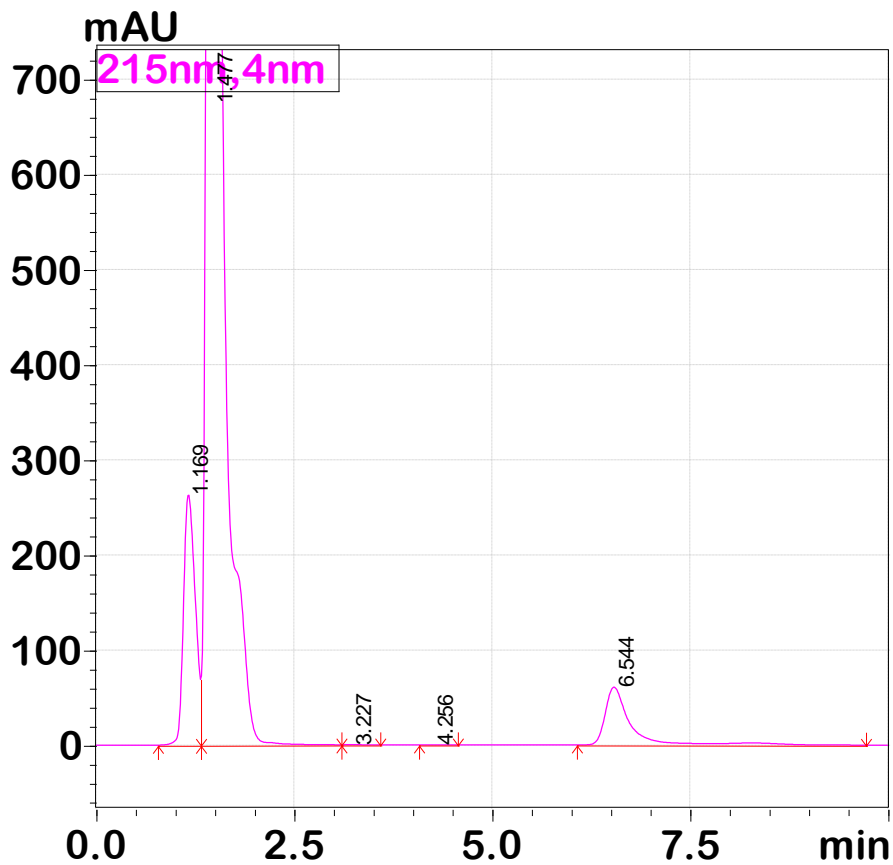


Figure 2-7 Representative chromatogram of the HPLC quantification of 2-aminoheptane

FDAA derivative:

Eluent ACN/H₂O (50/50 isocratic); flow 0.5 mL min⁻¹; temperature 40 °C; injection volume 4 μL; UV detection at $\lambda = 340$ nm. Peak at 9.564 minutes corresponds to the (*R*)-amine, no (*S*)-aminoheptane was detected in the reaction sample, indicating ee% greater than 99%.

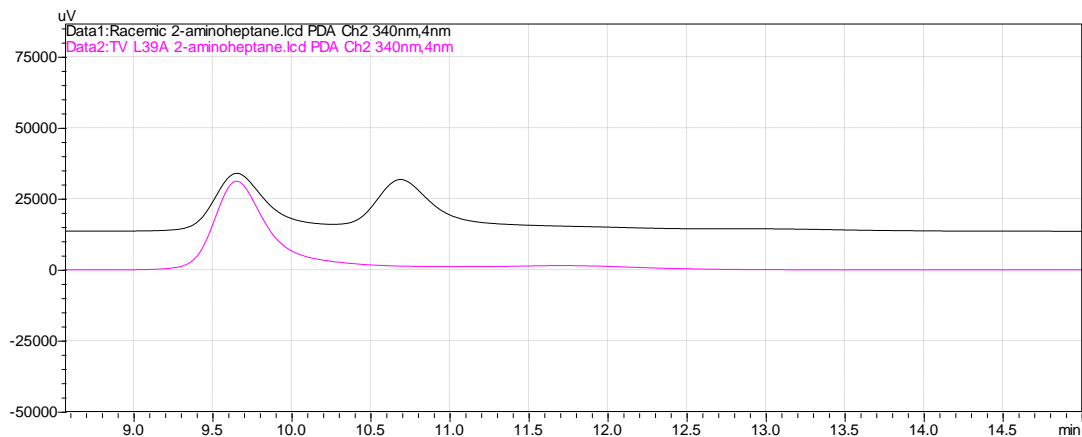


Figure 2-8 Comparison of HPLC chromatograms of 2-aminoheptane derivatized with FDAA. The racemic standard (black) showed two peaks of roughly equal size, while the 2-aminoheptane produced by L-AmDH TV/L39A produced one peak, indicating an ee% greater than 99%.

2.3.11.3 2-aminopentane

BzCl derivative:

Eluent ACN/H₂O (50/50 isocratic); flow 0.5 mL min⁻¹; temperature 29 °C; injection volume 4 μL; UV detection at $\lambda = 215$ nm. Peak at 3.269 minutes was integrated and the peak area of the reaction samples was divided by the peak area obtained from the derivatization of a 10 mM racemic 2-aminopentane standard solution to calculate conversion.

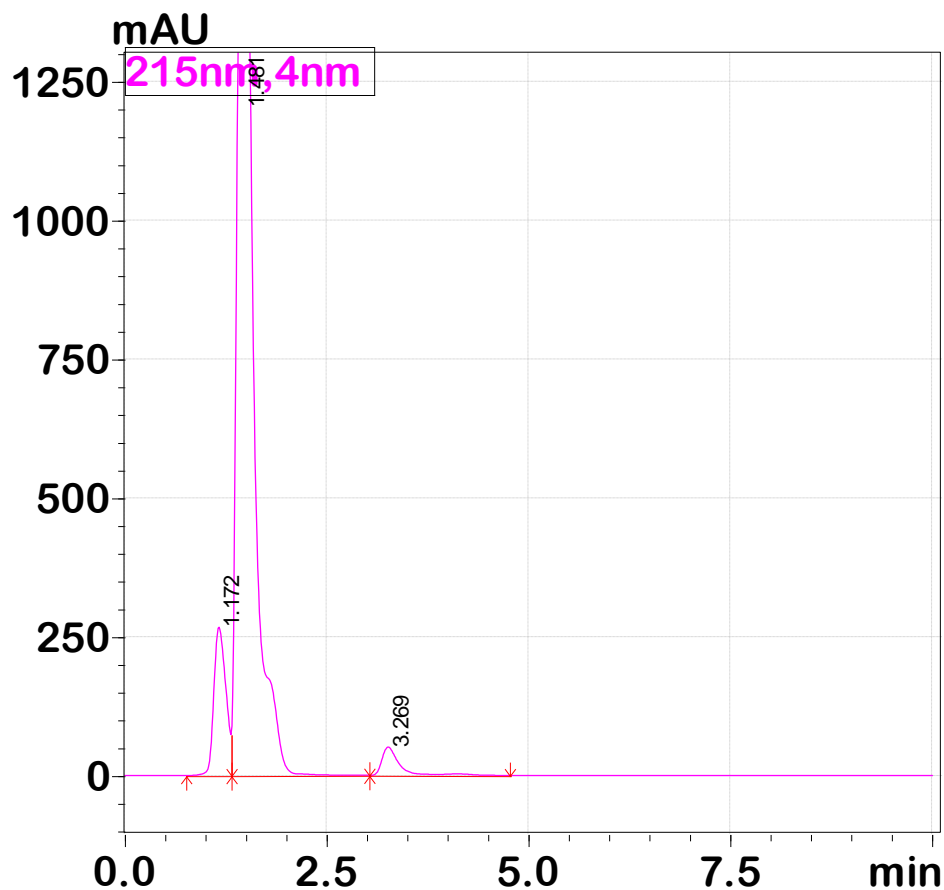


Figure 2-9 Representative chromatogram of the HPLC quantification of 2-aminopentane derivatized with benzoyl chloride

FDAA Derivative:

Eluent ACN/H₂O with a linear gradient (30/70 ratio for 1 minute, then 30/70 to 70/30 in 14 minutes, then hold at 70/30 for 1 minute); flow 0.5 mL min⁻¹; temperature 40 °C; detection at $\lambda = 340$ nm. The (R)- and (S)- enantiomers elute at 11.148 minutes and 11.415 minutes respectively.

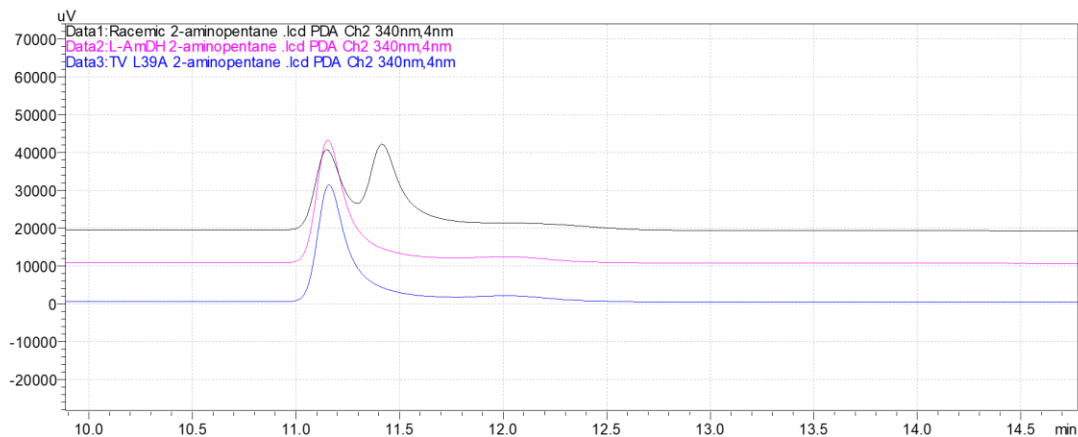


Figure 2-10 Comparison of HPLC chromatograms of 2-aminopentane derivatized with FDAA. The racemic standard (Black) showed two peaks of roughly equal size, while the two samples from 24-hours enzymatic conversions with L-AmDH (pink) and L-AmDH TV/L39A (blue) show just one peak.

2.4 Results

The L-AmDH mutations D32A, F101S, and C290V were generated sequentially using overlap extension PCR, followed by cloning and protein expression. Specific activity toward various aliphatic ketones was measured in 1 mL batch reactions by following the decrease in concentration of NADH with UV-visible spectrophotometry and is recorded in milliunits per milligram of enzyme, with one unit defined as the amount of enzyme required to catalyze the conversion of one micromole of substrate in one minute. The results of these assays are recorded in Table 2-1. Across the six substrates for which activity could be quantified, the combined D32A/F101S/C290V mutant (L-AmDH-TV) showed an average of a 2.5-fold increase in activity compared to the base case enzyme. The largest improvement was seen for 4-methyl-2-pentanone where L-AmDH-TV had 3.4-fold higher activity than the base case. Interestingly, the relative activity of the enzyme toward different substrates did not change due to the mutations, but rather the mutations increased activity for all substrates in roughly equal proportions. Additionally, differential scanning

fluorimetry (DSF) experiments showed the melting point of L-AmDH-TV to be 73.6 °C, an increase of 8.0 °C compared to L-AmDH at 65.6 °C. One possible explanation for the stabilization is the introduction of beneficial intermolecular interactions. Positions D32 and F101 lie at the interface between monomer subunits in the enzyme quaternary structure.

Table 2-1 Activity enhancement of L-AmDH toward aliphatic ketones and the generation of L-AmDH-TV

Substrate	Specific Activity (mU/mg)			
	L-AmDH	D32A	D32A/F101S	D32A/F101S/ C290V ("TV")
1	n.d. ^[a]	n.d.	n.d.	n.d.
2	87.9	61.4	181.7	225.5
3	430.5	888.3	1363.9	1303.6
4	144.8	172.2	278.6	266.4
5	n.d.	n.d.	n.d.	n.d.
6	n.d.	n.d.	n.d.	n.d.
7	n.d.	n.d.	n.d.	n.d.
8	n.d.	n.d.	n.d.	n.d.
9	453.4	945.3	959.2	1146.5
10	531.1	1406.5	1661.4	1808.5
11	549.6	1083.3	1145.1	1056.2

Reaction conditions: 0.4-1.0 μM enzyme, 20 mM substrate, 200 μM NADH, 4M NH₄Cl/NH₄OH, pH 9.6, 25 °C, 1 mL reaction volume. [a] n.d. denotes an activity level below the limit of detection

Sequence alignments of the active sites of multiple amino acid dehydrogenases suggested L-AmDH position L39 as a potential target for expansion of the substrate binding pocket to accommodate larger substrates.¹⁰⁹ Leucine is conserved at this position for leucine dehydrogenases, but a lysine at the homologous position in glutamate dehydrogenases is likely responsible for binding the acid group on the glutamate substrate

sidechain. The residue is positioned with its side chain pointing in toward the substrate binding site. The L-AmDH-TV scaffold presented in the previous section formed the basis for further mutations. L-AmDH-TV/L39A and L39G mutants were produced. Figure 2-11 shows a comparison of specific activities toward straight-chain ketones of varying lengths.

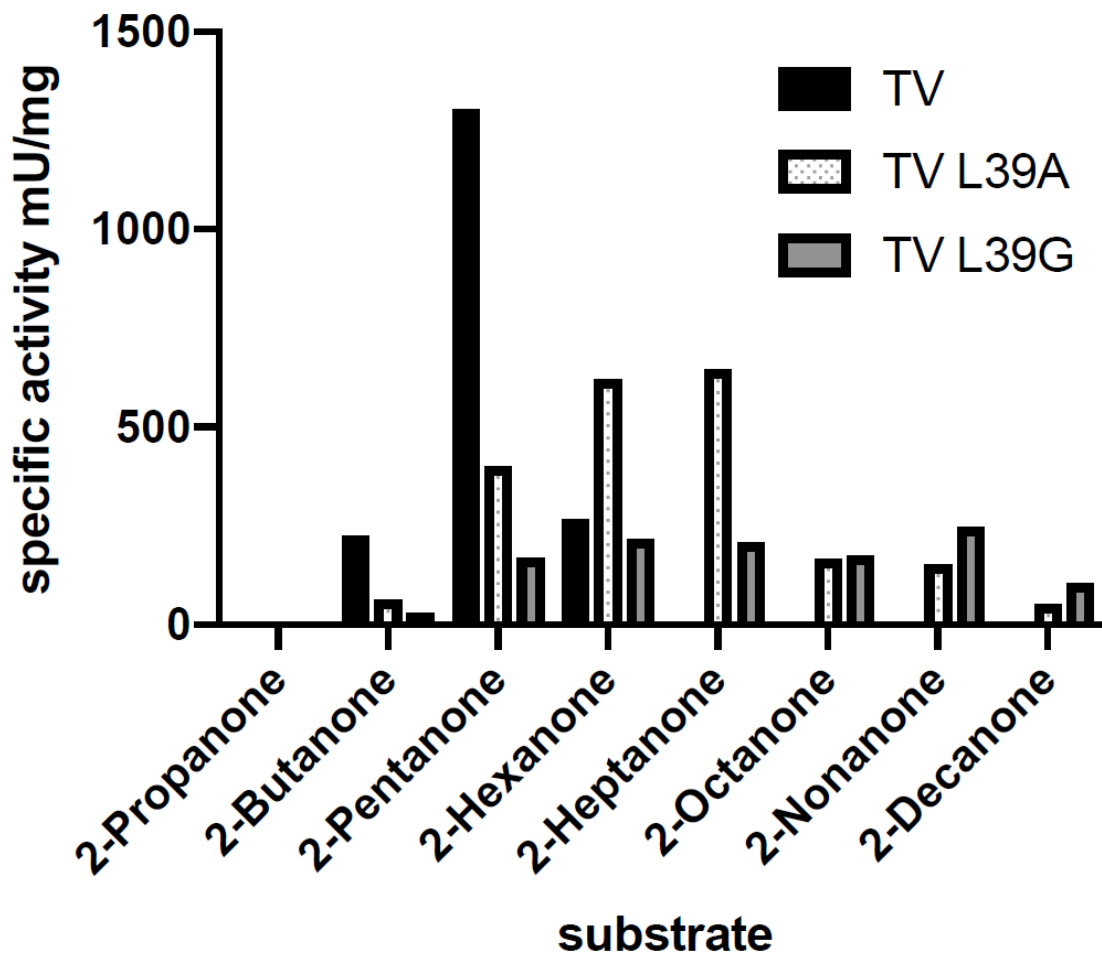


Figure 2-11 Expansion of the L-AmDH binding pocket to accommodate ketones of larger sizes due to mutations at position L39. Reaction conditions: 0.4-1.0 μM enzyme, 20 mM substrate, 200 μM NADH, 4M $\text{NH}_4\text{Cl}/\text{NH}_4\text{OH}$, pH 9.6, 25 $^\circ\text{C}$, 1 mL reaction volume.

For L-AmDH-TV, 2-pentanone shows the highest activity at 1.31 U/mg, while zero activity was observed for ketones longer than 2-hexanone. When the leucine at position L39 is

replaced with the smaller alanine, activity toward 2-butanone and 2-pentanone are greatly reduced, while activity was more than doubled for 2-hexanone. More interestingly, TV/L39A showed activity for ketones as large as 2-decanone, with the highest activity found for 2-heptanone at 644 mU/mg. When the residue was further mutated to glycine, the n-ketone with the highest activity shifted to 2-nonanone. While TV/L39G showed decreased activity for 2-butanone through 2-heptanone, activity was increased compared to TV/L39A for 2-octanone through 2-decanone.

Table 2-2 Effects of A112G and T133G on activity toward n-ketones

Substrate	Specific Activity (mU/mg)				
	TV	TV/ A112G	TV/ A112G/ T133G	TV/ L39A/ A112G	TV/ L39A/ A112G/ T133G
1	n.d. ^[a]	n.d.	n.d.	n.d.	n.d.
2	225.5	n.d.	n.d.	n.d.	n.d.
3	1303.6	80.5	565.1	35.1	19.0
4	266.4	166.6	777.3	308.9	177.7
5	n.d.	31.9	596.9	446.1	431.5
6	n.d.	n.d.	159.2	268.6	237.4
7	n.d.	n.d.	145.9	268.8	171.2
8	n.d.	n.d.	n.d.	140.5	92.9

Reaction conditions: 0.4-1.0 μ M enzyme, 20 mM substrate, 200 μ M NADH, 4M $\text{NH}_4\text{Cl}/\text{NH}_4\text{OH}$, pH 9.6, 25 $^\circ\text{C}$, 1 mL reaction volume. [a] n.d. denotes an activity level below the limit of detection.

Based on results reported for a different set of engineered L-AmDHs,⁸⁰ A112G and T133G were investigated as additional sites for binding pocket expansion. The TV/A112G variant shows new activity for 2-heptanone, and a new optimal substrate length of six carbons rather than five, as was found for TV (Table 2-2). The further addition of T133G

increased activity for 2-pentanone through 2-heptanone, while enabling new activity for 2-octanone and 2-nonanone. Finally, the addition of L39A to TV/A112G and TV/A112G/T133G shifted the optimal substrate length to 7 carbons and enabled activity toward 2-decanone. The addition of T133G to TV/L39A/A112G did not have the same synergistic effects as were found when TV/A112G, suggesting that the benefits of L39A and T133G are not additive.

Table 2-3 Activity of L-AmDH variants toward long branched ketones

Enzyme Variant	Activity Toward 12 (mU/mg)	Activity Toward 13 (mU/mg)
TV	n.d. ^[a]	n.d.
TV/L39A	n.d.	n.d.
TV/L39G	n.d.	39.4
TV/A112G	n.d.	n.d.
TV/A112G/T133G	n.d.	n.d.
TV/L39A/A112G	258.8	186.4
TV/L39A/A112G/T133G	177.9	161.5

Reaction conditions: 0.4-1.0 μ M enzyme, 20 mM substrate, 200 μ M NADH, 4M $\text{NH}_4\text{Cl}/\text{NH}_4\text{OH}$, pH 9.6, 25 $^\circ\text{C}$, 1 mL reaction volume. [a] n.d. denotes an activity level below the limit of detection.

The reported variants were also tested for their ability to convert longer branched ketones, **12** and **13** (Table 2-3). The combination of L39A and A112G allowed for the conversion of these bulky ketones, while each mutation on its own was insufficient. TV/L39G also showed low but measurable activity toward **13** at 39.4 mU/mg. As seen with the straight-chain ketones, T133G does not increase activity for larger substrates when in combination with L39A.

To further demonstrate the improvements to the applicability of L-AmDH to convert larger ketones, selected substrates were converted at a 50 mL preparative scale for

24 hours with both L-AmDH and TV/L39A. As shown in Table 2-4, relative conversion, (measured after derivatization with benzoyl chloride⁷⁷) between the two enzymes was in line with their relative specific activities. Additionally, the already exquisite enantioselectivity of the L-AmDH² was not impacted by the mutations, as measured after diastereomeric derivatization.¹¹⁶ Chromatograms in Figure 2-10 of the derivatized products from L-AmDH and L-AmDH-TV/L39A conversions to 2-aminopentane show no difference in enantioselectivity of the two variants. The lack of a second peak in both reaction samples indicates an ee% greater than 99%. The data shows there are no significant differences from previously reported results on L-AmDH due to the mutations. A racemic standard was used, but it is assumed that the first eluting peak is due to the (R)-amine, as is shown for 2-aminononane. Aggregation occurred in all samples over the course of the reaction and likely limited overall conversion. In the future, this could be mitigated through immobilization.

Table 2-4 Conversion values for preparative-scale reactions

Substrate	Concentration	Conversion after 24 hours	
		L-AmDH	TV/L39A
3	10 mM	65.4 ± 2.2%	48.5 ± 1.6%
5	10 mM	1.7 ± 0.1%	56.3 ± 4.4%
7	2 mM	n.d.	51.9 ± 0.5%

Reaction conditions: 2 mg each of AmDH and cbFDH, 1 mM NAD⁺, ketone concentration as listed, 2M NH₄COOH/NH₄OH, pH 8.5, 21 °C, 50 mL reaction volume, rotating at 20 rpm for 24 hours.

2.5 Conclusion

In conclusion, we found two sets of mutations to improve L-AmDH which result in either increased specific activity and thermodynamic stability, or in an altered substrate

specificity towards longer or branched methylketones. While the first set of mutations acts synergistically to increase L-AmDH activity and stability, the second set of three mutations for change substrate specificity does not. Instead, that second set enables picking a desired specificity trait, such as a long side chain of a methylketone or branched alkylmethylketone, with a specific mutation. Thus, the current work is an important step towards a differentiated family of sufficiently stable amine dehydrogenases.

CHAPTER 3. MECHANISTIC INSIGHT INTO AMINE DEHYDROGENASE KINETICS

The first portion of this chapter (up to and including section 3.5) is adapted from “Engineered amine dehydrogenase exhibits altered kinetic mechanism compared to parent with implications for industrial application”, which was authored by R.D. Franklin *et al.* and published in *Chemical Engineering Journal* in 2019.⁵⁵

3.1 Introduction

Amine Dehydrogenases (AmDHs) were first engineered in 2012² and catalyze the reductive amination of prochiral ketones to chiral amines and the oxidative deamination of primary (*R*)-amines to ketones. Because chiral amines are precursors for numerous active pharmaceutical ingredients (APIs) and enzymes promote intrinsic enantioselective chemistry, a requirement for chiral drug molecules, interest in the biocatalytic production of these amine compounds has been steadily growing for the past decade.^{82, 100, 117} Biocatalytic production of APIs has key advantages over chemical catalysis: operating conditions close to physiological conditions, temperatures below 50° C with pressure commonly at 1 bar, sustainable catalyst production in bacteria, absence of toxic metals, and high enantioselectivity. In addition to engineered AmDHs, wild AmDHs,¹⁰⁶ ω -transaminases,¹¹⁸⁻¹¹⁹ and recently reductive aminases⁵² have proven useful for conversion of ketones to chiral amines.

An AmDH is engineered by mutating two conserved amino acid residues in the active site of an amino acid dehydrogenase (AADH). Starting from the leucine

dehydrogenase (LeuDh) from *Bacillus stearothermophilus*, substituting a serine and leucine at the K68 and N261 positions, respectively, resulted in the leucine amine dehydrogenase (L-AmDH).² More than a dozen different AmDHs have since been generated by applying homologous mutations to AADHs.^{54, 69-70, 103-104} In the balanced reaction for L-AmDH in Figure 3-1, 2-pentanone (Pent) is reductively aminated to form (*R*)-2-aminopentane (AmPent). The reaction for LeuDh, also shown in Figure 3-1, is the reductive amination of ketoleucine (KLeu) to (*S*)-leucine (Leu). For both enzymes the NADH cofactor is oxidized to NAD⁺ through the hydride transfer step.¹¹⁴

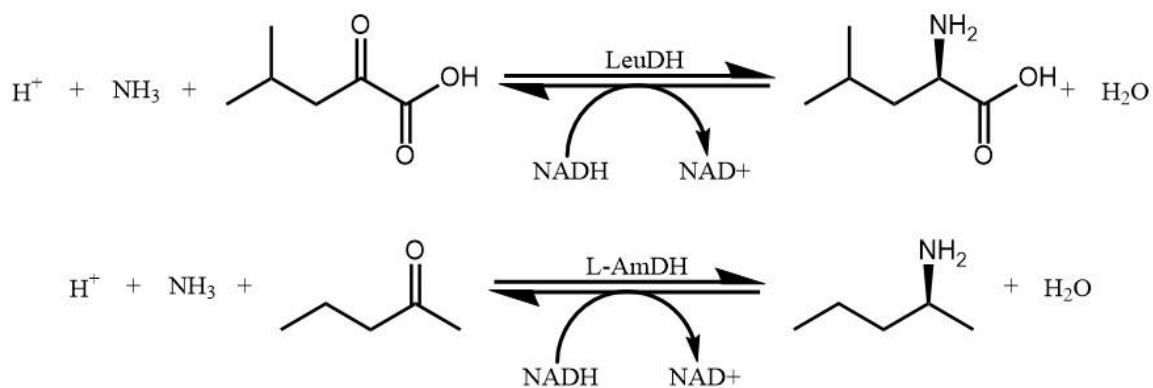


Figure 3-1 Balanced reactions for the leucine dehydrogenase (LeuDh) from *Bacillus stearothermophilus* and the engineered leucine amine dehydrogenase (L-AmDH)

The present work lays the groundwork for reactor engineering, required for proper scaling of synthesis. An enzyme's kinetic mechanism (the order and manner of substrate binding and product release) determines its kinetic rate law. The rate law defines the turnover rate as a function of substrate concentration and is required for the reactor design equations, which are used to determine proper reactor size and to predict yield. We have used the method of initial rates described by Cook and Cleland¹²⁰ to propose rate laws for both the reductive amination and oxidative deamination reactions for L-AmDH and

LeuDH. As their primary sequence differs by only a few amino acid residues, the kinetic mechanism of the engineered L-AmDH was assumed to be the same as its parent. However, the results of the present study surprisingly show that the mechanisms and thus the rate laws of the two enzymes are different.

Often, viscosogens (i.e. small sugars and sugar alcohols) are included in large-scale reaction solutions for enzyme stability and can affect overall enzyme reaction kinetics by way of a kinetic solvent viscosity effect (KSVE).¹²¹ These KSVEs are often the result of either an enzyme conformational change or the rate-limiting diffusion of substrates or products to or from the enzyme. Therefore, the potential impact of these KSVEs on the industrial scale is examined through the addition of viscosogens to small-scale reactions.

3.2 Materials and Methods

3.2.1 Materials Used

L-leucine 99% (Aldrich Chemical Company, Inc, Madison, WI, USA), 4-Methyl-2-oxopentanoic acid sodium salt >98% (Acros Organics, Morris, NJ, USA), 2-aminopentane >98% (Tokyo Chemical Industry, LTD., Tokyo, Japan), 2-pentanone 99% (Alfa Aesar, Tewksbury, MA, USA), sodium chloride 99% (BDH VWR Analytical, Radnor, PA, USA), tris base 99.8% (Fisher BioReagents, Fair Lawn, NJ, USA), ammonium chloride 99.5% (VWR Life Science AMRESCO, Solon, OH, USA), glycine 98.5% (Fisher BioReagents, Fair Lawn, NJ, USA), glycerol 99.9% (Fisher Chemicals, Fair Lawn, NJ, USA), sucrose 99.9% (VWR International, Radnor, PA, USA), NADH disodium salt trihydrate 99.6% (VWR Life Science AMRESCO, Solon, OH, USA), NAD trihydrate >98% (Gold Biotechnology, St Louis, MO, USA), xylitol 99% (Alfa Aesar,

Lancaster, United Kingdom), Overnight ExpressTM Instant TB Medium (Millipore Sigma, Burlington, MA, USA)

3.2.2 Enzyme Expression

Genes encoding leucine dehydrogenase (LeuDH) from *Bacillus stearothermophilus* (EC 1.4.1.9) and leucine amine dehydrogenase (L-AmDH, primary sequence as previously reported²) were codon-optimized for expression in *E. coli*, cloned into the pet28a expression vector, and stored in BL21(DE3) cells. Enzymes were expressed and purified using standard procedures described previously¹⁰⁵ with the modification that Overnight ExpressTM autoinduction media was used for growth. His-tagged enzymes were purified using Ni-NTA resin.

3.2.3 Spectrophotometer Assays

Solutions of the following were prepared: keto-substrate/amino-substrate (0.15 mM – 200 mM), ammonia (125 mM – 4000 mM), enzyme (0.01 μ M – 0.3 μ M); and NAD(H) (12.5 μ M – 1000 μ M). The reaction was initiated by addition of buffer, and the ΔA_{340} was monitored for 30 seconds at 25°C using a Cary 8454 UV-Vis (Agilent Technologies, Santa Clara, CA) equipped with a Quantum Northwest TC 1 Temperature Controller. Cofactor and enzyme solutions were kept on ice, buffer solutions were kept in a thermocycler at 25°C. Cuvettes were prepared with 1% (v/v) cofactor solution and 2% (v/v) enzyme solution with a final volume of 700 μ L. Enzyme and cofactor were placed in the cuvette first, on opposite sides of the cuvette floor to prevent mixing, before the insertion of buffer and final mixing of all three solutions. Test reactions with the lowest substrate concentrations were conducted for 120 seconds ensure linearity over the target experiment

time. If the rate was constant over 120 seconds, then the rate over 30 seconds could be assumed to approximate an initial rate.

3.2.4 Plate Reader Assays

The reaction was initiated by the addition of buffer to droplets of cofactor and enzyme sitting on opposite sides of the well floors, and the ΔA_{340} was monitored for 60 seconds at 25°C using a BioTek Synergy H4 Hybrid Reader (BioTek Instruments Inc., Winooski, VT). Cofactor and enzyme solutions were kept on ice, buffer solutions were kept in a thermocycler at 25°C. Plate wells were prepared with 1% (v/v) cofactor solution and enzyme (0.01 μM – 0.3 μM) solution to a final volume of 200 μL . The reactions were initiated with the addition of buffer solution containing the keto/amine substrate and ammonia to the enzyme and cofactor solutions. Test reactions with the lowest substrate concentrations were conducted for 120 seconds to ensure linearity over the target experiment time. If the rate was constant over 120 seconds, then the rate over 60 seconds could be assumed to approximate an initial rate.

3.2.5 Nonlinear Fitting to Find Rate Equation

For all enzyme assays, plots of initial absorbance vs time data were best fit to linear curves and converted to specific activity using Beer's law ($\epsilon_{340}(\text{NADH}) = 6.22 \text{ mM}^{-1} \text{ cm}^{-1}$) and the enzyme concentration. For all subsequent data analyses these specific activities were fit using the standard nonlinear model fitting function (NonlinearModelFit[]) in Mathematica^{®122} For fitting the general ter- and bi-reactant rate laws, equations 2 and 3 were used.¹²⁰

$$v_0 = \frac{V_{max}[A][B][C]}{Const + Coeff_a[A] + Coeff_b[B] + Coeff_c[C] + K_a[B][C] + K_b[A][C] + K_c[A][B] + [A][B][C]} \quad (2)$$

$$v_0 = \frac{V_{max}[P][Q]}{K_{iq}K_p + K_q[P] + K_p[Q] + [P][Q]} \quad (3)$$

Where v_0 = specific activity, A = NADH, B = 2-pentanone or ketoleucine, C = NH₄Cl, P = 2-aminopentane or leucine, and Q = NAD⁺. Coeff_x terms denotes binary complexes of enzyme and X, while K_x is the Michaelis complex for X and corresponds to complexes with enzyme and all substrates besides X. K_{iq} is the dissociation constant for substrate Q. Terms in the denominators of these equations were excluded from the model if the parameter value was less than zero, or the P-value for the parameter supplied by the fit function was less than 0.05 and their removal did not increase the mean squared error of the fit.

3.2.6 Kinetic Solvent Viscosity Effect Determination

Solvent viscosity was modulated through the addition of glycerol (0% - 30% v/v) to the reaction buffers. Viscosity was measured with a size 50 CANNON-Fenske Routine capillary viscometer in a water bath kept constant at 25 °C with an ANOVA® Precision Cooker. Density was measured with a handheld densitometer (Anton Paar, Graz, Austria). Solutions were prepared and incubated at 25 °C in an orbital shaker for 20 minutes. Assays were conducted using an Agilent Cary 8454 UV-Vis Diode Array System fitted with a temperature-controlled cell holder fixed at 25 °C. Initial rates were best fit to the Michaelis Menten equation. The resulting $^{app}k_{cat}$ and $^{app}k_{cat}/^{app}K_M$ values were normalized by dividing

the value obtained with no added viscogen by the value obtained at a higher viscosity, e.g. $(^{app}k_{cat})_0/(^{app}k_{cat})_\eta$. Viscosity was normalized by dividing the viscosity of the glycerol solution by the viscosity of reaction buffer with no viscogen. Plots of normalized rate constants versus normalized viscosity were fit to equation 4 if the relationship was linear, and equation 5 if the relationship had an inverse hyperbolic shape.¹²¹

$$\frac{(k)_0}{(k)_\eta} = m(\eta_{rel} - 1) + 1 \quad (4)$$

$$\frac{(k)_0}{(k)_\eta} = \frac{1}{1 + A \left[\frac{\eta_{rel} - 1}{(\eta_{rel} - 1) + B} \right]} \quad (5)$$

In equations 4 and 5, k is the rate constant in question, η_{rel} is the relative viscosity, and m , A , and B are parameters which describe the shape of the curve.

3.2.7 Product Inhibition

Initial reaction rates were collected at varying levels of inhibitor and substrate of interest. Other substrates were held at saturating levels whenever possible. The data of each single set of experiments were best fit to either the rate equations for competitive (Equation 6), noncompetitive (Equation 7), or uncompetitive (Equation 8) product inhibition¹²⁰ in Mathematica[®]. Assays were performed at 25 °C, pH 8.5.

$$v_0 = \frac{^{app}k_{cat}E_0[S]}{K_M \left(1 + \frac{[I]}{K_{is}} \right) + S} \quad (6)$$

$$v_0 = \frac{{}^{\text{app}}k_{\text{cat}}E_0[S]}{K_M \left(1 + \frac{[I]}{K_{is}}\right) + [S] \left(1 + \frac{[I]}{K_{ii}}\right)} \quad (7)$$

$$v_0 = \frac{{}^{\text{app}}k_{\text{cat}}E_0[S]}{K_M + [S] \left(1 + \frac{[I]}{K_{ii}}\right)} \quad (8)$$

In the above equations (6, 7, 8), v_0 = reaction rate, ${}^{\text{app}}k_{\text{cat}}$ = the first-order rate constant, E_0 = enzyme concentration, $[S]$ = substrate concentration, K_M = Michaelis constant, $[I]$ = inhibitor concentration, K_{ii} = the inhibition constant for intercept effects, and K_{is} = the inhibition constant for slope effects.

3.3 Results

3.3.1 Global Fit for the Reductive Amination Rate Law

To develop a kinetic rate law for LeuD_H and L-AmD_H, initial rates in the reductive amination direction at varied concentrations of NH₄Cl, keto/keto acid, and NADH were best fit to Equation 2 using the method described by Cleland¹²⁰. Terms in the denominator were omitted from the rate law based on their statistical significance (as defined by the P-value). Results of these fits are shown in Table 3-1. In the global fit for LeuD_H, the constant term and Coeff_b were found to be insignificant (P = 0.486 and 0.763, respectively) and were excluded from the final model. This result implied a lack of both a quaternary complex and binary enzyme-ketoleucine complex in solution. In the amination direction for L-AmD_H, the constant term and Coeff_c term were found to be insignificant (P = 0.561 and 0.395, respectively) and were excluded from the final model. Omission of the constant

term corresponds to the lack of the quaternary complex and the binary enzyme-NH₃ complex in solution.

Table 3-1 Global rate law fit parameters for reductive amination by L-AmDH and LeuDh

Parameter	Units	L-AmDH				LeuDh			
		General Model		Final Model		General Model		Final Model	
		value	P-value	value	P-value	value	P-value	value	P-value
V _{max}	U/mg	14.44 ± 1.958	< 10 ⁻⁵	14.72 ± 1.794	< 10 ⁻⁵	456.5 ± 46.56	< 10 ⁻⁵	467.6 ± 41.3	< 10 ⁻⁵
Const	mM ³	230.6 ± 396.4	0.561	---	---	-8.404 ± 12.07	0.486	---	---
Coeff ₁	mM ²	12850. ± 5675.	0.024	16300. ± 4693.	7.7x10 ⁻⁵	1484. ± 221.4	< 10 ⁻⁵	1407. ± 190.9	< 10 ⁻⁵
Coeff ₂	mM ²	53.85 ± 20.23	0.0079	67.61 ± 17.03	5.4x10 ⁻⁴	4.057 ± 12.06	0.736	---	---
Coeff ₃	mM ²	0.2052 ± 0.241	0.395	---	---	0.0391 ± 0.00954	< 10 ⁻⁵	0.0353 ± 0.00786	< 10 ⁻⁵
K ₁	mM	0.1848 ± 0.0343	< 10 ⁻⁵	0.192 ± 0.0219	< 10 ⁻⁵	0.1179 ± 0.01884	< 10 ⁻⁵	0.123 ± 0.01486	< 10 ⁻⁵
K ₂	mM	59.39 ± 10.71	< 10 ⁻⁵	62.06 ± 9.363	< 10 ⁻⁵	1.487 ± 0.2717	< 10 ⁻⁵	1.577 ± 0.2449	< 10 ⁻⁵
K ₃	mM	7795. ± 1334.	< 10 ⁻⁵	7797. ± 1205.	< 10 ⁻⁵	3803. ± 572.6	< 10 ⁻⁵	3949. ± 487.4	< 10 ⁻⁵
MSE	U/mg	0.0275		0.0275		61.41		61.25	

Fit parameters are the constant terms from (2). A=NADH, B=2-pentanone (L-AmDH)/leucine (LeuDh), C=NH₄Cl. V_{max} is reported in terms of specific activity. Reaction conditions for L-AmDH: 4000, 2000, 1000, 500, 250, and 125 mM NH₄Cl/NH₄OH, 100, 50, 25, 12.5, 6.25, and 3.125 mM 2-pentanone, 0.4, 0.2, 0.1, 0.05, 0.025, and 0.0125 mM NADH. Assays were run at 25 °C in with a constant pH of 8.5 and ionic strength maintained at 4M using NaCl. Reaction conditions for LeuDh: 4000, 2000, 1000, 500, 250, and 125 mM NH₄Cl/NH₄OH, 4, 2, 1, 0.5, 0.25, and 0.125 mM ketoleucine, 0.4, 0.2, 0.1, 0.05, 0.025, and 0.0125mM NADH. Assays were run at 25 °C in with a constant pH of 8.5 and ionic strength maintained at 4M using NaCl. MSE indicates the mean square error of the fit results.

The high values for ^{app}K_{M,NH4} prevented determination of the true value of k_{cat} for either enzyme. The solubility of ammonium chloride in solution was observed to be around 6000 mM, so measurement of enzyme activity at [NH₄Cl] > ^{app}K_{M,NH4} value was not possible. Note also the general trend of smaller ^{app}K_M values in the case of LeuDh when compared to L-AmDH, indicating stronger substrate binding.

3.3.2 Global Fit for the Oxidative Deamination Rate Law

For the deamination of leucine by LeuDh, no terms were excluded from the final model (Table 3-2), which was consistent with a sequential mechanism. For the deamination

of (R)-2-aminopentane by L-AmDH, the constant term was found to be insignificant ($P = 0.637$) and was excluded from the final model. This corresponds to the lack of a ternary complex in solution.

Table 3-2 Global rate law fit parameters for oxidative deamination by L-AmDH and LeuDh

Parameter	Units	L-AmDH				LeuDh			
		General Model		Final Model		General Model		Final Model	
		value	P-Value	value	P-Value	value	P Value	value	P-Value
V_{max}	U/mg	0.7055 ± 0.152	1.4×10^{-4}	0.7605 ± 0.1333	$< 10^{-5}$	0.9488 ± 0.04514	$< 10^{-5}$		
K_{iq}	mM	0.01207 ± 0.02517	0.637	---	---	0.3693 ± 0.09167	9.9×10^{-5}	Unchanged	
K_q	mM	0.4623 ± 0.1437	4.1×10^{-3}	0.5178 ± 0.12	2.7×10^{-4}	0.1474 ± 0.0174	$< 10^{-5}$		
K_p	mM	62.01 ± 20.34	6.1×10^{-3}	70.46 ± 16.05	2.3×10^{-4}	0.4782 ± 0.091	$< 10^{-5}$		
MSE	U/mg	0.000107		0.000104		0.000387			---

Fit parameters are the constant terms from (3). P =leucine (LeuDh)/(R)-2-aminopentane (L-AmDH), and Q = NAD^+ . V_{max} is reported in terms of specific activity. Assays were carried out at 25 °C in 500 mM Tris/HCl buffer at pH 8.5 with a constant ionic strength of 4 M, adjusted with NaCl. Substrate concentrations for LeuDh: 4, 2, 1, 0.5, 0.25, and 0.125 mM leucine, 0.4, 0.2, 0.1, 0.05, 0.025, and 0.0125 mM NAD^+ . Substrate concentrations for L-AmDH: 200, 100, 50, 25, and 12.5 mM 2-aminopentane (racemic), 0.4, 0.2, 0.1, 0.05, 0.025 mM NAD^+ . MSE indicates the mean square error of the fit results.

3.3.3 First- and Second-Order Rate Constants

The first- and second-order rate constants for both enzymes are listed in Table 3-3. For deamination, both enzymes had similar $^{app}k_{cat}$ values. However, the maximum amination rate for L-AmDH was 30-fold lower than the value for LeuDh. The $^{app}k_{cat}/K_{M,NH_4}$ and $^{app}k_{cat}/K_{M,NADH}$ values both were 50-fold higher in LeuDh than L-AmDH,

Table 3-3 Comparison of first and second order rate constants between L-AmDH and LeuDh

Reaction Direction	Substrate	LeuDh		L-AmDH	
		$^{app}k_{cat}$ s ⁻¹	$^{app}k_{cat}/K_M$ M ⁻¹ s ⁻¹	$^{app}k_{cat}$ s ⁻¹	$^{app}k_{cat}/K_M$ M ⁻¹ s ⁻¹
Amination	ketoleucine		2.10×10^5	2-pentanone	1.68×10^2
	NADH	331.9	2.82×10^6	NADH	10.45
	NH ₄ Cl		84.0	NH ₄ Cl	1.34
Deamination	leucine		1.41×10^3	2-aminopentane	8.71
	NAD^+	0.673	4.58×10^3	NAD^+	1.04×10^3

however, the $^{app}k_{cat}/K_{M,keto}$ value was 1000-fold higher for ketoleucine than for 2-pentanone. In the deamination direction, the $^{app}k_{cat}/K_{M,NAD}$ was the same across both enzymes, while the $^{app}k_{cat}/K_{M,Leu}$ again was almost 3 orders of magnitude larger than $^{app}k_{cat}/K_{M,AmPent}$. These results countered the hypothesis that weak ammonia binding was the greatest driver of decreased enzyme activity; instead, the binding of the keto substrate had the greatest effect.

3.3.4 Product Inhibition

Product inhibition studies were conducted in the reductive amination direction to elucidate the binding order of the cofactor and keto substrates. For LeuDh, leucine was found to be uncompetitively inhibitive to NADH; for L-AmDH, 2-aminopentane noncompetitively inhibited NADH. Aside from that distinction, the inhibition profiles of the two enzymes are the same. Competitive inhibition of NAD^+ on NADH was found for both enzymes. Additionally, the amino product for both enzymes was found to be a competitive inhibitor for the keto substrate. The inhibition ratios (K_M/K_I) for the L-AmDH-catalyzed reaction (Table 3-4) showed a decrease in reaction efficiency when compared to LeuDh. The inhibition ratio describes the ratio of the amount of substrate needed to saturate the enzyme versus the amount of product which becomes strongly inhibitory; at higher values, less product per enzyme per unit time can be produced. Product inhibition by both the cofactor and amino products was stronger for the engineered enzyme. For experiments with 2-aminopentane, only a racemic mixture was available. For the results in Table 3-4, it was assumed that (*S*)-2-aminopentane did not interact with the enzyme. If (*S*)-2-aminopentane is not inert, the real $K_{I,AmPent}$ would be higher, leading to a smaller inhibition ratio.

Table 3-4 Summary of product inhibition patterns for LeuDh and L-AmDH

Enzyme	Varied substrate	^{app} K_M mM	Product Inhibitor	Inhibition Type	K_{is} mM	K_{ii} mM	K_M/K_I
L-AmDH	NADH	0.0594	NAD ⁺	C	0.0669	---	0.888
			(<i>R</i>)-2-aminopentane	NC	30.18	15.05	
	2-pentanone	16.904	NAD ⁺	NC	0.498	0.422	
			(<i>R</i>)-2-aminopentane	C	9.713	---	1.740
LeuDh	NADH	0.205	NAD ⁺	C	1.11	---	0.185
			leucine	UC	---	13.55	
	ketoleucine	0.878	NAD ⁺	NC	5.343	2.328	
			leucine	C	18.74	---	0.047

C=competitive inhibition, NC=noncompetitive inhibition, UC=uncompetitive inhibition. Inhibition constants correspond to the constant parameters in Equations (6), (7), and (8). The inhibition ratio (K_M/K_I) is reported in cases where competitive inhibition was observed.

3.3.5 Kinetic Solvent Viscosity Effects

Glycerol was included to increase buffer viscosity and the resulting effects on k_{cat} and k_{cat}/K_M were observed to determine the differences, if any, in the dependence of the rate-limiting steps of L-AmDH and LeuDh on diffusion. For LeuDh-catalyzed deamination, $^{app}k_{cat}/K_{M,Leu}$ increased with viscosity in an inverse hyperbolic pattern, while the k_{cat} value was not dependent on viscosity (Figure 3-2B). For amination of ketoleucine by LeuDh, the $k_{cat}/K_{M,KLeu}$ again exhibited an inverse hyperbolic KSVE and overall turnover was mostly limited by diffusion, with a slope of 0.7 (Figure 3-2A). For amination with L-AmDH, the $^{app}k_{cat}/K_{M,AmPent}$ value was not viscosity dependent but the $^{app}k_{cat}$ value was (Figure 3-2C). In the deamination direction, the k_{cat}/K_M value was viscosity dependent with a slope of 0.76 and the k_{cat} value was not viscosity dependent (Figure 3-2D), a reversal of the KSVE on k_{cat}/K_M compared to LeuDh. The KSVEs on LeuDh catalysis suggested that a diffusion-dependent conformational change was required for turnover but did not limit the overall rate. A similar conformational change for L-AmDH was not indicated.

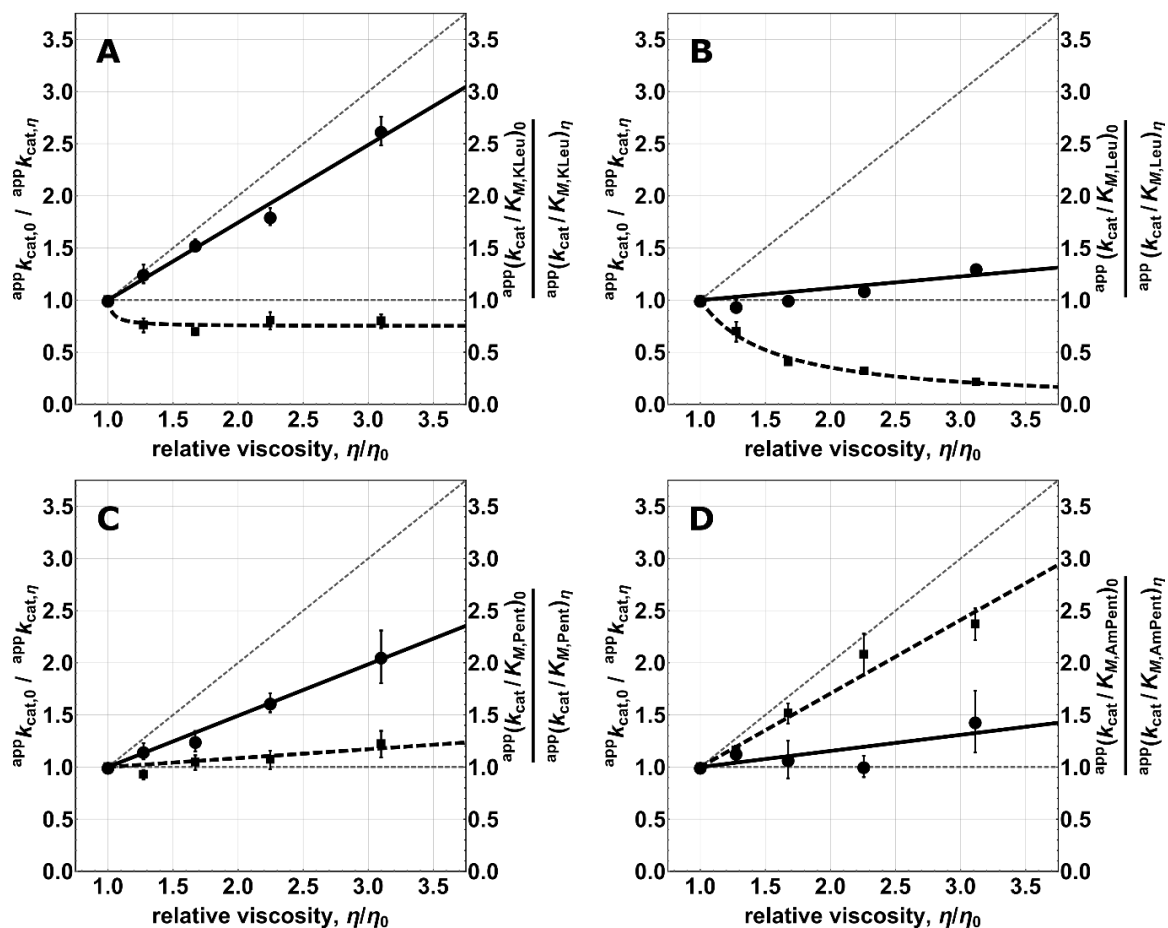


Figure 3-2 Kinetic Solvent Viscosity Effects on L-AmDH and LeuDh. Normalized reaction rate constants versus normalized viscosity. Dashed gray lines with slope = 1 represents complete diffusion control. Dashed gray lines with slope = 0 represents no impact of diffusion. Circles and solid lines represent effect on appkcat. Squares and dashed lines represent effect on appkcat/KM for the indicated substrate. For all experiments, glycerol concentrations used were 0%, 7.5%, 15%, 22.5%, and 30% V/V with temperature fixed at 25 °C. Individual conditions: A) amination of ketoleucine. 4.8, 2.4, 1.2, 0.6, 0.3, 0.15, and 0.075 mM ketoleucine, 2.4 M NH₄Cl, 200 μM NADH, pH 8.5. B) deamination of leucine. 20, 10, 5, 2.5, 1.25, 0.625 mM leucine, 200 μM NAD⁺, 500 mM glycine buffer, pH 9.5. C) amination of 2-pentanone. 100, 50, 25, 12.5, 6.25, 3.125 mM pentanone, 2.4 M NH₄Cl, 200 μM NADH, pH 8.5. D) deamination of (R)-2-aminopentane. 200, 100, 50, 25, 12.5, 6.25 mM 2-aminopentane (racemic), 200 μM NAD⁺, 500 glycine buffer, pH 9.5.

3.4 Discussion

The differences in the kinetic properties of L-AmDH and LeuDh presented herein reflect a different kinetic mechanism. When compared to its parent enzyme, L-AmDH

displayed a different substrate binding order, lower affinity for the keto substrate, and stronger product inhibition. The two key residues which must be mutated to produce an AmDH from an amino acid dehydrogenase (K68 and N261 for L-AmDH) form hydrogen bonds with the acid group on the substrate.² The mutations to serine and leucine, respectively, permit the binding of methyl ketones but with lower affinity compared to keto acids (Table 3-1). The second-order rate constants for pentanone and 2-aminopentane are both three orders of magnitude lower than those for leucine and ketoleucine. Additionally, solvent viscosity effects demonstrated that an isomerization of the enzyme-substrate complex, important for LeuDh catalysis, was not observed for L-AmDH, likely owing to a change in rate-limiting step from LeuDh to L-AmDH functionality.

Poor NH₃ binding was previously hypothesized to cause the 30-fold decrease in activity between L-AmDH and LeuDh.¹²³ However, at reaction conditions relevant for large-scale synthesis, i.e. high concentrations of all substrates and pH value of 8.5, the K_{M,NH_4} values for LeuDh and L-AmDH are much closer than had been expected based on reports at pH ~9.6, where K_{M,NH_4} values of < 300 mM were reported for LeuDhs.¹²⁴⁻¹²⁶ Since the calculated K_{M,NH_4} value for each enzyme was near the solubility limit of NH₄Cl of ~6 M, saturating conditions for NH₄Cl substrate could not be realized. The large K_{M,NH_4} values paired with the lack of a constant kinetic term for LeuDh or L-AmDH suggests that ammonia in neutral or ionic form (NH₃ or NH₄⁺) does not bind to the enzyme at all, but rather that free ammonia attacks the bound ketone or keto-acid directly, as previously proposed for PheDH¹²⁷ and glutamate dehydrogenase (GluDH).¹²⁸

The pH value of 8.5 was chosen for the present study to match the pH value for large-scale synthesis, where a cofactor regeneration enzyme must be employed to

economize cofactor use and to drive high conversion. The most common of these regeneration enzymes are formate dehydrogenase (FDH), with a pH optimum around pH 7.5,¹²⁹ and glucose dehydrogenase (GDH), with a pH optimum of 8.5.¹³⁰ Additionally, L-AmDH and FDH are destabilized at higher pH values (unpublished data). Both L-AmDH and LeuDh have lower activity at pH 8.5 than at pH 9.6, the most common pH value for conversions with AmDHs.^{80, 103-104} The pH optima of ketoleucine amination and leucine deamination for LeuDh are at pH 9.5 and pH 11, respectively.¹³¹ The pKa value for ammonium at ionic strength of 4 M is around pH 9.7,¹³²⁻¹³³ so at pH 8.5 the protonated form (NH_4^+) dominates, which contributes to the high values of K_{M,NH_4} . A standard ionic strength of 4 M, (equal to the maximum NH_4Cl concentration used), was maintained for

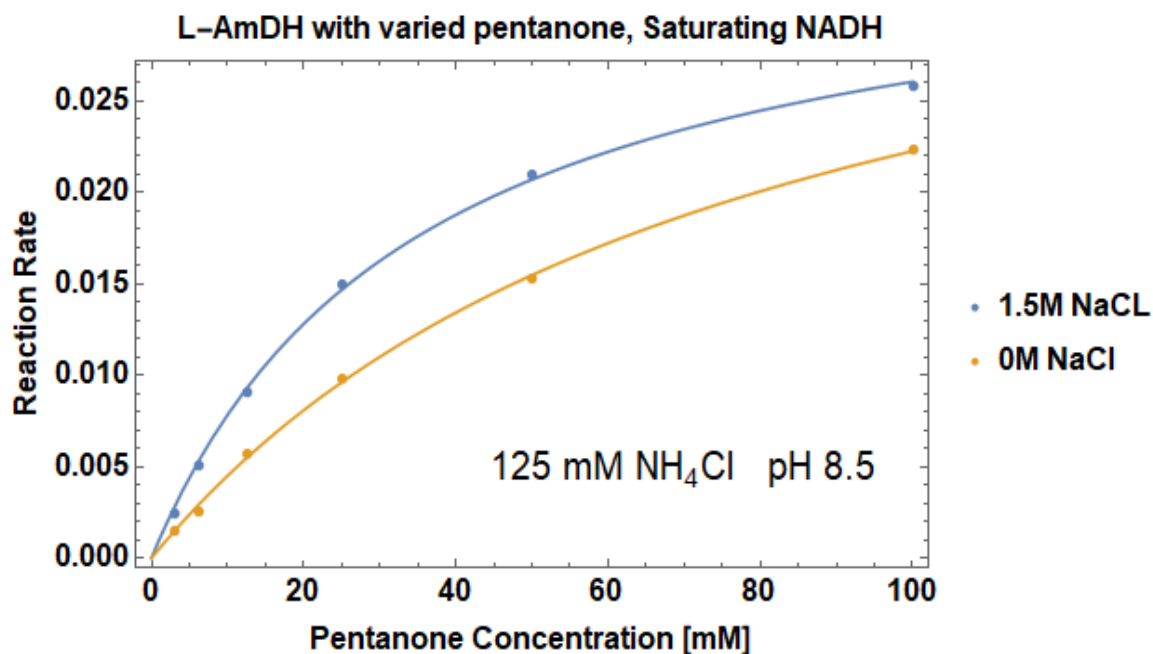


Figure 3-3 Effect of increasing ionic strength on the kinetic parameters for reductive amination of 2-pentanone by L-AmDH.

both amination and deamination, as a change of 1.5 M ionic strength can double/half the $K_{M,keto}$ value (see Figure 3-3)

The results for the kinetic mechanism of LeuDH are consistent with previously reported data, except for the observed competitive inhibition by leucine on ketoleucine (Table 3-4). For reductive amination, there is wide agreement for a strictly ordered sequential mechanism of substrate binding, though the exact order has not been consistent. There is broad agreement that NAD(P)H binds first, supported by the observation of competitive inhibition between $NAD(P)^+$ and NAD(P)H, indicating both forms of the cofactor can bind to free enzyme. For LeuDH^{124-126, 134}, AlaDH¹³⁵⁻¹³⁶, and PheDH^{114, 137-138}, previous studies have indicated that ammonia binds either second or third. Other than the lack of the constant term in the reductive amination direction (Table 3-1), the fitted rate laws for LeuDH in both directions are consistent with an ordered sequential mechanism in which NADH binds first, followed by ketoleucine, and then ammonia. This binding order is consistent with the lack of a [B] term in the denominator of the rate equation, i.e. absence of an enzyme-ketoleucine complex, and has been proposed for other leucine dehydrogenases.^{126, 134}

For reductive amination by L-AmDH, the term related to the enzyme-ammonia complex is excluded rather than the enzyme-pentanone term (Table 3-1). If this were an ordered mechanism, this would imply ammonia binds second, after NADH and before 2-pentanone. However, a large K_{M,NH_4} value renders ammonia binding to the enzyme itself unlikely. More likely, the mechanism calls for ordered addition of ammonia after 2-pentanone, whereas NADH and 2-pentanone bind randomly. Product inhibition patterns (Table 3-4) gave further insight into substrate binding order for LeuDH and L-AmDH. For

L-AmDH, competitive inhibition observed for NAD^+ on NADH is consistent with previous observations for other amino acid dehydrogenases.^{114, 124, 139} However, competitive inhibition observed by 2-aminopentane on 2-pentanone at both half and full saturation of NADH has not been reported previously for amino acid dehydrogenases and indicates random binding of NADH and 2-pentanone. Additionally, the presence of noncompetitive inhibition by NAD^+ on 2-pentanone and 2-aminopentane on NADH suggests the presence of dead-end complexes of enzyme-NADH-aminopentane and enzyme- NAD^+ -pentanone. Because an uncompetitive inhibitor cannot bind to the free enzyme, the lack of uncompetitive inhibition by 2-aminopentane on NADH at saturated 2-pentanone in the reductive amination direction rules out a kinetic mechanism where the cofactor must bind first.¹⁴⁰ For LeuDh, an ordered sequential mechanism was expected based on the literature^{124-126, 134}. For a strictly ordered mechanism, uncompetitive inhibition is expected for all pairs listed in Table 3-4 except for NAD^+ versus NADH, as observed for the LeuDh from *Bacillus sphaericus*.¹²⁴ Instead, we see competitive inhibition for leucine versus ketoleucine and noncompetitive inhibition for leucine versus NADH, which indicates that cofactor binding is not necessarily required for leucine binding.

L-AmDH and parent LeuDh differed in response to increasing solution viscosity, indicating a change in the rate-limiting steps of catalysis. For LeuDh, both the amination and deamination directions showed an inverse hyperbolic viscosity effect on normalized $^{\text{app}}k_{\text{cat}}/K_{\text{M}}$ value for the amino/amino acid substrate. An inverse hyperbolic KSVE indicates that an isomerization of the enzyme-substrate or enzyme-product complex contributes to catalysis.¹²¹ The k_{cat} value encompasses all first-order rate constants in the reaction while the $k_{\text{cat}}/K_{\text{M}}$ value reflects all kinetic steps starting from binding of the substrate to the first

irreversible step. If the effects on the k_{cat} and $k_{\text{cat}}/K_{\text{M}}$ values were the same, then the rate-determining step would occur between substrate binding and the first irreversible step.¹²⁰ However, because the KSVEs were different, k_{cat} reflects a step that occurs after the first irreversible step (likely the product release step). Because the effect on $^{\text{app}}k_{\text{cat}}/K_{\text{M}}$ was hyperbolic rather than linear, diffusion effects limiting substrate capture are ruled out.¹⁴¹ A similar hyperbolic KSVE pattern was seen for the deamination of D-histidine by D-arginine dehydrogenase.¹⁴² Recently, a conformational change upon binding of NADPH and α -ketoglutarate by the GluDH from *Aspergillus niger* (*An*-GluDH) was demonstrated through x-ray crystallography.¹⁴³ LeuDH and L-AmDH have a similar clamshell-like structure to *An*-GluDH, with two domains connected by a hinge region. The active site lies in the cleft between the two domains. Residues on both sides of the cleft have been identified as being important for either substrate binding or catalysis.^{114, 127} Upon binding of the substrate and cofactor, the two halves of *An*-GluDH move closer together by as much as 15 Å. Likely, the equilibrium relationship between open and closed conformations of LeuDH is perturbed by an increase in viscosity and favors the closed conformation and thus the formation of products.¹⁴⁴

For LeuDH, a normal viscosity effect on the $^{\text{app}}k_{\text{cat}}$ value was shown for reductive amination, meaning that increasing solvent viscosity decreases the overall turnover rate at substrate saturation. This effect indicates that overall turnover is partially limited by product release.¹²¹ The diffusion dependence is much stronger for reductive amination than for oxidative deamination. In the amination direction, a strong viscosity limitation on product release was not surprising given the large $^{\text{app}}k_{\text{cat}}$ value of 330 s^{-1} , as other enzymes with similar k_{cat} values show similar results.¹⁴⁵⁻¹⁴⁷ In the deamination direction at pH 9.5,

the $^{app}k_{cat}$ value is 20 s^{-1} (data not shown); as a result, the viscosity effect in this direction is weaker. Interestingly, an inverse hyperbolic effect on the $^{app}k_{cat}/K_{M,AmPent}$ value was not observed for L-AmDH. Instead, a strong normal viscosity effect with slope of 0.75 was seen, despite the low $^{app}k_{cat}/K_{M,AmPent}$ value of $8.7 \text{ M}^{-1} \text{ s}^{-1}$. This effect is the opposite of what was seen for the reductive amination direction and demonstrates that a viscosity effect drives an increase in concentration of the Michaelis complex in both directions. A decreased $^{app}k_{cat}/K_{M,AmPent}$ in the deamination direction indicates slow substrate release while a decreasing $^{app}k_{cat}$ in the amination direction suggests slow product release; viscosity is likely affecting the same common step in each reaction direction as the substrate for the deamination direction is the product for the amination direction.

The results described in the present study confirm key restrictions on reaction conditions which must be considered to maximize reactor productivity. Increased viscosity should be avoided for the amination of ketones by L-AmDH, as a 4-fold increase in viscosity can lower the reaction rate by as much as 50% at saturating ketone concentration (Figure 2C). In a reactor setting, detrimental and beneficial KSVEs may be realized through the deliberate addition of glycerol to stabilize the biocatalyst¹⁴⁸ and unintentionally through the introduction of kosmotropic anions such as formate or sulfate.¹⁴⁹⁻¹⁵⁰ As a result, engineers must optimize processes to balance stability and catalytic efficiency based on relative costs of catalyst and products. Additionally, it is important to avoid the strong product inhibition seen for L-AmDH to optimize amine production, especially, as competitive inhibition by 2-aminopentane on the already slow-binding 2-pentanone increases with conversion. Inhibition by NAD^+ can be avoided by employing a large amount of the cofactor regeneration enzyme, which lowers $[\text{NAD}^+]$.

3.5 Conclusion

Through initial rate, product inhibition, and KSVE experiments, we have demonstrated key differences between the kinetic mechanisms of L-AmDH and its parent enzyme, LeuDH. The 40-fold decrease in the $^{app}k_{cat}$ value between the two enzymes can largely be explained by the much lower affinity for the ketone or amine substrate rather than affinity for ammonia. Kinetic viscosity effects elucidated the importance of an isomerization of the Michaelis complex for determining the rate of LeuDH catalysis, but the rate-limiting step is shifted for L-AmDH. A change in substrate binding order between the two enzymes was indicated by the differences in the fitted rate laws and inhibition patterns. An understanding of the kinetic properties of L-AmDH will enable its use in the biocatalytic production of chiral amines and is a required input for reactor design and scale-up.

CHAPTER 4. THE JOURNEY TOWARD CONTINUOUS MANUFACTURING OF CHIRAL AMINES

4.1 Motivation and Introduction

Of the four Aims which were initially set out for this thesis, continuous manufacturing of chiral amines with AmDHs was the most important. By 2016, the AmDH project in the Bommarius lab was already ten years old, with three previous graduate students and one lab manager involved in creating and improving the enzymes.^{2, 69, 103, 105, 123, 151-152} Given the engineering background of the Bommarius group, it was important to move the use of AmDHs from cuvettes and test tubes into a scalable process which could produce tangible amounts of product. The primary deliverable of the entire thesis project from day one was a vial containing at least one gram of a pure (*R*)-amine. While CHAPTER 5 presents the successful implementation of a continuous AmDH process, it does not tell most of the story of how we got there. CHAPTER 4 will give an overview of the ideas which were tried along the way but were ultimately not successful. As such, it will have a different format and style compared to the other chapters which surround it.

4.2 The Enzyme Membrane Reactor

4.2.1 Overview and Initial Setup

The first attempt at continuous amine production utilized an enzyme membrane reactor (EMR), which was a 10 mL continuously stirred tank and would convert ketones to amines using soluble AmDH and FDH. The reactor was jacketed and fully watertight and was topped with a 10 kDa ultrafiltration membrane to retain the soluble enzymes while

allowing substrates and products to pass through freely. Because the products of AmDHs are chiral and the reactants achiral (except for the negligible concentration of NAD^+/NADH), the plan was to measure conversion in the reactor continuously with a polarimeter equipped with a jacketed flow cell (Autopol® III, Rudolph Research Analytical, Hackettstown, NJ, USA). Temperature in the reactor and the polarimeter cell were controlled separately with circulating water baths. The enzyme membrane reactor used for AmDH catalysis was originally commissioned by the Bommarius lab for a study helmed by Dr. Thomas Rogers which sought to understand the thermal deactivation of TEM-1 β -Lactamase in a continuous, non-isothermal assay.¹⁵³ The system worked quite well for Rogers, and was used again in the lab for a similar study by McDonald *et al.* in 2018.¹⁵⁴

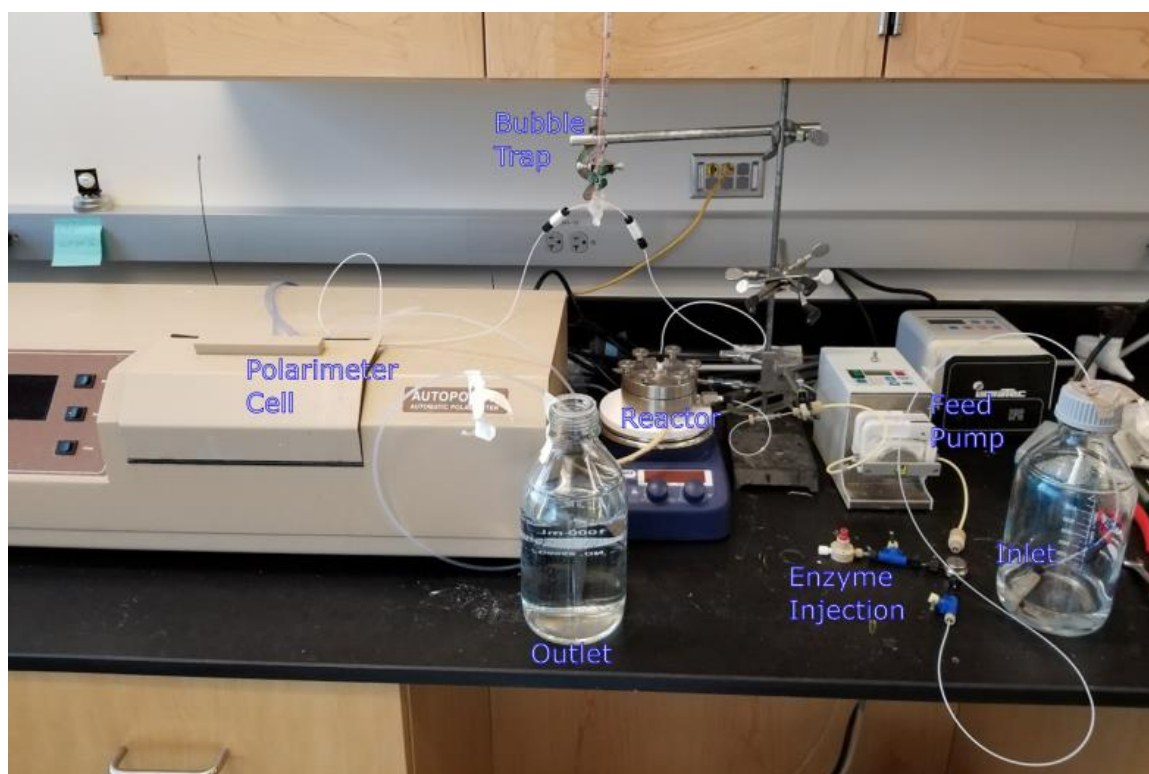


Figure 4-1 Photo of the continuous enzyme membrane reactor setup

4.2.2 *Results and Challenges*

The continuous flow reaction system was set up as pictured in Figure 4-1. Conversion of multiple substrates (methyl-isobutyl ketone and acetophenone) with both L-AmDH and cFL1-AmDH was attempted with formate dehydrogenase for cofactor regeneration. Very slight changes in optical rotation were seen over time, but they were barely above the limit of detection of the polarimeter. For the previous work in the group with polarimetry, the molecules being studied were β -lactam antibiotics, which have specific optical rotation values that are between one and two orders of magnitude higher than those for any of the amines that the AmDHs can produce. The lack of sensitivity of the polarimeter toward detecting the amines produced in the reaction meant that polarimetry could not be used to measure conversion moving forward.

Ultimately, the use of the EMR was abandoned due to stability problems with the amine dehydrogenases. Both AmDHs used in the study are not stable enough to be used continuously in solution overnight and tend to aggregate. Multiple days of operation were desired for a truly continuous process, the aggregation problem ended up being serious enough that other options were needed.

4.3 Immobilization Onto Immo beads in a Packed Bed Reactor

4.3.1 *Rationale*

After the failure of the initial experiments with the EMR, it was clear that immobilization would be necessary to prevent aggregation and subsequent deactivation of the enzymes. The EMR is unsuitable for biocatalysts immobilized onto solid supports

because the action of the magnetic stir bar will grind any porous polymer over time and eventually deactivate the catalyst. As a result, a new platform for immobilizing the enzymes onto macroporous beads and subsequently packing into a tubular reactor was explored. In February of 2019, a screening kit containing twelve different macroporous resins marketed especially for enzyme immobilization called Immobeads® was acquired (Chiralvision B.V., Den Hoorn, the Netherlands). The types of binding chemistries offered in the kit are shown in Figure 4-2. Three of the beads use covalent immobilization via ring opening reactions between epoxide groups on the bead surface and lysine residues on the protein surface. A further four beads use adsorption interactions, including polar and nonpolar adsorption. The final five resins are ion exchange resins, which include one cation exchange and four amine anion exchange resins with primary, secondary, tertiary amine and a quaternary ammonium options. Depending on the protein of interest and its surface chemistry, different binding chemistries would be most effective at binding and retaining enzyme. As such, it was useful to try a wide range of options, rather than assuming a single chemistry would work. Importantly, all of the resins in the kit bind nonspecifically, so it is important to purify proteins prior to immobilization.

4.3.2 Initial Immobilization Screening

The immobilization procedure for all 12 beads in the kit is straightforward: purified protein at a known concentration is incubated with a defined mass of the beads overnight without shaking at 4 °C. Following the incubation time, the beads are filtered, and washed with water to remove traces of unbound enzyme. Afterward, the beads are ready to be screened for activity. The degree of binding to the beads can be quantified by measuring

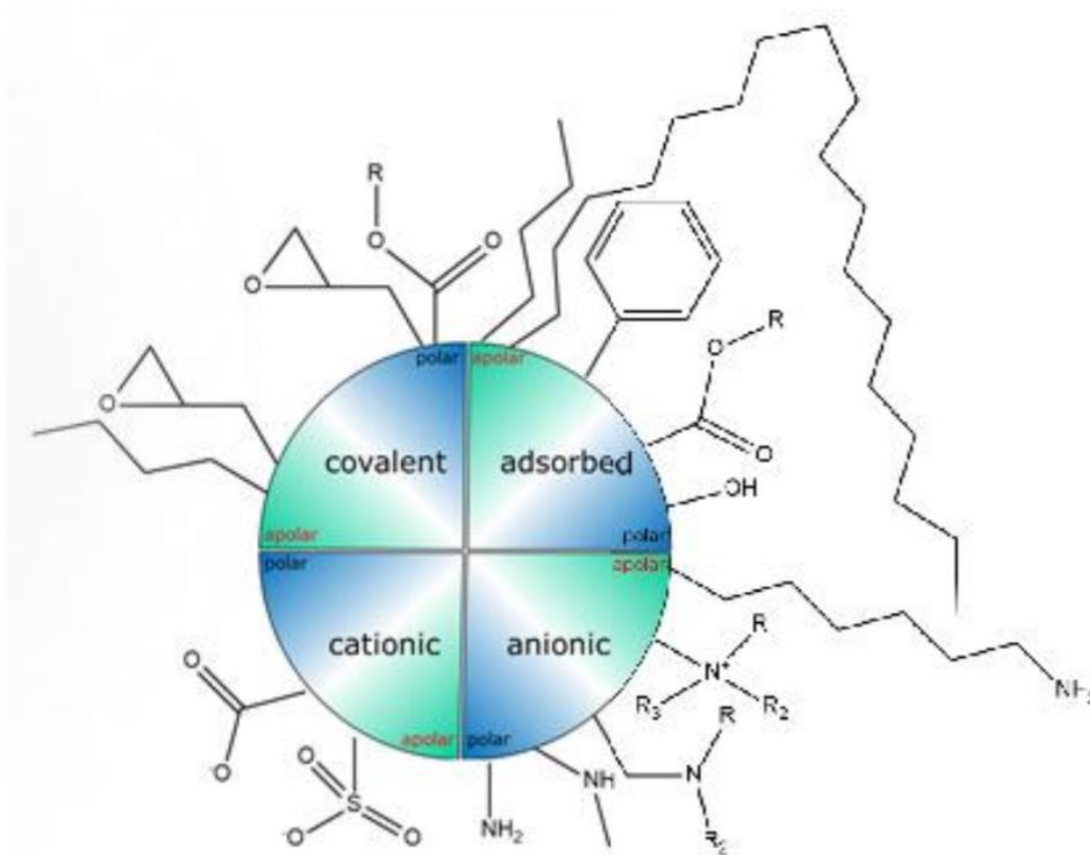


Figure 4-2 Promotional image from ChiralVision outlining their available enzyme binding chemistries

the concentration of protein in the supernatant after filtering and comparing to the concentration of enzyme in solution prior to immobilization. Immobilization of both cFL1-AmDH¹⁰³ and the formate dehydrogenase from *Candida boidinii* (FDH) were screened

against all twelve bead types, to assess their binding and immobilized activity, the results can be seen in Table 4-1. The degree of binding is defined as the residual enzyme concentration after binding divided by the initial enzyme concentration.

Table 4-1 Degree of binding of cFL1-AmDH and FDH to various enzyme immobilization beads

Bead Name	Binding mode	Functional Group	Degree of Binding	
			cFL1-AmDH	FDH
covalent 1	apolar	epoxide/butyl	< 96%	< 92%
covalent 2	polar	epoxide	< 96%	< 92%
covalent 3	polar	epoxide	< 96%	87.9%
adsorption 1	apolar	phenyl	78.9%	80.7%
adsorption 2	apolar	carboxylic ester	94.3%	< 92%
adsorption 3	apolar	octadecyl	< 96%	< 92%
adsorption 4	polar	styrene/methyl	71.3%	76.7%
cationic 1	strong	sulphonic	31.6%	34.4%
anionic 1	apolar	primary amine	< 96%	< 92%
anionic 2	weak	tertiary amine	82.7%	68.5%
anionic 3	weak	quaternary ammonia	88.3%	52.7%
anionic 4	strong	quaternary ammonia	84.8%	47.2%

For the binding screen shown in Table 4-1, the initial concentrations of cFL1-AmDH and FDH were 2.42 mg/mL and 1.24 mg/mL, respectively as measured by the Bradford Assay.¹¹⁵ The limit of detection of the Bradford assay kit used for this study is about 0.1 mg/mL, which is why quantification of binding efficiency was limited to a range above a certain percentage. Of the twelve beads in the kit, only five showed complete binding of both enzymes, this group included two of the covalent beads, two adsorption beads, and one anionic exchange bead.

After the binding screen, the immobilized enzymes were screened for activity by flowing a solution containing reaction substrates through a gravity flow column containing the beads and measuring absorbance before and after. For AmDH, activity toward 50 mM 2-hexanone with 200 μ M NADH in 1M NH_4COOH pH 8.5 was measured and for FDH the reaction contained 400 μ M in 1M NH_4COOH at pH 8.5. Absorbance values of repeated flow-throughs of the same 1 mL of reaction solution were measured to estimate the reaction rate. Both AmDH and FDH were active on the two covalent immobilization resins, but at levels at least 100x slower than the expected rates in free solution, which is too much of an activity decrease to be acceptable. The two adsorption beads exhibited significant leaching of enzyme almost immediately when exposed to the reaction buffer, so they were also removed from consideration. The anion exchange resin seemed to show initial promise in the 1 mL reactions, with initial activity and no detectable leaching of either enzymes at pH 8.5. As the pH was increased to 9.5, some enzyme was removed from the resin, likely due to deprotonation of the primary amine groups on the bead surface. Despite the leaching at pH 8.5 the results were promising, and the beads were tested for their suitability in continuous flow mode.

4.3.3 Continuous amine Production Results

The anion exchange resin with co-immobilized cFL1-AmDH and FDH (4 mg of each) was packed into a 1 mL disposable flow cartridge (EB-Ctg1-5, Agarose Bead Technologies, Miami, FL, USA) and incorporated into a continuous flow setup with a recycle loop (see 4.5 for a discussion of the recycle system). To accomplish the binding, empty resin was first packed into the reactor, then a solution containing both enzymes in PBS was continuously circulated through the resin with a peristaltic pump until the

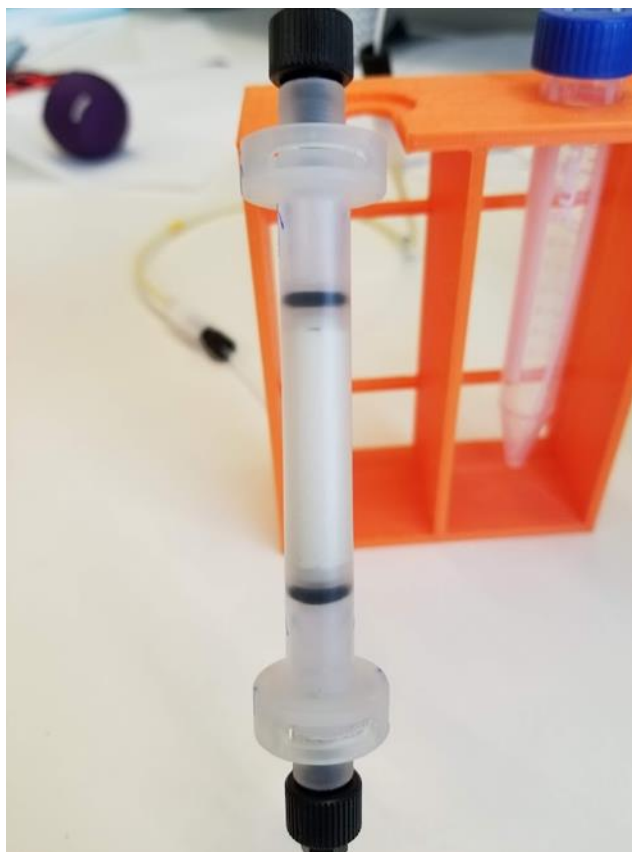


Figure 4-3 Reactor cartridge packed with Immobeads®

concentration of enzyme in the bulk solution was negligible. After binding, the resin was rinsed with fresh PBS, and no enzyme was present in the runoff. An image of the reactor cartridge is shown in Figure 4-3. At the time of their use, these cartridges appeared to be the best option for this reactor setup. However, they had two large disadvantages: they do not have an adjustable volume, and they can only be used once because the tabs that keep the reactor sealed cannot be undone without damage.

The feed solution contained 20 mM acetophenone, 0.5 M NH_4COOH , 1.5 M NH_4Cl , 1 mM NAD^+ and was adjusted to a pH value of 8.5. Temperature of the reactor was held constant with the use of a large water bath and a *sous vide* circulating heater. A photo of

the setup is shown in Figure 4-4. Feed solution was fed at a rate of 150 $\mu\text{L}/\text{min}$ and the recycle flow rate was set at 3000 $\mu\text{L}/\text{min}$. Samples were taken at regular intervals over the course of five days. Flow through the reactor was unstable, with sudden partial clogging events which would eventually become unblocked. The experiment eventually ended when a clog caused the peristaltic tubing to burst off its barbed fitting. Examination of the samples taken from the first hours of the experiment identified large amounts of protein in

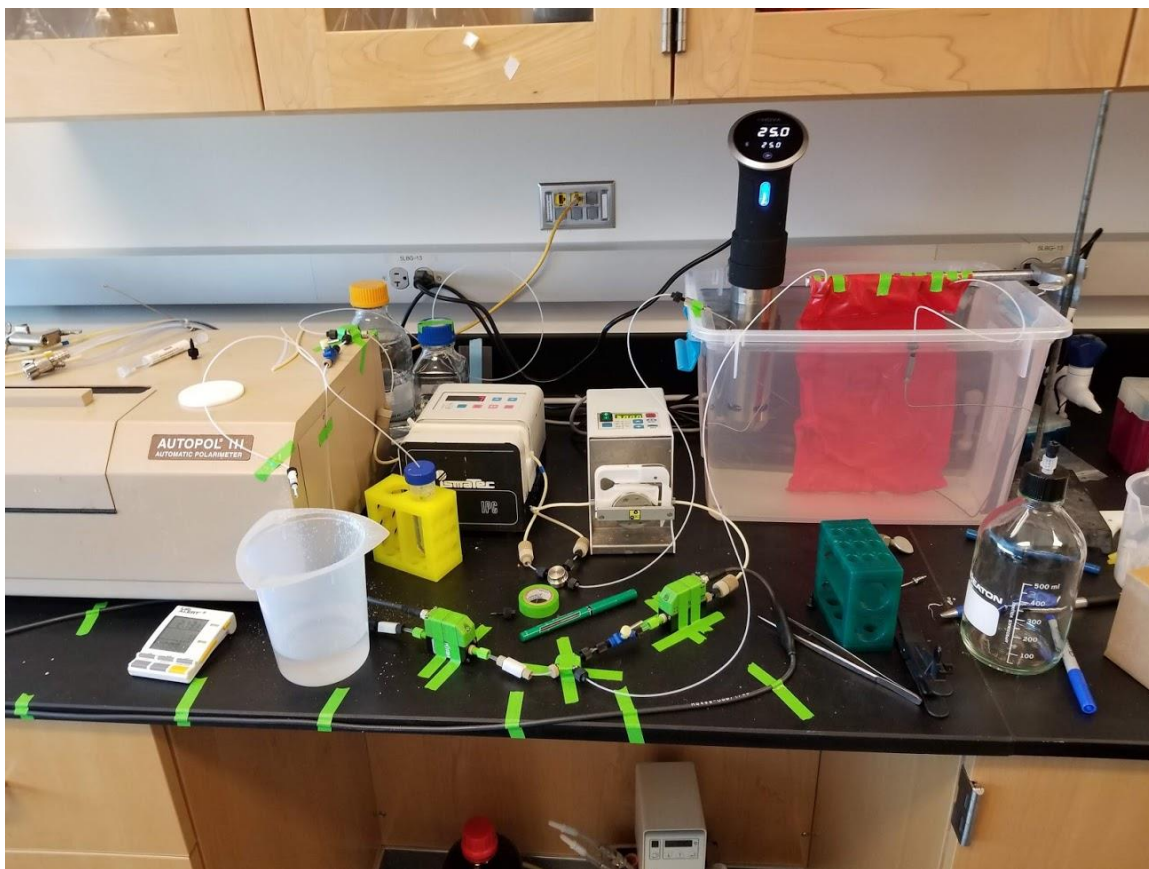


Figure 4-4 Photo of the first packed bed reactor setup with AmDH and FDH. The reactor located inside the red plastic bag.

the outlet. The level of enzyme leaching in prior batch experiments was likely not large enough to be detected, but the continuous flow and high recycle ratio likely contributed to the leaching. Any amount of significant leaching is unacceptable for continuous operation,

so the use of these beads was immediately abandoned. Due to difficulties with HPLC method development, the conversion for this continuous trial was never measured, but it is assumed that conversion was very low.

4.4 Immobilization onto Immobeads® Modified with Leucine Zippers

4.4.1 Leucine Zipper Binding Scheme

After all the 12 binding chemistries from ChiralVision were ruled out, a different strategy was developed in collaboration with Adam Caparco to utilize the covalent binding chemistry of the Immobeads® with the leucine zipper immobilization technology developed by the Champion group at Georgia Tech. Leucine zippers, originally found in DNA binding protein, are protein structures consisting of pairs of alpha helices, one rich in glutamate (Z_E) and another rich in arginine (Z_R), which form very tight and specific heterodimers.⁹⁸⁻⁹⁹ The Z_E zipper was attached to both cFL1-AmdH and *cb*-FDH using an engineered linker, generating AmdH-ZE and FDH-ZE. In a separate peptide, two copies

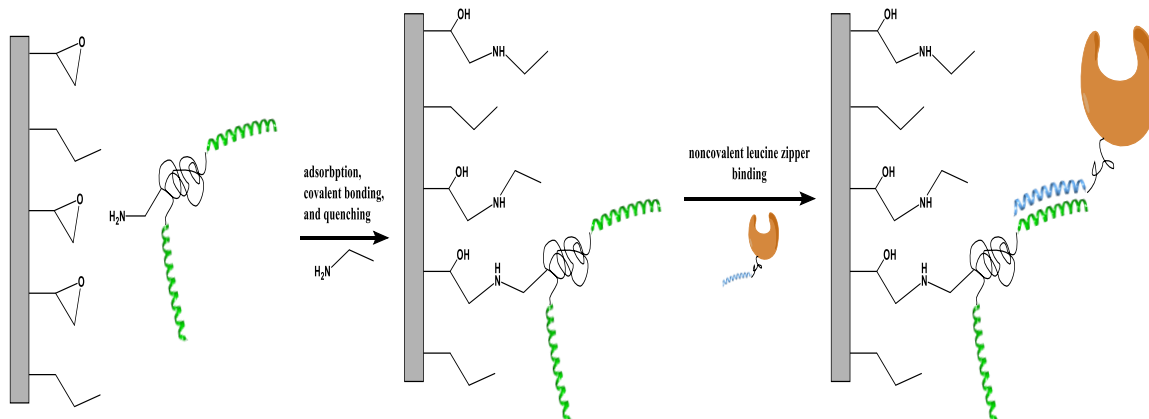


Figure 4-5 Covalent binding of $Z_R C_{10} Z_R$ to Immobeads® followed by noncovalent binding of AmdH-ZE via leucine zipper interactions

of the Z_R zipper are attached by an unstructured linker to form construct called $Z_R C_{10} Z_R$.

If $Z_R C_{10} Z_R$ is immobilized onto a solid support, then the Z_E tags attached the enzymes will bind tightly, allowing for noncovalent, but very strong immobilization. It has been shown previously by Caparco *et al.* that enzymes immobilized with this chemistry retained their structure and activity. The sequences of the enzymes involved, $Z_R C_{10} Z_R$, and methods for their expression and purification have been published previously.⁹⁸⁻⁹⁹ Importantly, the linker sequence of $Z_R C_{10} Z_R$ contains exactly one lysine residue, which meant it could be covalently immobilized to the one of the Immobeads® (IB-COV2) using epoxide ring opening chemistry. A general schematic of the binding strategy is shown in Figure 4-5.

4.4.2 Immobilization Results

Covalent conjugation of $Z_R C_{10} Z_R$ to IB-COV2 was accomplished by incubating a solution containing the pure protein in PBS overnight rotating in a cold room at 4 °C. After washing off excess unbound protein, the remaining epoxide groups which had not reacted with protein were quenched with 250 mM methylamine. This was done to prevent unwanted covalent binding, and deactivation, of AmDH and FDH to the beads. After quenching, the beads were washed again with PBS, and then incubated with a PBS solution containing AmDH-ZE, FDH-ZE, or both. As expected, $Z_R C_{10} Z_R$ was readily able to bind to the bead, as measured by absorbance at 280 nm before and after incubation. Additionally, AmDH-ZE and FDH-ZE were both able to bind to the beads after conjugation with $Z_R C_{10} Z_R$ and quenching. Finally, both enzymes retained their activity when immobilized separately. The precise specific activity of the enzymes compared to the values in free solution was not measured. After incubation of the beads for 24 hours in 2 M NH_4COOH , no protein was detectable by the Bradford assay in the aqueous phase,

which indicated the leucine zipper immobilization did not suffer the same leaching problem as the anion exchange binding chemistry.

4.4.3 *Continuous Amine Production Results*

The leucine zipper immobilization strategy did not end up being successful. While two continuous reactor assays were attempted, neither produced measurable conversion. One possible reason for this is channelling effects within the beads due to the reaction solution. Additionally, expression of AmDH-ZE and FDH-ZE at the time was very difficult, with yields as low as 10 mg of protein per liter of culture. Further development of the AmDH-ZE based reactor stopped when the BioRad Nuvia IMAC resin showed positive results (see CHAPTER 5). Use of the Nuvia resin allowed for the use of the standard 6xHis-tagged AmDH and FDH, which have much higher expression levels.

4.5 The Packed Bed Recycle Reactor (PBRR)

The successful packed bed flow reactor described in CHAPTER 5 was originally intended to include a recycle stream that would return a portion of the reactor outlet directly back to the inlet. It was assumed that the recycle stream would increase the mean residence time of the reactor without decreasing the inlet flow rate, thus increasing productivity. The reactor configuration was inspired by the circulating batch or fed-batch plug flow reactors which have been used periodically for enzyme-catalyzed reactions.¹⁵⁵⁻¹⁵⁸ These batch systems consist of a packed bed tubular reactor and a stirred reservoir. Fluid is continuously pumped from the reservoir, through the packed bed, and back into the reservoir. A second potential benefit of a rapid recycle stream is that the real flow rate in the reactor is much faster for a given inlet flow rate compared to a single-pass reactor. An increase in the flow

rate will increase the external mass transfer coefficient, k_{LA} , and would potentially alleviate any external mass transfer limitations in the system. See 5.5.4 for a more detailed discussion of external mass transfer limitations in packed bed reactors. The PBRR setup went through multiple iterations with improvements to the reactor, sample collection, air removal, and flow characterization along the way.

4.5.1 System Setup

The final setup of the PBRR is shown in Figure 4-6. Flow into the system comes either from the substrate inlet bottle or tracer inlet tube. A selection valve (V-100L, IDEX Health & Science, Oak Harbor, WA, USA) allows for rapid switching between inlets. A peristaltic pump (Ismatec™ IPC-4, Cole-Parmer, Vernon Hills, IL, USA) with 1.30 mm ID 2-stop santoprene tubing (Precision Glassblowing, Centennial, CO, USA) pumps fluid first through a bubble trap (Omnifit™ 006BT, Diba Industries, Danbury, CT, USA). The

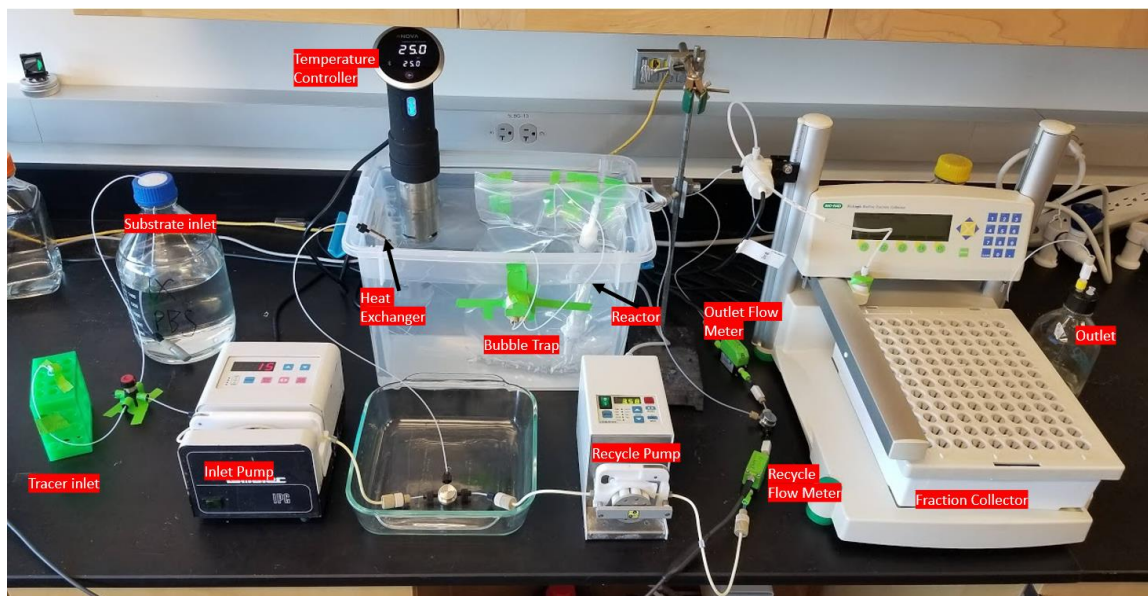


Figure 4-6 Photo of the final packed bed recycle reactor setup

fluid then flows through 1.6 meters of 1/16 inch O.D. stainless steel tubing followed by the

reactor (Omnifit™ EZ SolventPlus™ 10mm x 100 mm chromatography column with one adjustable endpiece, Diba Industries, Danbury, CT, USA). The steel tubing and reactor are both submerged in a water bath with the temperature controlled by a thermal immersion circulator (Precision™ Cooker, Anova Culinary, San Francisco, CA, USA). The fluid from the reactor outlet is split into two streams at a steel T-shaped union. The outlet stream flows through a digital flow meter (SLI-1000, Sensirion AG, Stäfa, Switzerland) and then into an automated fraction collector (BioFrac™ Fraction Collector, Bio-Rad Laboratories, Hercules, CA, USA). From the outlet splitter, the recycle stream is pulled through a digital flow meter (SLI-2000, Sensirion AG, Stäfa, Switzerland) by a second peristaltic pump (Ismatec™ REGLO Digital MS-4/12, Cole-Parmer, Vernon Hills, IL, USA) equipped with tubing with the same composition and internal diameter as the feed pump. The recycle stream then travels from recycle pump to a T-junction located directly downstream of the feed pump, where the two streams are mixed and fed to the reactor.

4.5.2 Residence Time Distributions in the PBRR

Residence time distributions at various flow rates and recycle ratios were collected for the PBRR system using the same methods described in 5.3.10. Four RTDs all collected at the same inlet flow rate (344 $\mu\text{L}/\text{min}$), but different values of R, the recycle ratio are shown in Figure 4-7. At small recycle ratios, individual peaks are baseline-separated in the RTD. Each peak in the RTD is a single pass through the reactor loop. As the recycle ratio increases, the separation between peaks in the RTD decreases. As the recycle ratio increases beyond the 5.9 value shown in the figure, the RTD approaches an ideal CSTR with a delay time. The single pass residence time was 15.8 minutes, while the residence

time for recycle ratios of 1.2, 3.6, and 5.9 were 20.9 minutes, 20.8 minutes, and 18.8 minutes, respectively.

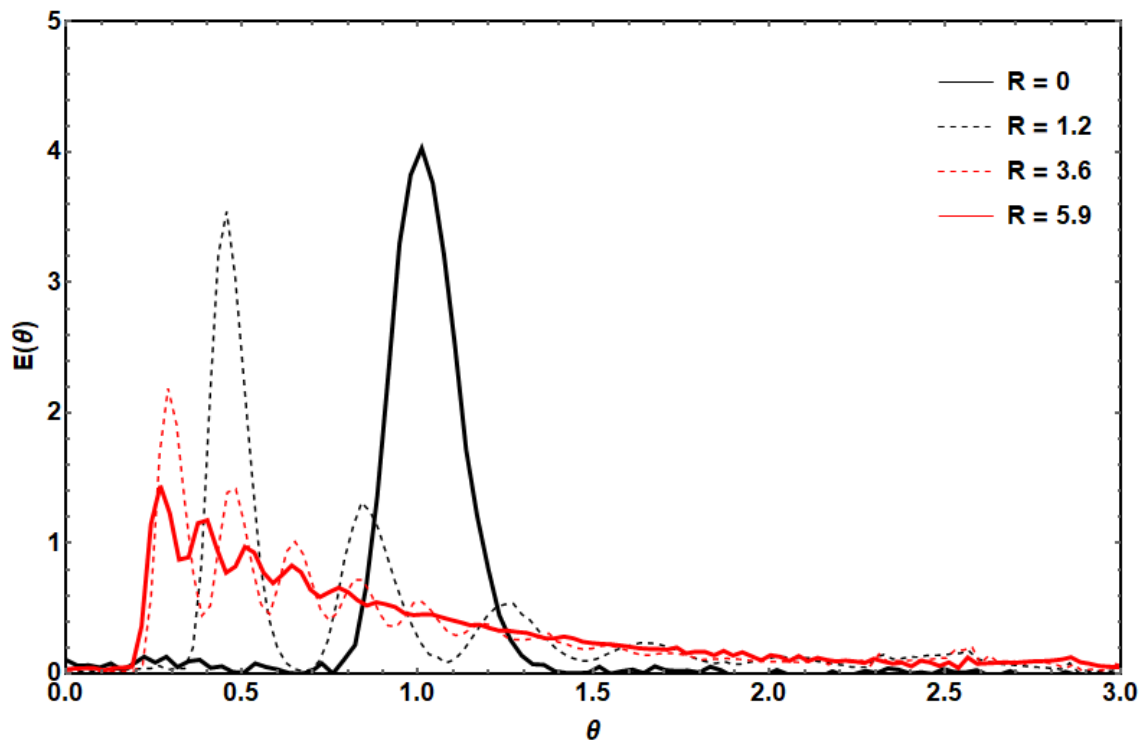


Figure 4-7 Residence time distributions in the PBRR for various recycle ratios. For all residence time distributions in this plot, inlet the inlet flow rate was fixed at 344 $\mu\text{L}/\text{min}$

4.5.3 Conversion Results and Why it Would Not Have Worked

In parallel to the work on characterizing the flow behavior in the PBRR, work was ongoing to develop an enzyme immobilization strategy and product quantification strategy which would enable continuous operation. The assumptions about the possible benefits of an increased recycle ratio were not really put to the test until all the other pieces were in place, which did not happen until January 2020. Once the first continuous assays were performed, it was found that running the reaction at a recycle ratio of 10 resulted in a decrease in conversion of 20% compared to a single pass at the same inlet flow rate (data

not shown). Once this result was obtained, it was quickly decided to remove the recycle stream and stop working on characterizing its performance.

Ultimately, the recycle ratio for this type of reactor system has absolutely no impact on the mean residence time in the reactor, despite the apparent increases in τ indicated by the collected residence time distributions. The proof of this is described below, and is adapted from a 1967 paper by David Rippin on using a recycle reactor to model incomplete mixing.¹⁵⁹

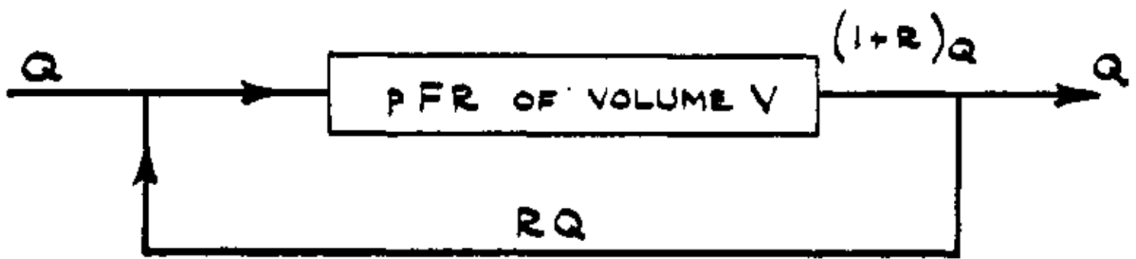


Figure 4-8 Flow diagram of a recycle reactor from Rippin, 1967

Consider a system as shown in Figure 4-8 which has inlet flow rate Q , reactor volume V , and recycle ratio R . For the purposes of this derivation it is assumed that the inlet, outlet, and recycle lines have zero volume. The flow rate in the recycle stream is equal to RQ , and the flow rate through the reactor is equal to $(1+R)Q$. Now, a pulse with a differential duration is introduced to the inlet. It will spend an amount of time in τ_1 in the reactor before it reaches the outlet where $\tau_1 = V / (1 + R)Q$. At the outlet a fraction f_1 of the initial tracer leaves the reactor, where $f_1 = 1 / (1+R)$, and the remaining fraction, $R / (1+R)$, is recycled. The fraction of the tracer that is left travels through the reactor again and reaches the outlet, where a fraction f_2 of the remaining tracer exits, where f_2 is given by (9).

$$f_2 = f_1 \frac{R}{1+R} = \frac{1}{1+R} \left(\frac{R}{1+R} \right) \quad (9)$$

The fraction of the tracer which leaves after two passes spent a total amount of time τ_2 in the reactor, where $\tau_2 = 2V / (1 + R)Q$. This process repeats continuously, with more and more of the tracer leaving after each pass. The total residence time of pass i , is τ_i , where $\tau_i = iV / (1 + R)Q$. The fraction, f_i , of the original tracer which exits the reactor after pass i is given by (10).

$$f_i = \frac{1}{1+R} \left(\frac{R}{1+R} \right)^{i-1} \quad (10)$$

The mean residence time of the entire tracer pulse, τ , is thus given by (11).

$$\tau = \sum_{i=1}^{\infty} f_i \tau_i = \sum_{i=1}^{\infty} \frac{iV}{(1+R)Q} \left(\frac{1}{1+R} \right) \left(\frac{R}{1+R} \right)^{i-1} \quad (11)$$

This sum, when evaluated out to infinity, reduces to $\tau = V / Q$, meaning the mean residence time is independent of the recycle ratio.

Unlike the ideal PBRR from the above derivation, the recycle loop in the real PBRR had a nonzero volume. The measured increases in mean residence time due to elevated recycle ratio thus represented the time that the tracer spent in the recycle loops between passes, not extra time in the reactor. Because the enzyme is immobilized, the time spent in the recycle loop is non-productive and should be ignored when considering reactor performance. At high recycle ratios, the PBRR acted as a CSTR with a certain dead volume. Despite the unproductive dead volume, effective reactor volume of the simulated CSTR is

the same as the packed bed volume. In the PBRR, conversion was 20% lower when the reactor was operated at a high recycle ratio compared to the level of conversion when the reactor was operated in single-pass mode at the same inlet flow rate. The results of the recycle experiment show that for an AmDH reaction at these reactor conditions, a CSTR will give a lower conversion than a PFR of the same volume. This is consistent with the expected behavior for product inhibition-limited reactions taught in introductory reactor design courses.¹⁶⁰ There are a couple of examples in the literature of a PBRR being used with the intention of enhancing enzymatic reactions. In one case, increasing the recycle ratio did not negatively impact reaction kinetics. The authors spoke of the lack of significant product inhibition, as the reason high amounts of product recycling would not harm reaction rates.¹⁶¹ In another study, the use of a PBRR actually enhanced conversion for an autocatalytic protease-driven process.¹⁶²

CHAPTER 5. CONTINUOUS PRODUCTION OF CHIRAL AMINES IN A PACKED BED REACTOR

5.1 Introduction

Amine dehydrogenases (AmDHs), first engineered in 2012,² are a family of enzymes which catalyze the reductive amination of prochiral ketones to form chiral amines. Chiral amine functional groups can be found in many of the current top selling small molecule drugs like sitagliptin (Januvia®), oseltamivir phosphate (Tamiflu®), and dolutegravir (Tivicay®)⁷ and their efficient production is an important challenge in the pharmaceutical industry. The chiral purity of many active pharmaceutical ingredients (APIs) must be greater than 99% to ensure efficacy or avoid adverse side effects.¹⁶³ The naturally high enantioselectivity of enzyme catalysts, among other benefits, have made them increasingly interesting to the industry and academics^{82, 100, 164-165} for the production of chiral APIs including amines.

The application of continuous flow chemistry to biocatalysis has also been increasingly attractive in the pharmaceutical and fine chemical industries.¹⁶⁶ The current paradigm for biocatalysis in most of the pharmaceutical industry calls for large stirred batch reactors into which enzyme, either soluble or immobilized, is added as a reagent. After the reaction is complete, processing steps are required to remove the enzyme. Continuous flow reactions with immobilized enzymes combine the reaction and biocatalyst separation steps into a single unit operation. The operational lifespan of the enzyme, known as the total turnover

number (TTN), can also be significantly higher in flow reactors due to the stabilizing effects of immobilization⁹⁴ and the ease of enzyme reuse compared to batch reactors.

The family of AmDHs has been under continuous development by groups around the world since their first publication eight years ago. The first examples were the leucine amine dehydrogenase (L-AmDH) engineered from the natural leucine dehydrogenase (LeuDh) from *Geobacillus stearothermophilus*² and the phenylalanine amine dehydrogenase (F-AmDH) engineered from the natural phenylalanine dehydrogenase (PheDH) from *Bacillus badius*.⁶⁹ For both L-AmDH and F-AmDH, homologous residues in the active site responsible for binding the carboxylic acid group on the natural amino acid substrate were mutated to instead promote binding to methyl ketones. A similar strategy has been employed by other groups to generate AmDHs based on other PheDH and LeuDh scaffolds.^{70, 74, 104} Recently the Mutti group were able to generate an AmDH from the ϵ -deaminating L-lysine dehydrogenase from *Geobacillus stearothermophilus* which showed activity toward substrates not as easily accessible with the previous engineered AmDHs.⁷⁶ Work has also been done through high-throughput screening and metagenomic mining to identify naturally occurring AmDHs.^{78, 106}

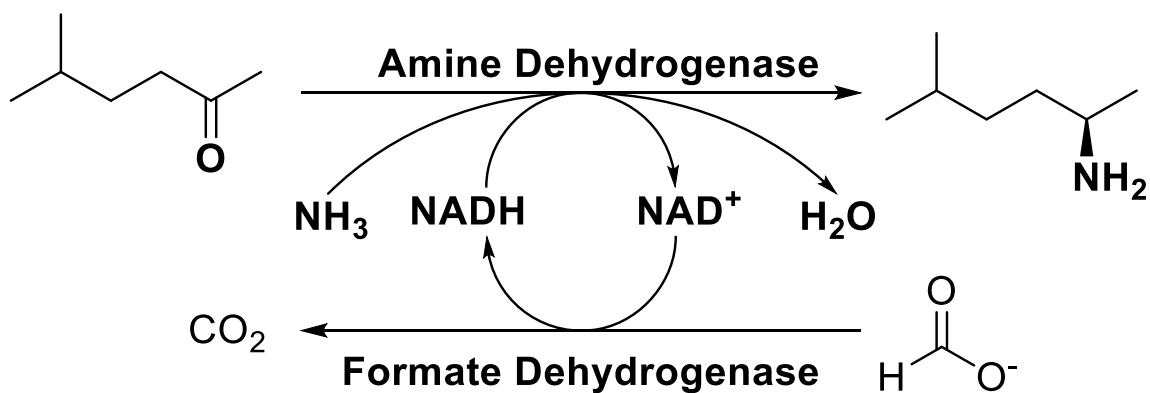


Figure 5-1 Reductive amination of 5-methyl-2-hexanone with cofactor regeneration

There is a growing interest in the pharmaceutical industry to replace the nearly ubiquitous batch reactors with continuous flow chemistry where possible.¹⁶⁷ Continuous processing can offer key advantages over batch reactors in terms of reducing manufacturing time, plant footprint, and waste. Since 2013, the U.S. Food and Drug Administration has been encouraging pharmaceutical companies to pursue continuous processes.¹⁶⁸ Continuous processing is especially attractive for heterogeneous catalysis, as product separation from the solid phase occurs simultaneously with reaction. Continuous flow processes are also easier to monitor and control, as they tend to operate at steady state rather than in a transient mode. Ease of control over reaction conditions can yield tighter control over product purity. For enzymes specifically, continuous processing can alleviate product inhibitions due to the *in-situ* removal of products. Additionally, the total turnover numbers of enzymes in continuous processes tend to be higher than for batch reactions, leading to more efficient use of resources.¹⁶⁶

The primary goal of the reported work was to demonstrate a stable application of continuous flow chemistry to the production of chiral amines with an AmDH. The chimeric amine dehydrogenase cFL1-AmDH,¹⁰³ which will subsequently be referred to here as AmDH, was chosen for its thermostability and high expression levels. AmDH, along with the formate dehydrogenase (FDH) from *Candida boidinii*, was used to convert 5-methyl-2-hexanone (5M2H) to (*R*)-5-methyl-2-aminohexane with ammonium formate and NADH as co-substrates (see Figure 5-1). Initially, the biocatalysts in solution were fed into a continuously stirred enzyme membrane reactor like the one employed by Rogers *et al.* to study the deactivation of TEM-1 beta-lactamase.¹⁵³ Unfortunately, the tendency of AmDH to aggregate in solution under reaction conditions rendered continuous soluble operation

impossible. Our focus then shifted toward co-immobilizing AmDH and FDH onto a solid support for use in a packed bed reactor (PBR), which showed much greater promise.

5.2 Enzyme immobilization

The immobilization support for AmDH and FDH needed to be robust under reaction conditions, have tight binding without significant leaching, be amenable to packing into a flow column with good flow properties, and be readily available. Multiple groups in the past 5 years have explored co-immobilization of AmDHs with FDH and with other enzymes like ω -transaminases and alcohol dehydrogenases.^{88, 97-98, 107} While the reported immobilization strategies met some of the listed criteria, none seemed to meet all of them. In this work, all twelve of the Immobead® enzyme carriers offered commercially by ChiralVision, which included 10 different binding chemistries, were screened for their effectiveness. Despite promising binding efficiency on a few of the beads, the physical properties of the Immobeads yielded significant channeling effects when tightly packed into a column which rendered them unsuitable.

Ultimately the immobilization strategy chosen for this study was to use a commercial immobilized metal affinity chromatography (IMAC) resin from Bio-Rad called Nuvia IMAC. This resin is charged with divalent nickel ions which have been immobilized to the 49 μm acrylamido polymer beads with covalently bound nitriloacetic acid (NTA). A polyhistidine (6xHis) tag is recombinantly expressed at either the C- or N- terminus of a target enzyme, and under the right conditions this 6xHis tag tightly chelates the immobilized nickel ion.¹⁶⁹ Once chelated to the nickel, the 6xHis-tagged proteins are tightly bound, but still retain their folded structure and activity. While IMAC resins have

traditionally been used for protein purification rather than enzyme immobilization, Merck and Co. recently demonstrated the use of Nuvia IMAC for the production-scale immobilization of multiple enzymes in the production of their Phase 3 HIV drug islatravir (MK-8591).¹⁷⁰ EnginZyme in Sweden has also developed a range of IMAC resins for enzyme immobilization with slightly different metal ion immobilization chemistry. The Turner group demonstrated the use of EziG Amber, which employs immobilized Fe^{3+} rather than Ni^{2+} , for use with co-immobilized AmDH and FDH in a packed bed flow reactor.⁹⁶ The authors in that study reported 68% conversion of a 10 mM inlet stream of 4-fluorophenylacetone to form 4-fluoroamphetamine and a volumetric productivity over 300 g/L/day. However, this level of productivity was only stable for a reported 3 hours before rapid deactivation of the catalyst. In the present study, we report the successful application of the Nuvia IMAC resin to immobilize AmDH and FDH in a flow reactor with productivity values similar to those found for the EziG immobilization, but with an apparent half-life exceeding five days.

5.3 Materials and Methods

5.3.1 Sources of Raw Materials

Materials used for enzyme expression and purification, as well as product quantification with benzoyl chloride were published previously.⁷⁹ Additional materials are listed below.

Ni-charged Nuvia® IMAC resin (Bio-Rad Laboratories, Hercules, CA, USA), 5-methyl-2-hexanone 99% (Alfa Aesar, Ward Hill, MA, USA), 5-methyl-2-aminohexane 98% (Santa Cruz Biotechnology, Dallas, TX, USA)

5.3.2 Buffers Used for Expression, Immobilization and Reaction

Binding Buffer: 1X phosphate-buffered saline (PBS), 300 mM additional NaCl, 10 mM imidazole; **Wash Buffer 1:** 1X PBS, 300 mM additional NaCl, 20 mM imidazole; **Wash Buffer 2:** 1X PBS, 300 mM additional NaCl, 40 mM imidazole; **Elution Buffer:** 1X PBS, 300 mM additional NaCl, 250 mM imidazole; **Reaction Buffer:** 2M ammonium formate (NH_4COOH) adjusted to pH 8.5 with 2M NH_4OH , 20 mM 5-methyl-2-hexanone, variable concentration of NAD^+ between 0.1 and 4 mM; **Autoinduction Media:** 1X PBS, 5 g/L NaCl, 20 g/L tryptone broth, 5 g/L yeast extract. This solution is autoclaved in 500 mL batches in 2.8 L baffled shake flasks. After it has cooled, a 50 mL mixture containing 12.5 mg kanamycin, 6 mL glycerol, 0.5 g glucose, and 2 g lactose is filtered through a 0.22 μm syringe filter into the baffled flask.

5.3.3 Enzyme Expression

Engineered cFL1-AmDH¹⁰³ and wild-type *cb*-FDH are expressed separately, but with identical procedures. The gene is stored in the pet28a vector with NdeI and XhoI restriction sites, giving the enzyme an N-terminal 6xHis-tag. After transformation into *E. coli* BL21(DE3) cells, frozen cell stocks are stored at -80 °C in 10% DMSO. 5 mL (standard LB media with 25 mg/L kanamycin) overnight cultures are seeded from the frozen stock and allowed to grow for 16 hours shaking at 37 °C and 250 RPM. The 5 mL starter culture is used to seed 500 mL of autoinduction media. After incubation for 24 hours at room temperature in a 125 RPM orbital shaker, cells are spun down at 2,800 g for 35 minutes. The supernatant is removed, and cell pellets stored at -20 °C or -80 °C for short-term or long-term storage, respectively.

5.3.4 *Enzyme Purification*

Frozen cell pellets resuspended are in an amount of binding buffer based on the size of the expression culture which produced the pellet. A pellet from a 500 mL expression is resuspended in 40 mL of binding buffer. After resuspension, the mixture is split into 20 mL aliquots and sonicated to break open the cells. After cell lysis, the crude lysate is centrifuged at 12,000 g for 40 minutes at 4 °C. Each 20 mL aliquot of clarified lysate is incubated in a separate gravity filtration column for 1 hour at room temperature with 2 mL of Bio-Rad Nuvia IMAC resin which had been previously washed with 30 mL of DI water and 40 mL of binding buffer. After incubation, the column is drained, and subsequent washes are completed first with 10 mL of wash buffer 1 followed by 10 mL of wash buffer 2. After washing, elution buffer is added in 2.5 mL increments and is collected after incubation at room temperature for 5 minutes. Subsequent fractions are collected until the protein concentration in the outlet is less than 1 mg/mL as measured by the Bradford assay¹¹⁵. Elution fractions are buffer exchanged back into the binding buffer using a PD10 desalting column (GE Lifesciences, Chicago, USA) with standard procedures. After desalting, pure protein solutions are stored at 4 °C until needed.

5.3.5 *Enzyme Immobilization*

Empty Nuvia IMAC Ni-NTA resin is stored as a 66% slurry in 20% ethanol. For immobilization, the desired quantity of resin was first washed in a gravity filtration column with 10 bed volumes of deionized water, followed by 10 column volumes of binding buffer. With the column equilibrated in binding buffer, enzyme can be introduced to the resin in form either of purified protein or clarified lysate. After incubation overnight on a rotary

mixer (Roto-Mini™ Rotator Series R2020, Benchmark Scientific Inc, Sayreville, NJ, USA), the resin is washed with 10 bed volumes of wash buffer 1, followed by 10 bed volumes of 2.0 M NH₄COOH/NH₄OH at pH 8.5. The resin is now ready to be packed into a column or transferred to a batch reaction.

5.3.6 *Binding Capacity Determination*

The binding capacity of the Nuvia IMAC resin was determined for both AmDH and FDH separately in a continuous flow binding experiment. The reactor system was set up as shown in Figure 5-2. Stock solutions of AmDH (100 mL, 0.72 mg/mL) and FDH (100 mL, 0.468 mg/mL) in Binding Buffer were prepared and kept at 4 °C or on ice for the duration of the experiment. For each enzyme, 0.666 mL (settled bed) of fresh resin were packed into the reactor column (Omnifit™ EZ SolventPlus™ 10mm x 100 mm chromatography column with one adjustable endpiece, Diba Industries, Danbury, CT, USA) and the column was attached into the flow system. After equilibration of the column with at least 20 mL of binding buffer, the inlet was switched to the enzyme solution, which flowed slowly at 0.168 mL/min through the column. 384 fractions of 230 µL were collected into four UV-transparent 96-well plates using a programmable fraction collector. The change in absorbance at 280 nm between the enzyme stock solution and the reactor outlet could then be used to determine the amount of enzyme which had bound to the enzyme out of each mL that flowed through the resin. For both enzymes, the amount of stock solution was not large enough to fully saturate the resin, so the remaining portion of the binding isotherm was extrapolated. Integration of the binding curves (see Figure 5-4) yields the specific binding capacities of the resin for each enzyme.

5.3.7 *AmDH to FDH Binding Ratio Optimization*

Based on the binding capacities obtained from 5.3.6, and the assumption that the two enzymes have the same rate of binding, the amount of AmDH and FDH needed to saturate 0.2 mL of Nuvia IMAC resin plus 25% was calculated for 5 mass ratios. The ratios and masses of each enzyme required for each ratio are listed in Table 5-1. For each ratio, 0.2 mL of resin are prepared as described in 5.3.5, and purified enzyme is prepared as described in 5.3.4. The required amounts of each enzyme (in binding buffer) are mixed together in a 15 mL conical tube and diluted up to 15 mL with binding buffer. The enzyme mixtures are then used to slurry transfer the resin from the gravity columns to the conical tubes. After incubation overnight, rotating at 20 RPM at room temperature, the 5 immobilized biocatalyst samples are washed with 20 bed volumes of 2.0 M $\text{NH}_4\text{COOH}/\text{NH}_4\text{OH}$ at pH 8.5 and then transferred to 50 mL conical tubes, each containing 50 mL of reaction buffer with 1 mM NAD^+ . The batch reactions proceed for 21 hours at room temperature and rotating at 20 rpm, with samples taken at selected timepoints by stopping the rotisserie mixer and allowing the resin to settle for 5 minutes before collecting 100 μL of supernatant, which is stored at 4 °C until all timepoints have been collected. Quantification of conversion is described in 5.3.11.

5.3.8 *Continuous Flow Reactor System Setup*

A representative schematic of the continuous flow reactor used in the present study can be found in Figure 5-2.

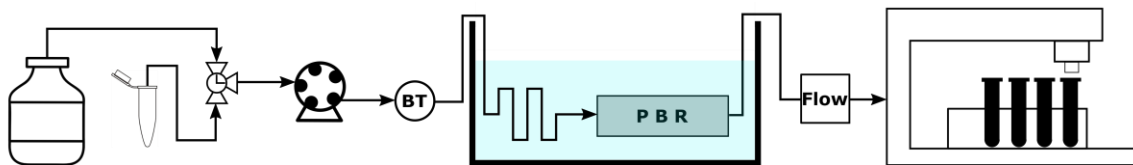


Figure 5-2 Block flow diagram of the continuous flow packed bed reactor system

Flow into the system comes either from the substrate feed bottle or tracer inlet tube. A selection valve (V-100L, Idex Health & Science, Oak Harbor, WA, USA) allows for rapid switching between inlets. A peristaltic pump (Ismatec™ IPC-4, Cole-Parmer, Vernon Hills, IL, USA) with 1.30 mm ID 2-stop santoprene tubing (Precision Glassblowing, Centennial, CO, USA) pumps fluid first through a bubble trap (Omnifit™ 006BT, Diba Industries, Danbury, CT, USA). The fluid then flows through 1.6 meters of 1/16 inch O.D. stainless steel tubing followed by the reactor (Omnifit™ EZ SolventPlus™ 10mm x 100 mm chromatography column with one adjustable endpiece, Diba Industries, Danbury, CT, USA). The steel tubing and reactor are both submerged in a water bath with the temperature controlled by a thermal immersion circulator (Precision™ Cooker, Anova Culinary, San Francisco, CA, USA). Once through the reactor, fluid flows through a digital flow meter (SLI-1000, Sensirion AG, Stäfa, Switzerland) and finally into an automated fraction collector (BioFrac™ Fraction Collector, Bio-Rad Laboratories, Hercules, CA, USA).

5.3.9 Flow Meter Calibration

The flow meter used in this study must be calibrated for each solution it is used for. At various pump speed settings, the desired fluid is pumped through the flow meter, and is collected for precise amounts of time into pre-tared tubes with the fraction collector. The mass of fluid in each tube is converted to a volumetric flow rate by dividing by the collection time and by the density as measured by an Anton Parr Density Meter DMA35.

Comparison of the real flow rate to averaged flow rate as measured by the flow meter is used to produce a pump curve and calibration curve (not shown).

5.3.10 Residence Time Distributions

Flow through the reactor was characterized through the measurement of the residence time distribution at various flow rates. The reaction system is set up as described in 5.3.8 with 1X PBS in the substrate feed bottle and 20 mM NADH in the tracer inlet tube. The reactor column was packed with 2 mL (settled bed) of empty Nuvia IMAC resin. The fraction collector was configured to collect with the required sampling time collect 200 μ L samples into the wells of two 96-well flat bottom polystyrene plates. After purging of the tracer inlet line and subsequent equilibration with 1X PBS, an RTD experiment was commenced by simultaneously starting the fraction collector sequence and rapidly switching the selection valve to allow for the flow of the tracer solution into the reactor for one second, then rapidly switching back to PBS. Once 186 fractions were collected into the two plates, the absorbance of each well at 340 nm was measured in using BioTek Synergy H4 Hybrid Reader (BioTek Instruments Inc., Winooski, VT). Absorbance values were normalized by dividing by the average absorbance of the process fluid at steady state.

For each experiment, the residence time distribution, $E(t)$, was obtained from the normalized absorbance values, $C(t)$, with (12).

$$E(t) = \frac{C(t)}{\int_0^{\infty} C(t) dt} \quad (12)$$

The mean residence time between the tracer inlet valve and the fraction collector outlet, τ_{sys} , is obtained from the $E(t)$ by (13).

$$\tau_{sys} = \int_0^{\infty} t E(t) dt \quad (13)$$

Once the mean residence time has been determined, the residence time distribution can be nondimensionalized to obtain $E(\theta)$ by dividing the function by τ_{sys} as shown in (14).

$$E(\theta) = \frac{E(t)}{\tau_{sys}} \quad (14)$$

The dimensionless time, θ , is defined as t/τ_{sys} . Finally, the variance, σ^2 of the residence time distribution is given by (15).

$$\sigma^2 = \int_0^{\infty} (t - \tau_{sys})^2 E(t) dt \quad (15)$$

The one-dimensional dispersion model with Dankwerts boundary conditions was utilized to estimate the Peclet number (Pe) for each of the collected RTDs by solving (16) numerically for Pe in Excel or Mathematica.¹⁶⁰

$$\frac{\sigma^2}{\tau_{sys}^2} = \frac{2}{Pe} - \frac{2}{Pe^2} (1 - e^{-Pe}) \quad (16)$$

5.3.11 Conversion Determination With HPLC

Conversion in the reactor was determined by direct measurement 5-methyl-2-aminohexane concentration after derivatization with benzoyl chloride. The procedures for

derivatization and quantification of primary amines with reverse-phase HPLC have been described previously.⁷⁹

5.4 Results

5.4.1 Enzyme Leaching Under Reaction Conditions

It had been previously speculated that high concentrations of ammonia/ammonium in solution could lead to elution of bound proteins from Ni-NTA resins. To test this hypothesis, AmDH (11.3 mg) and FDH (5.1 mg) were each immobilized separately onto 0.25 mL of resin. After incubation of the samples at room temperature in 10 mL of a 2.5 M NH₄COOH solution at pH 8.5 for two hours, no protein was detectable by the Bradford assay in the bulk solution for either enzyme. The absence of detectable enzyme leaching in the short term indicated the resin was suitable for further testing.

5.4.2 Enzymatic Activity and Stability in Reaction Conditions

The two samples of separately immobilized biocatalyst from 5.4.1 were combined and employed in a 10 mL batch conversion of 20 mM 5M2H for 24 hours at room temperature. The immobilized enzyme was then left in the solution from the completed batch experiment for 30 days on the bench. After 30 days, there was no detectable protein concentration in the supernatant, which confirms the lack of significant leeching of either enzyme from the resin due to the reaction buffer. After the resin was washed with NH₄COOH solution at pH 8.5 to remove any remaining amine product, the 10 mL batch conversion was repeated to assess the long-term stability of the immobilized enzymes. In both cases, roughly 85% conversion was reached. Importantly, the measured time course

for day 30 was virtually indistinguishable from the one measured on day 0, as can be seen in Figure 5-3.

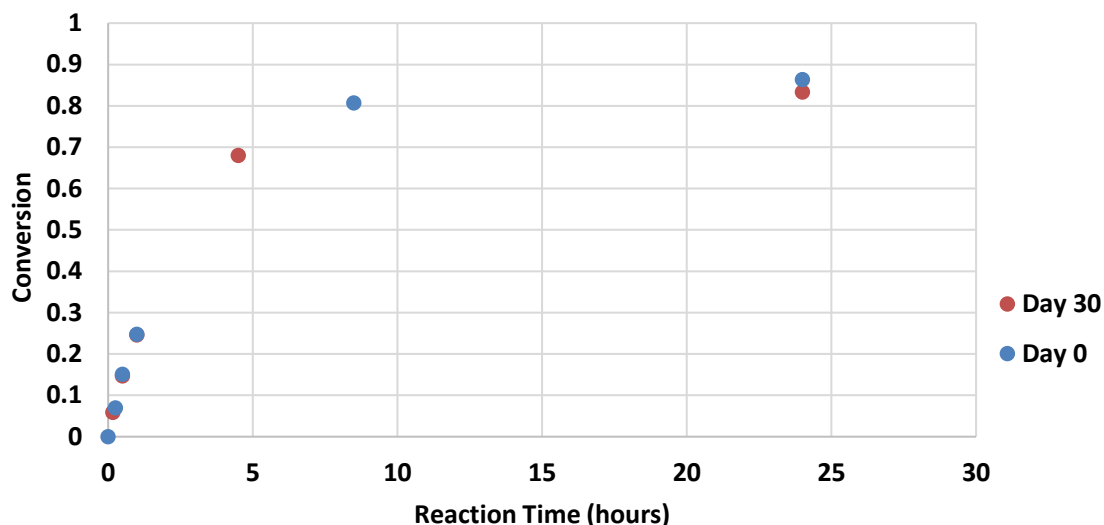


Figure 5-3 Batch conversions of 5-methyl-2-aminohexane by AmDH and FDH immobilized on Nuvia IMAC before and after 30 days of storage in NH_4COOH buffer

5.4.3 Binding Capacity

The binding capacities of the Nuvia IMAC resin for both AmDH and FDH were determined using a continuous flow experiment through a packed column. A known concentration of enzyme was pumped through a packed column with a known quantity of empty Nuvia IMAC resin. The outlet from the reactor was collected into 96-well plates, and the change in enzyme concentration from the stock solution of each fraction was determined by measuring the absorbance at 280 nm. All the enzyme which is missing in the outlet solution was assumed to have bound to the resin. For both experiments, the enzyme stock solution ran out before the resin was completely saturated, so the binding curve was extrapolated to infinite time by assuming the binding isotherm is symmetric about the inflection point. Integration of the binding curves shown in Figure 5-4 yields the total binding capacity of the resin for each of the two enzymes. The resin can bind 78.3 mg

of AmDH per mL of settled bed, or 440 mg per gram of dry resin. However, the binding capacity for FDH was just 42.1 mg per mL of settled bed, or 236 mg per gram of dry resin. Dry resin weight was calculated based on 64% random packing efficiency for spheres, the 80% reported pore volume for Nuvia IMAC resin,¹⁷¹ and 1.11 g/mL density of polyacrylamide. The difference in binding capacity cannot be explained by differences in molecular weight, as the monomer masses of AmDH and FDH are 43.3 and 42.5 kDa, respectively. Instead, the inconsistency in binding capacity is likely due to differences in quaternary structure. FDH is known to form dimers in solution,¹⁷² while the AmDH likely shows a different dominant oligomeric state, likely a tetramer.

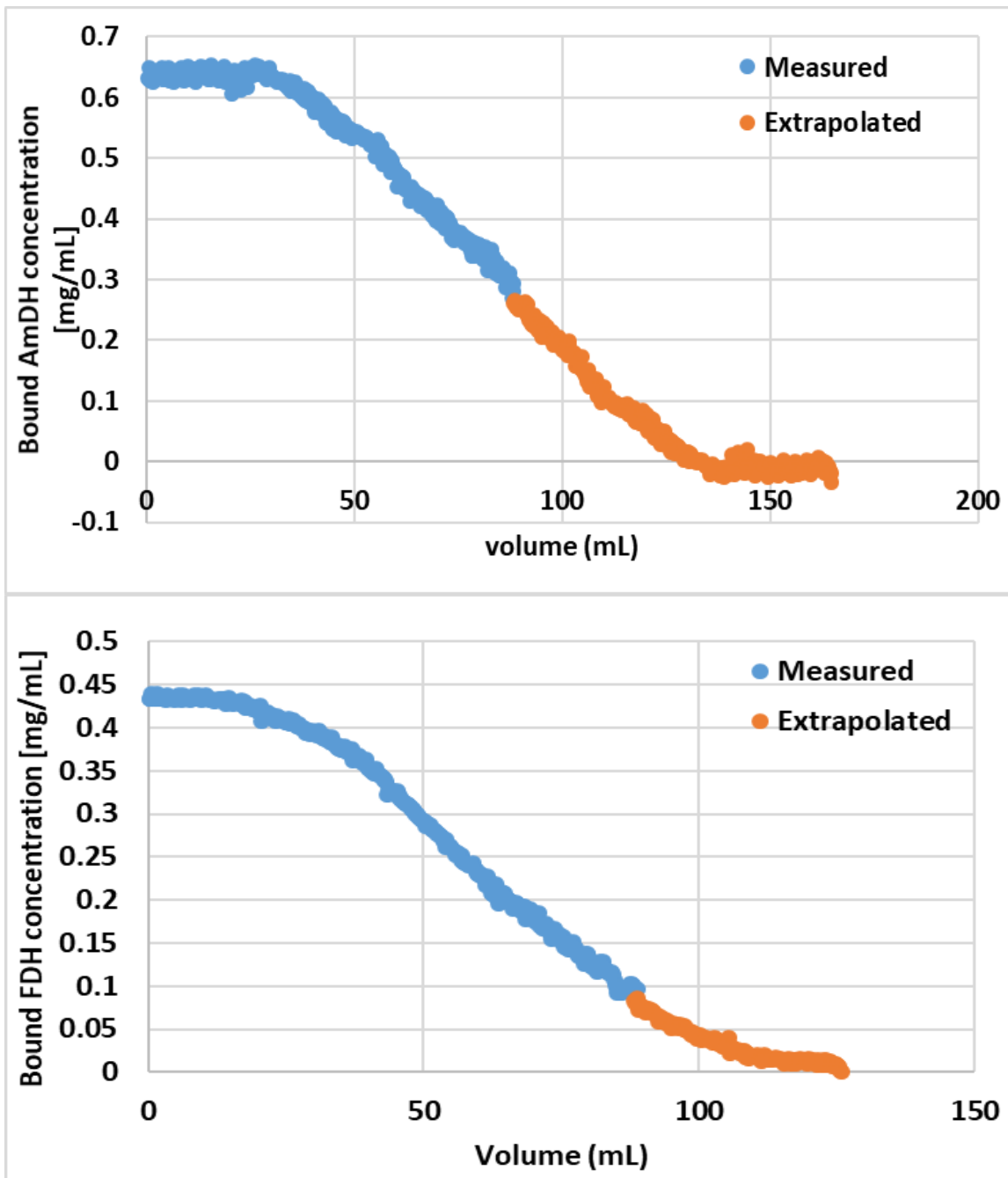


Figure 5-4 Experimental binding curves of AmDH and FDH to Nuvia IMAC resin.

5.4.4 *AmDH to FDH Binding Ratio*

While the binding capacities of the two enzymes on Nuvia IMAC resin are significantly different, the rate of binding was assumed to be the same. Mixtures containing saturating enzyme concentrations at different mass ratios of AmDH to FDH were incubated with 0.2 mL of resin for 24 hours. Then, the immobilized biocatalyst beads were employed in 50 mL scale for conversions of 20 mM 5M2H for 21 hours. As seen in Table 5-1, for the conditions tested, there was no optimum enzyme ratio. The condition which showed the maximum conversion after 21 hours was a 5:1 AmDH to FDH case. The benefits of increased AmDH concentration were likely offset by slower cofactor regeneration. An optimum AmDH to FDH ratio must exist somewhere above 5:1, but it was not investigated further in the reported work.

Table 5-1 Comparison of enzyme binding ratios and the effect on batch conversion

Enzyme Ratio	total capacity	25% excess	mg enzyme		Conversion
AmDH:FDH	mg	mg	AmDH	FDH	%
5:1	13.98	17.475	13.98	2.796	51.5
2:1	12.18	15.225	9.744	4.872	48.8
1:1	10.8	13.5	6.48	6.48	46.7
1:2	9.7	12.125	3.88	7.76	44.8
1:5	8.8	11	1.76	8.8	38.8

5.4.5 *Flow Characteristics of the Reactor System*

After the full flow reactor setup described in 5.3.8 was assembled, the physical parameters and flow characteristics were characterized first using empty resin absent of bound enzyme. After calibration of the electronic flow meters and generation of pump curves, the flow properties of the packed bed could be examined. When the Nuvia IMAC resin is properly packed, 2 mL of settled bed compresses to 1.58 mL in the column. The

flow properties of the system were examined using standard pulsed tracer experiments with NADH as the tracer. By following the absorbance at 340 nm in the outlet over time, the residence time distribution of the system at varying flow rates could be determined. A

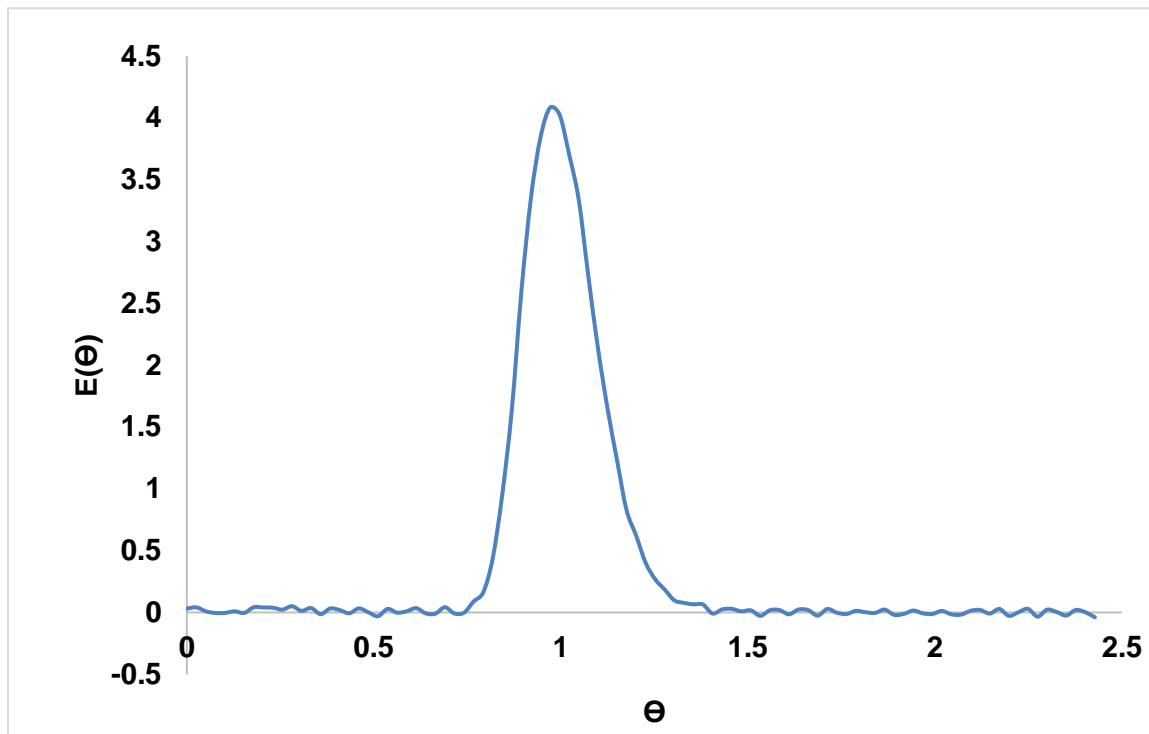


Figure 5-5 Residence time distribution at 0.574 mL/min

representative example of a collected RTD is shown in Figure 5-5. For an inlet flow rate of 0.574 mL/min, the mean residence time of the system, τ_{sys} was determined to be 9.78 minutes. Importantly, this residence time includes not just the reactor, but all the tubing between the tracer injection point and the outlet of the fraction collector. The shape of the RTD shown in Figure 5-5 indicates a flow pattern in the system similar to a plug-flow reactor with a small dispersion effect, as evidenced by an estimated axial Péclet number of 128. The RTD of the reactor alone in the absence of the rest of the system could not be measured experimentally, so it is unknown how much of the observed dispersion occurs in

the actual packed bed. Also, the single clean peak in the RTD indicates proper packing of the reactor without significant channelling or dead volume.

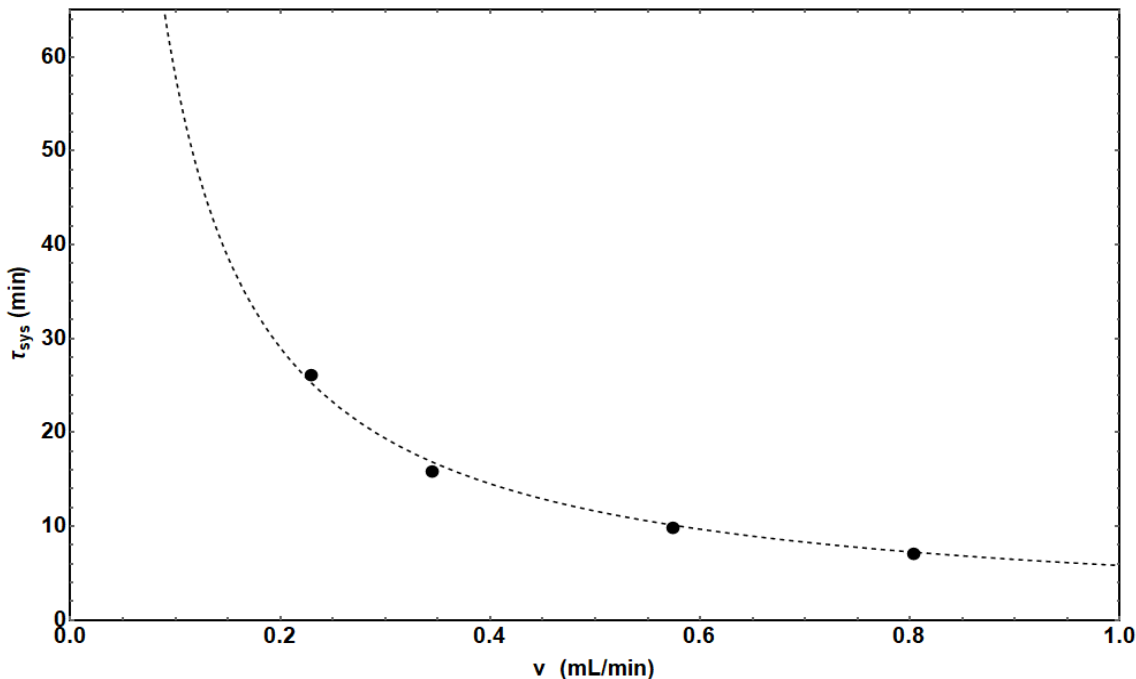


Figure 5-6 Dependence of mean residence time on flow rate in the packed bed reactor. The dashed line represents the function $\tau_{sys} = V_{sys}/\nu$ where V_{sys} was determined to be 5.80 mL.

Prediction of the time to reach steady state without measuring conversion on-line was vital to operation of subsequent experiments. The total system volume V_{sys} was determined to be 5.80 mL by measuring τ_{sys} at various flow rates and fitting the resulting data to the simple relation $\tau_{sys} = V_{sys}/\nu$ where ν is the volumetric flow rate in mL/min (see Figure 5-6). Once V_{sys} was determined, τ_{sys} could be predicted at any flow rate, and Figure 5-5 shows that after two mean residence times have passed since tracer injection, the system has returned to a steady state. Thus, after any change in conditions, samples could be confidently collected after at least two times τ_{sys} and saved for later quantification. A similar set of experiments was conducted with twice the volume of resin, and V_{sys} was

determined to be 7.07 mL. Thus, the actual reactor volume in the first set of RTD experiments, V_{bed} is the difference between the two measured system volumes, or 1.27 mL. V_{bed} was used to predict τ_{bed} , which is the residence time of the actual reactor for use in subsequent characterization.

5.4.6 *Continuous Amine Production: Initial Tests*

For an initial proof of concept, AmDH and FDH were coimmobilized directly from clarified lysate onto 2 mL (settled bed) of Nuvia IMAC resin. While the exact amount of protein immobilized onto the resin for this test is not known, it is estimated that roughly 25 mg of FDH and 60 mg of AmDH were bound to the resin. This estimate comes from the measured yields of protein purified from a fraction of the same fermentation batch as was used for immobilization. The total amount of enzyme on the beads could be measured by elution of the bound protein from the resin with either a high concentration of imidazole or EDTA followed by quantification with the Bradford Assay. However, because the two enzymes were co-immobilized, it is not possible to determine the relative concentration of the two enzymes after elution with benchtop assays. Further development of the reactor platform was conducted with purified enzyme rather than lysate in order to give better control over relative enzyme concentrations on the beads. After packing the resin into a column, the effect of temperature on conversion was determined. As shown in Figure 5-7, increasing the temperature from 25 °C to 40 °C increased conversion by roughly 2.5-fold. When the natural log of the relative conversion is plotted versus the inverse of absolute temperature to produce an Arrhenius plot, a linear relationship is observed as expected.

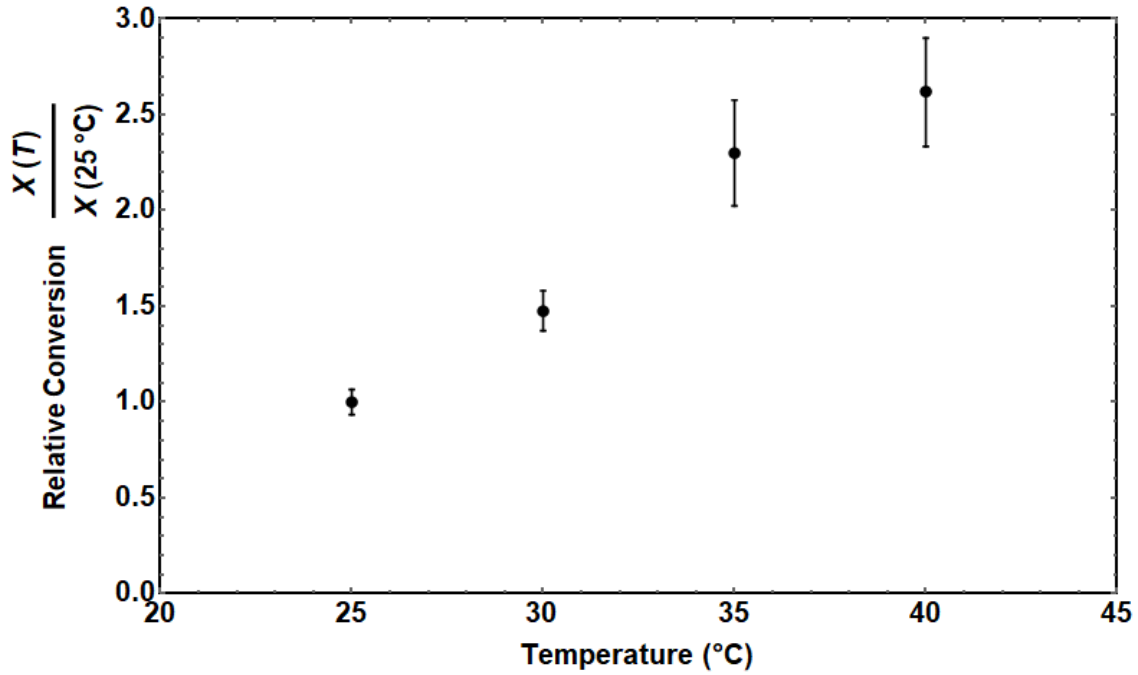


Figure 5-7 Effect of temperature on reaction conversion of 5-methyl-2-hexanone in the packed bed reactor. Feed to the reactor consisted of 20 mM 5M2H, 1 mM NAD⁺, and 2 M NH₄COOH/NH₄OH adjusted to pH 8.5.

The relative conversion has a linear relationship to the apparent rate constant, so its use in an Arrhenius plot is valid. Based on (17), the apparent activation energy, E_a^{app} , of the AmDH/FDH system is given by the slope of the Arrhenius plot multiplied by the gas constant, R, which has a value of $1.987 \times 10^{-3} \text{ kcal mol}^{-1} \text{ K}^{-1}$. Based on the slope in Figure 5-8 and (17), the apparent activation energy of the combined AmDH/FDH reactions was calculated to be 12.4 kcal/mol.

$$\ln \left(\frac{X(T)}{X(25^\circ\text{C})} \right) = \frac{-E_a^{app}}{R} \left(\frac{1}{T} \right) + \ln(A_0) \quad (17)$$

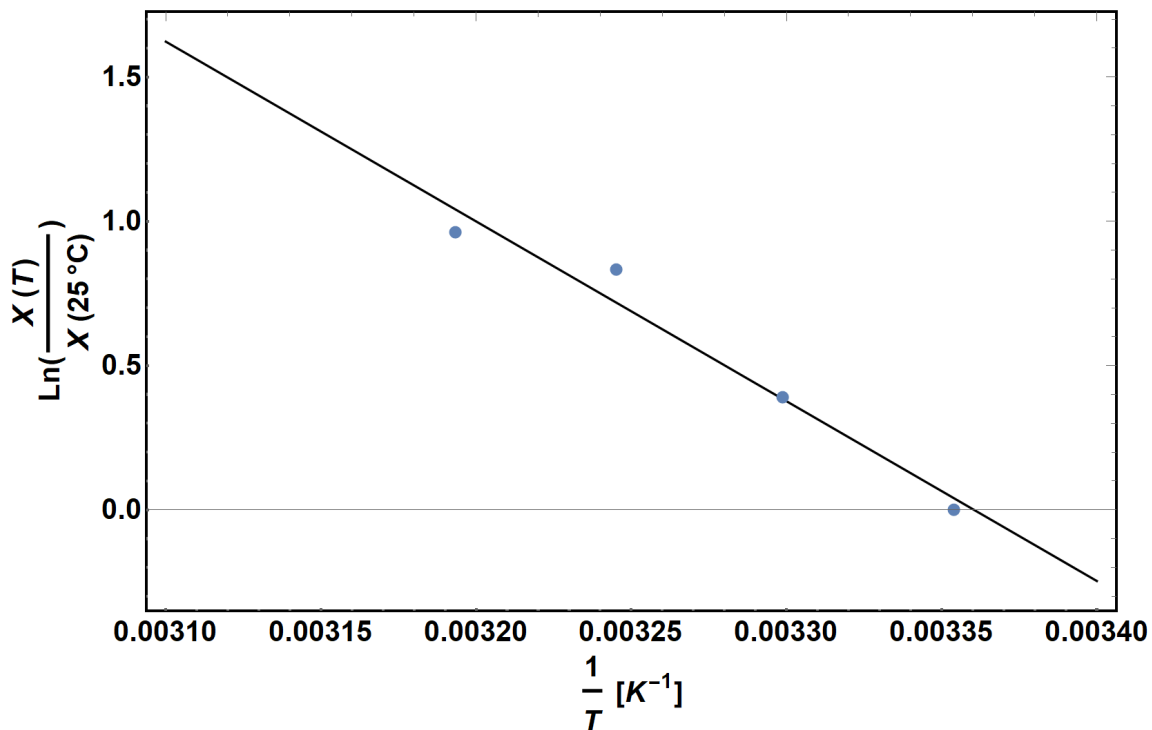


Figure 5-8 Arrhenius plot of the observed relationship between conversion and temperature in the packed bed reactor

Because increasing temperatures often leads to decreases in enzyme stability, the apparent deactivation rates of the immobilized biocatalysts were determined at two temperatures. For both 30 °C and 40 °C, the change in conversion over five days appeared to follow a first order deactivation kinetic. Deactivation profiles over 120 hours at the two temperatures are shown in Figure 5-9. There was no significant decrease in stability at 40 °C compared to 30 °C. The apparent half-life at 30 °C was 124 hours, while the apparent half-life at 40 °C was even longer, at 159 hours.

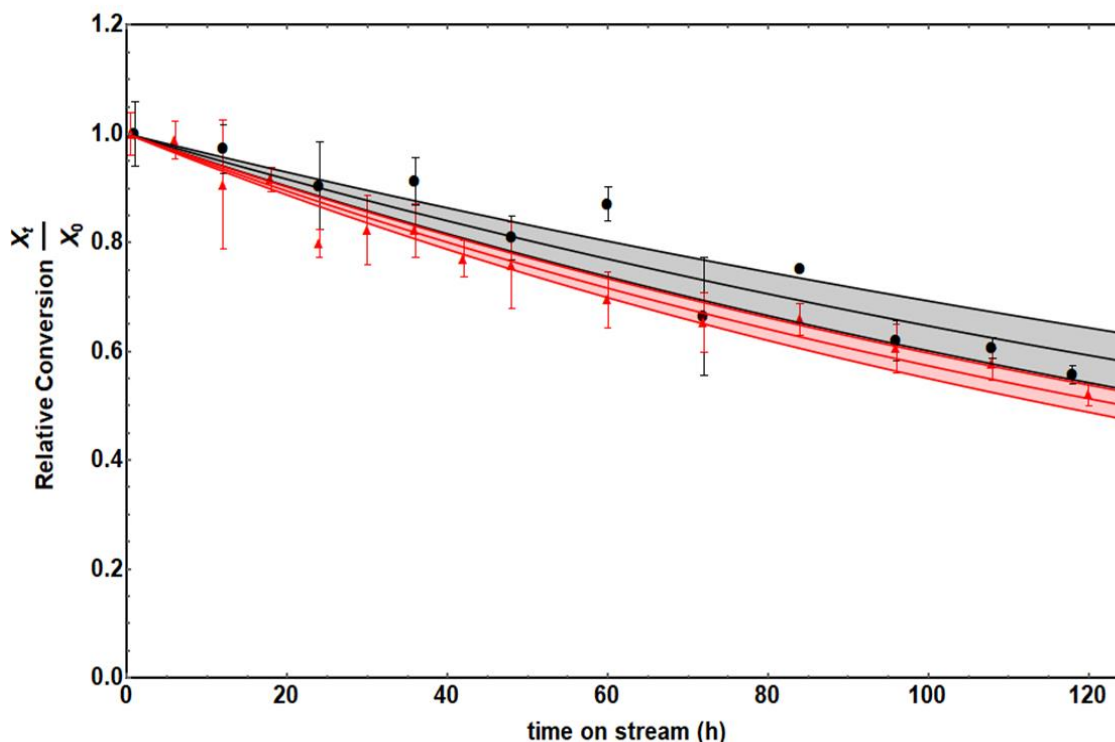


Figure 5-9 Apparent deactivation kinetics of immobilized FDH and AmDH under continuous flow conditions. Red points and curves represent reaction at 30 °C, while black points and curves and points represent reaction at 40 °C. Shaded regions represent the 95% confidence region on the first order deactivation fit.

5.4.7 Improved Reaction Conditions

Using the lessons learned from previous experiments, a final batch of immobilized enzyme was prepared and characterized. A 2 mL sample of Nuvia IMAC resin was saturated with AmDH and FDH in a 5:1 ratio by mass. With the reactor held at 40 °C, inlet flow rate was varied to determine the effect of residence time on conversion and productivity. The results of this experiment are displayed in Figure 5-10.

Figure 5-10A shows the relationship between flow rate and reactor performance, while Figure 5-10B displays data from the same experiment, but in terms of residence time in the reactor rather than flow rate. The two different views of the data are useful for

different ways of thinking about the experiment. The shape of the residence time versus conversion plot indicates an asymptotic conversion somewhat less than 100% at very long residence times. The flow rate plot, Figure 5-10A is more useful as a tool for actually operating the reactor, as flow rate is a readably controllable parameter. The maximum observed conversion, 48%, was at the largest residence time of 11.9 minutes and a flow rate of 106.8 $\mu\text{L}/\text{min}$, as expected. Conversion steadily decreased as flow rate was increased, with a minimum of 18.8% at 816 $\mu\text{L}/\text{min}$ and a residence time of 1.55 minutes. Productivity was reasonably high at all flow rates, with a minimum value of 166 g/L/day at 106 $\mu\text{L}/\text{min}$ and a maximum of 433 g/L/day at the second highest flow rate, 715 $\mu\text{L}/\text{min}$.

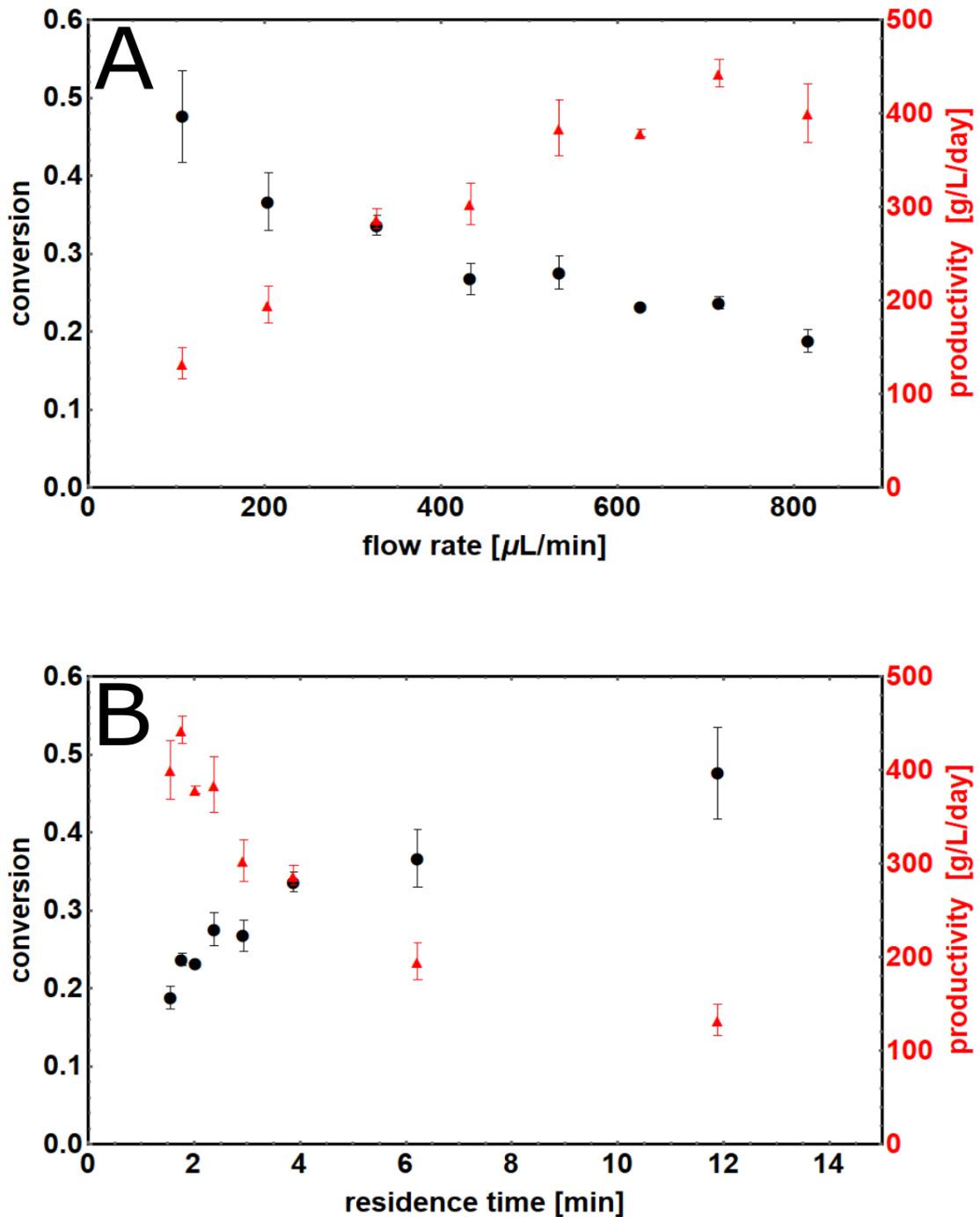


Figure 5-10 Impact of flow rate on conversion and productivity in the AmDH/FDH packed bed reactor. Feed to the reactor consisted of 20 mM 5M2H, 0.5 mM NAD^+ , and 2 M $\text{NH}_4\text{COOH}/\text{NH}_4\text{OH}$ adjusted to pH 8.5. Temperature was fixed at 40 °C.

5.5 Estimation of Limitations to Conversion

Despite high volumetric productivities reported in 5.4.6, overall conversion was limited to just under 50% for the longest included residence time. Batch reactions with immobilized AmDH and FDH showed that conversions of 5-methyl-2-hexanone exceeding 85% are possible. However, the shape of the residence time vs. conversion plot in Figure 5-10B indicates it would likely require a residence time in excess of one hour to reach 90% conversion at the given reaction conditions, which would yield much decreased volumetric productivity. An exploration of the possible causes of limited conversion is important for future reactor development.

5.5.1 Damköhler Numbers

In 1936, Gerhard Damköhler published his seminal paper on the relationship between flow, diffusion, and kinetics in continuous reactors.¹⁷³ In this discussion, we will focus on a set of parameters that have since become known as Damköhler Numbers (*Da*). A Damköhler number, broadly speaking, is the ratio of the chemical flux (the reaction rate per unit area) in a reactor to the mass flux (mass transfer rate per unit area). Put another way, it is the ratio of the characteristic time scale for mass transfer to the characteristic time scale for chemical reaction.¹⁷⁴

$$Da \equiv \frac{\text{Chemical Flux}}{\text{Mass Flux}} = \frac{\text{Mass Transfer Time}}{\text{Reaction Time}} \quad (18)$$

The desired form of *Da* depends on the type of reaction in the reactor and the type of mass flux to be examined. The first form of *Da* described by Damköhler relates the

reaction rate to the rate of convective mass flux, and here will be called $Da_{(I)}$ and is defined in (19) for a reaction with rate $-r_A$ per unit volume, reactor with length L , substrate concentration C_A and superficial fluid velocity U_{SF} . The length of the reactor divided by the superficial velocity is equivalent to the mean residence time, τ .

$$Da_{(I)} \equiv \frac{\text{Reaction Rate}}{\text{Convection Rate}} = \frac{\text{Convective Flow Time}}{\text{Reaction Time}} = \frac{-r_A L}{C_A U_{SF}} = \frac{-r_A \tau}{C_A} \quad (19)$$

A value of $Da_{(I)} \gg 1$ indicates the time it takes for the substrate to flow through the reactor is much longer than the time it takes for the substrate to react. Thus, at high values of $Da_{(I)}$, complete conversion is expected. Likewise, low conversion is expected at low values of $Da_{(I)}$. For a first order reaction in an ideal plug flow reactor, the expression for $Da_{(I)}$ and the expected relationship between $Da_{(I)}$ and X is shown in (20) and (21).¹⁶⁰

$$Da_{(I)} = \frac{-r_A \tau}{C_A} = k\tau \quad (20)$$

$$X = 1 - e^{-Da_{(I)}} \quad (21)$$

Section 5.5.2 will discuss modifications to (19) and (21) necessary to adequately describe the enzymatic reaction system used in this study.

The second Damköhler number relates the reaction rate to the rate of diffusive mass transfer. The Definition Damköhler gave for $Da_{(II)}$ is shown in (22).

$$Da_{(II)} \equiv \frac{\text{Reaction Rate}}{\text{Diffusion Rate}} = \frac{\text{Diffusive Flow Time}}{\text{Reaction Time}} = \frac{-r_A l^2}{D_A C_A} \quad (22)$$

In (22), l is some characteristic length, C_A is the concentration of species A, $-r_A$ is the reaction rate per unit volume, and D_A is the diffusion coefficient of species A. The value of $Da_{(II)}$ can reveal information about the timescales required for reaction and for diffusion. If $Da_{(II)}$ is very large, then the intrinsic rate of reaction is much larger than the rate of diffusion. As such, the catalyst will react with the substrate much faster than the substrate can diffuse from the bulk to the catalyst. A large value of $Da_{(II)}$ results in a lower than expected observed reaction rate and an under-utilized catalyst. The relationship between the observed reaction rate and the maximum reaction rate that would be observed without diffusion limitations is known as the effectiveness factor, η . In a packed bed reactor with porous beads, the specific form of $Da_{(II)}$ depends on whether one is interested in diffusion limitations inside the beads or limitations between the bulk fluid and the bead surface. Internal mass transfer limitations will be discussed in 5.5.3 while external mass transfer limitations will be discussed in 5.5.4.

5.5.2 Enzyme Kinetics

5.5.2.1 Assumptions

The most basic analyses of biocatalytic processes assume that the expression for the rate of reaction takes the form of the Michaelis Menten equation.

$$-r_A = \frac{V_{max} [S]}{K_M + [S]} = \frac{k_{cat} [E][S]}{K_M + [S]} \quad (23)$$

While reaction kinetics of the reactor system presented in this study are much more complicated than (23), as was discussed in detail in CHAPTER 3, the simplifying assumptions needed for (23) to be potentially useful are reasonable and are listed below.

- 1) Full conversion of NAD^+ by FDH is fast enough that the concentration of NADH is constant over the length of the reactor and is close to the inlet concentration of NAD^+ , 0.5 mM.
- 2) The concentration of NH_3 in the reaction is constant over time.
- 3) There is no significant product inhibition.
- 4) The expression $V_{\max} = k_{\text{cat}}[E]$ is true for the relevant enzyme concentration $[E]$ in the reactor of 2.5 mM

Based on reported literature values for FDH, the k_{cat} value is estimated to be 8.06 s^{-1} , which is significantly higher than estimated value for AmDH of 1.75 s^{-1} . Thus, Assumption 1 is likely valid to a reasonable approximation. Since the concentration of NH_4COOH in the feed is 2.0 M and the maximum possible change in ammonia concentration is 20 mM, Assumption 2 is also reasonable.

In the literature on continuous reaction engineering with immobilized enzymes, it is common to further assume (Assumption 5) the rate of the reaction in the reactor can be accurately described as a first order reaction with a rate constant equal to either V_{\max}/K_M or $V_{\max}/C_{A,0}$ where $C_{A,0}$ is the inlet concentration of the substrate.¹⁷⁵⁻¹⁸⁵ This results in a very simple expression for $Da_{(I)}$ shown in (24) and equally simple expressions for $Da_{(II)}$ and the Thiele modulus ϕ_m .

$$Da_{(t)} = \frac{k_{cat}[E]}{K_M} \tau \quad (24)$$

For the experimental results shown in Figure 5-10, the enzyme concentration [E] was 2.5 mM, and initial rate experiments yielded k_{cat} and K_M values of 1.75 s⁻¹ and 4 mM, respectively. Applying (24) with these values at a residence time of 3.9 minutes yields an expected value for $Da_{(t)}$ of 254.6, and conversion based on (21) of 100%. Experimental results, instead, showed a conversion of 33.6% when the residence time was set at 3.9 minutes. In fact, conversion would be expected to be 99.5% with a residence time of 5.0 seconds if (24) were valid for the reactor system studied here.

5.5.2.2 High Enzyme Concentration

One of the fundamental assumptions of the Michaelis Menten equation is that the concentration of enzyme in solution is much less than the concentrations of and K_M values of the substrates involved in the reaction. In the experiments which produced Figure 5-10, the enzyme concentration was 2.5 mM, while the concentration on NADH in the reactor was at most 0.5 mM. Additionally, the $K_{M,NADH}$ for AmDH is approximately 0.0125 mM. The reaction conditions are not consistent with the low enzyme concentration assumption when NADH is concerned. A more general rate law, (25), can be used to describe single-substrate kinetics without inhibition at any ratio of enzyme to substrate.¹⁸⁶⁻¹⁸⁷ The magnitude of the relative error between (23) and (25) at various concentrations of enzyme and substrate can be seen in Figure 5-11, which is adapted from Cha, 1970.¹⁸⁶

$$-r_A = \frac{2 k_{cat}[E] [S]}{K_M + [S] + [E] + \sqrt{(K_M + [S] + [E])^2 - 4[S][E]}} \quad (25)$$

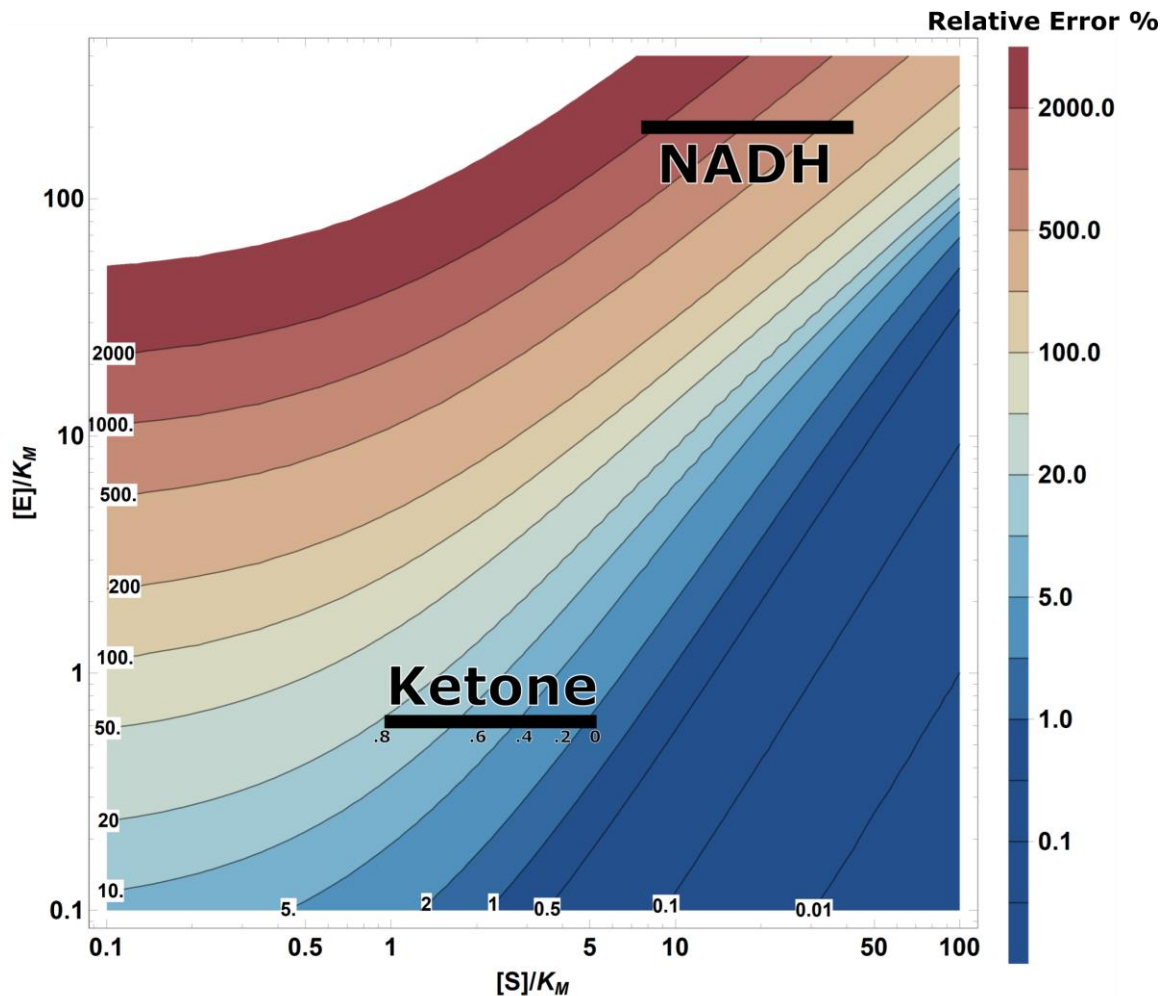


Figure 5-11 Relative percent error in the Michaelis Menten equation at various enzyme and substrate concentrations. The black bars represent the accessible concentration ranges for 5-methyl-2-hexanone and NADH in the experiments which produced Figure 5-10. The numbers below the “Ketone” bar refer to the conversion value at the location along the bar. Numbers in the white boxes inside the plot refer to the value of the relative error along that line.

Based on assumption 1 from 5.5.2.1, the concentration of NADH is expected to be relatively constant at around 0.5 mM, which is much higher than the K_M value of 0.0125 mM and much lower than the 2.5 mM AmDH concentration. As a result, the substrate is

completely saturated with enzyme, and adding additional enzyme will not increase the reaction rate. This is the opposite situation of the classic Michaelis-Menten case, where enzyme is saturated when $[S] \gg K_M$. Under the chosen reaction conditions, Assumption 4 from 5.5.2.1 is clearly invalid. The apparent maximum velocity $V_{max,app}$ is given by (26), where V_{max} is multiplied by the ratio of (25) and (23) and then simplified for the case that $[NADH] \gg K_M$ and $[E] \gg K_M$, as is the case in the reactor.

$$V_{max,app} = \frac{2([S] + K_M)}{K_M + [S] + [E] + \sqrt{(K_M + [S] + [E])^2 - 4[S][E]}} k_{cat}[E]$$

$$V_{max,app} = \frac{2[S]}{[S] + [E] + \sqrt{([S] - [E])^2}} k_{cat}[E] \quad (26)$$

Equation (26) was evaluated for $[NADH] = 0.5$ mM and $[E] = 2.5$ mM to give the final expression for $V_{max,app}$ shown in (27).

$$V_{max,app} = 0.203k_{cat}[E] \quad (27)$$

5.5.2.3 Product Inhibition

The extent of product inhibition of AmDH by 5-methyl-2-amino-hexane was examined *via* initial rate experiments with soluble enzyme. The reaction rate was determined at various simulated levels of conversion by mixing various combinations of concentrations amine and ketone, each of which added to a total of 20 mM. Figure 5-12 shows that, like was seen for a different amine dehydrogenase in CHAPTER 3, AmDH is competitively inhibited by the amine product, and fits to (28) reasonably well.

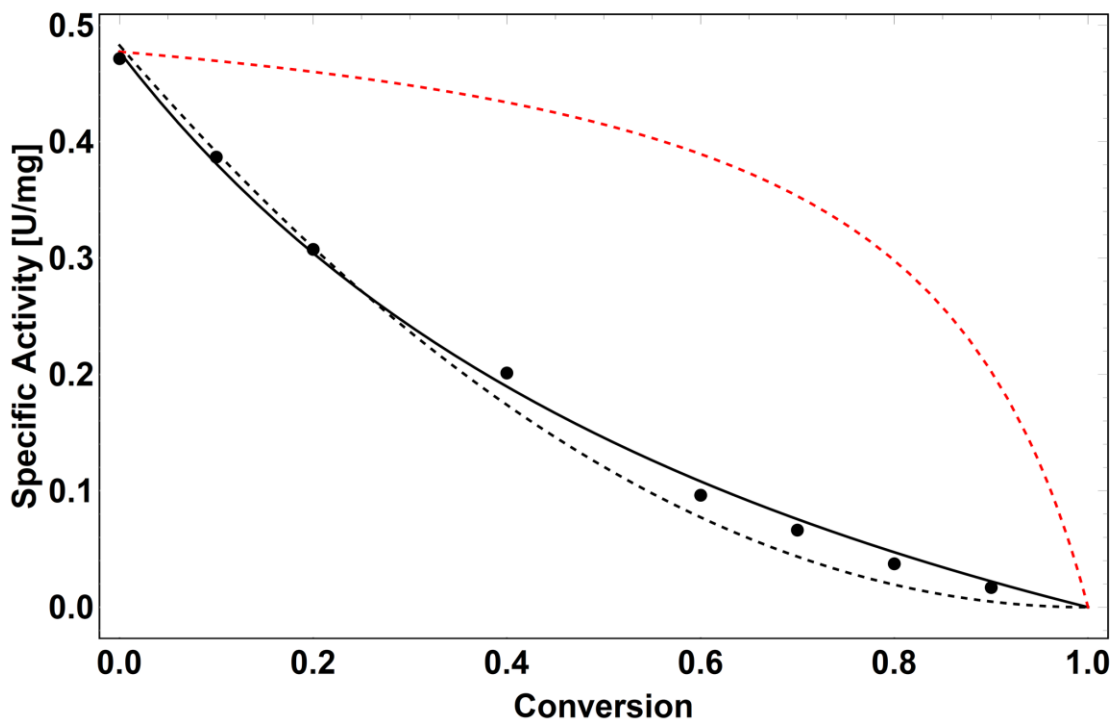


Figure 5-12 Relationship between conversion and reaction rate for AmDH amination of 5-methyl-2-hexanone. Circular data points represent the results of individual initial rate assays with simulated levels of conversion of 20 mM 5-methyl-2-hexanone between 0.0 and 0.9. The solid black curve represents a nonlinear fit of the initial rate data to (28), the rate law for competitive inhibition, the hashed red curve represents the expected activity vs. conversion curve for Michaelis Menten kinetics, and the hashed black curve is a fit of the initial rate data to a standard second order reaction kinetic.

$$-r_A = \frac{V_{max,app}C_{A,0}(1 - X)}{K_M \left(1 + \frac{C_{A,0}X}{K_I}\right) + C_{A,0}(1 - X)} \quad (28)$$

In this rate law, $C_{A,0}$ is the starting ketone concentration, X is conversion, K_M is the Michaelis constant for the ketone, and K_I is the inhibition constant for the amine product. The fit values for K_M and K_I were 3.54 mM and 1.54 mM, respectively. Given these results, both Assumption 3 and Assumption 5 from 5.5.2.1 are invalid for the current AmDH reaction.

5.5.2.4 The Improved Rate Law and $Da_{(l)}$

Given the results from 5.5.2.2 and 5.5.2.3, an improved form of the rate law as a function of conversion was developed which will be used in reactor characterization calculations in subsequent sections.

$$-r_A = \frac{V_{max,app} C_{A,0} (1 - X)}{K_M \left(1 + \frac{C_{A,0} X}{K_I}\right) + C_{A,0} (1 - X)} = \frac{0.203 k_{cat} [E] C_{A,0} (1 - X)}{K_M \left(1 + \frac{C_{A,0} X}{K_I}\right) + C_{A,0} (1 - X)} \quad (29)$$

As shown in Figure 5-12, the rate of reaction changes constantly with conversion, and is neither in the first-order nor the zero-order regime. Thus, there is not a single value of $Da_{(l)}$ which is valid over the entire length of the reactor. To arrive at a single average value for $Da_{(l)}$, one can take the integral of $Da_{(l)}$ with respect to conversion from 0% to 100% at a given residence time τ , as shown in (30).

$$Da_{(l)} = \int_0^1 Da_{(l)}[X] dX = \int_0^1 \frac{-r_A[X]}{C_{A,0}(1 - X)} \tau dX \quad (30)$$

For a residence time of 3.9 minutes, (30) predicts a $Da_{(l)}$ value of 4.6. Because the AmDH kinetics roughly approximate a second order power law kinetic (see Figure 5-12), (31) can be used to give an estimate of expected conversion for a 3.9 minute residence time.¹⁶⁰

$$X \approx \frac{Da_{(l)}}{1 + Da_{(l)}} = \frac{4.6}{1 + 4.6} = 0.82 \quad (31)$$

While 82% conversion is still much higher than the observed conversion of 33.6%, it is not unreasonably high, and is much more accurate than the conversion value estimated in 5.5.2.1.

5.5.3 Internal Mass Transfer

If the rate of internal diffusion through the pores of the beads in a packed bed is slower than the rate of intrinsic kinetics, then the overall conversion in the reactor will be lower than would be observed if all the enzyme were at the bead surface and thus internal diffusion were unimportant. The Thiele modulus, ϕ_m , is often used to describe the relationship between a reaction rate at the catalyst surface to a rate of diffusion within the catalyst particle.¹⁶⁰ The American engineer Ernst Thiele and German Damköhler both worked in this area in parallel but separate fashions in the late 1930s.¹⁸⁸ Although Thiele likely was not aware of Damköhler's work at the time, his modulus can be defined in terms of a form of a Damköhler number for internal pore diffusion, $Da_{(II),i}$ where the characteristic length l is defined as $0.5d_p/6$, the ratio of the volume of a sphere with diameter d_p to its surface area.

$$Da_{(II),i} = \phi_m^2 = \left(\frac{0.5d_p}{3} \right)^2 \frac{-r_{As}}{D_{A,eff}C_{As}} \quad (32)$$

In (32), d_p is the bead diameter (49×10^{-6} m) and $-r_{As}$ is the reaction rate per unit volume at surface concentration C_{As} of 5-methyl-2-hexanone as defined in 5.5.2.4. The effective diffusivity of ketone inside the pores, $D_{A,eff}$, is the bulk diffusivity multiplied by a factor of $\epsilon_{bead}/\tau_{bead}$ which is defined as the porosity ($\epsilon_{bead} = 0.8$)¹⁷¹ divided by the tortuosity (estimated to be 3.0) of the Nuvia IMAC beads. The bulk diffusivity of 5M2H at 40 °C

was assumed to be roughly equal to the infinite dilution diffusivity at that temperature, $1.06 \times 10^{-9} \text{ m}^2/\text{s}$.¹⁸⁹ This results in an effective diffusivity inside the pores of $2.83 \times 10^{-10} \text{ m}^2/\text{s}$. While the assumed value of the diffusivity is likely inaccurate due to the high ionic strength present in the reaction buffer, recalculation of the transport parameters in the following sections with a 100-fold lower estimation of the diffusivity did not change the conclusions. At very low values of the ϕ_m , pore diffusion is much faster than the reaction, so diffusion limitations can be neglected. At the reactor inlet, where the reaction rate is the highest and the effects of mass transfer limitations would be greatest, ϕ_m was estimated to be 0.091. The very low value of ϕ_m yields an internal effectiveness factor, η_I , greater than 0.99 which indicates no impact of internal mass transfer limitations in the reactor.¹⁶⁰

The volumetric productivities (in g/L/day) from the continuous reactor measured in 5.4.6, after unit conversion to mol/m³/s, are equivalent to the average observed rate of reaction over the entire reactor, $-r_A(\text{obs})$, and were used to further verify the absence of limitations due to pore diffusion using the Weisz-Prater criterion.¹⁹⁰

$$C_{W-P} = \frac{-r_A(\text{obs})(0.5 d_p)^2}{9D_{A,eff}C_{A,f}} \ll 1 \quad (33)$$

$C_{A,f}$ in (33) is the outlet concentration of ketone after the system had reached steady state. For all inlet flow rates recorded C_{W-P} was less than 0.01, which satisfies the criterion. The very small 49 μm particle diameter of the Nuvia IMAC resin is very effective at avoiding internal diffusion resistance for small molecules.

5.5.4 External Mass Transfer

Even though internal mass transfer limitations can be neglected, the impact of external mass transfer from the bulk fluid to the resin beads needed to be considered. Predictions of the impact of external mass transfer were made by computing the external mass transfer Damköhler number, $Da_{(II),ex}$, which is the ratio of the reaction rate to the rate of diffusive mass transfer from the bulk fluid to the bead surface. The value for $Da_{(II),ex}(X)$ at any point along the reactor is a function of the conversion, because the reaction rate and diffusion rate are both strongly dependent on the concentration of substrate. To give an average value of $Da_{(II),ex}$ across all concentration ranges, the instantaneous Damköhler number is integrated from $X=0$ to $X=1$.

$$Da_{(II),ex} = \int_0^1 Da_{(II),ex}[X]dX = \int_0^1 \frac{\phi_{bed}}{1 - \phi_{bed}} \frac{-r_A[X]}{k_L a C_{A,0}(1 - X)} dX \quad (34)$$

In (34), X is conversion, $C_{A,0}$ is the inlet ketone concentration (20 mol/m³), and ϕ_{bed} is the packed bed void fraction which was assumed to be 0.3. The values of k_L , the external mass transfer coefficient, and a , the volume averaged interfacial area, were estimated using (35) and (36).

$$k_L = \frac{D_A}{d_p} Sh \quad (35)$$

$$a = \frac{6(1 - \phi_{bed})}{d_p} \quad (36)$$

The Sherwood number, Sh was estimated based on (37), a correlation incorporates the Reynolds (Re) and Schmidt (Sc) numbers and is valid under conditions of creeping flow.¹⁹¹

For all flow rates in the reported work, Re is less than 1×10^{-4} , which is consistent with creeping flow. Sc , which is independent of flow rate, is estimated to be 8.04×10^5 .

$$Sh = 2 + 0.991(Re Sc)^{1/3} \quad (37)$$

Where,

$$Sc = \frac{\nu}{D_A}, \quad Re = \frac{U_{SF} d_p}{\nu}, \quad \text{and} \quad U_{SF} = \frac{v_f}{3.141(0.5 d_r)^2}$$

The kinematic viscosity ν for 2M NH_4COOH was measured using a capillary viscometer at 22 °C and was found to be 30% higher than that of pure water at the same temperature and it was assumed the relationship holds true at 40 °C.¹⁹² In the equation above for superficial fluid velocity, U_{SF} , the reactor diameter d_r and volumetric flow rate v_f were measured directly. Typical values of Sh for the flow rates relevant to this study are predicted to be between 3.0 and 4.2. For all flow rates and conversion values relevant to the reported reaction system, the predicted value of $Da_{(II),ex}$ is less than 0.003. From the Damköhler number, the external effectiveness factor, η_E was determined using (38) and was greater than 0.99 for all relevant flow rates and conversions.¹⁷⁶ While (38) is only strictly valid for a second order kinetics, Figure 5-12 shows that a second order rate law is a reasonable approximation for the real kinetics in the system.

$$\eta_E = \frac{\sqrt{1 + 4Da_{(II),ex}} - 1}{2Da_{(II),ex}} \quad (38)$$

As was the case with internal mass transfer, no limitations on conversion are expected due to external mass transfer. This is due to the very small diameter of the Nuvia

IMAC beads. A 10-fold increase in the bead diameter to 490 μm would yield a 100-fold increase in $Da_{(II),ex}$, and η_E values as low as 0.8. Further confirmation of the lack of external mass transfer limitations was accomplished with a version of the Mears criterion which has been modified for enzyme kinetics.¹⁹³⁻¹⁹⁴ External mass transfer limitations can be ignored if (39) is satisfied.

$$\frac{-r_A(obs)}{k_L C_{A,f}} \left(\frac{d_p}{6} \right) < 0.05 \frac{1 + \hat{K}}{\hat{K}} \quad (39)$$

Where,

$$\hat{K} = \frac{K_{M,eff}}{C_{A,f}}, \text{ and } K_{M,eff} = K_M \left(1 + \frac{C_{A,0} - C_{A,f}}{K_I} \right)$$

Over the range of flow rates relevant to this study, values of the left-hand side of (39) ranged from 1.59×10^{-4} to 2.34×10^{-4} while the values of the right-hand side of (39) ranged from 0.06 to 0.08. Thus, for all flow rates examined in the reported work, the modified Mears criterion is satisfied and external mass transfer limitations can be neglected.

5.6 Discussion

We have demonstrated the first continuous flow reaction system to enantiomerically pure (*R*)-amines with co-immobilized AmDH and FDH which is stable for more than 24 hours of operation. Additionally, the system remained operational, with reductions in activity, for more than a week and the system is as stable at 40 °C as it is at 30 °C. Conversion of 20 mM 5-methyl-2-hexanone increased with decreasing flow rate and ranged between 19% and 48%. However, decreased conversion resulted in increased

volumetric productivity, which ranged from 107 g/L/day at 48% conversion up to a maximum of 443 g/L/day at 24% conversion.

The relationship between conversion and productivity is a key design constraint to consider when engineering a continuous chemical process. The choice of whether to favor conversion at the expense of productivity in the reactor or *vice versa* should be based on the requirements and costs of the unit operations surrounding it and cannot be made based solely on the results in the present study. Without knowledge of the economics of the rest of the process, the optimal operating point for the enzyme reactor cannot be determined. If enzyme and resin are expensive, but separation is cheap, then operating at a lower conversion with a post-separation recycle stream might be preferable. However, if separating ketone from amine is expensive, then higher conversion per-pass would be desired at the expense of higher costs for enzyme or resin.

Binding of the enzyme to the Nuvia IMAC resin was shown to be tight and stable under reaction conditions. The very small diameter of the resin beads of 49 μm resulted in excellent mass transfer properties and no limitations due to internal or external diffusion rates. The specific binding capacities of the resin for AmDH and FDH were determined to be 78.3 mg/mL and 42.1 mg/mL respectively. After batch experiments at varying enzyme ratios, a 5:1 ratio of AmDH to FDH was chosen to maximize conversion. However, when saturated resin was packed into the reactor, the AmDH concentration was much higher than the cofactor concentration, which caused 80% of the enzyme to go un-utilized. Depending on the costs of the components involved, the underutilization of enzyme could be alleviated by increasing the cofactor concentration, or by utilizing the same amount of enzyme but

spread over more resin. Inhibition by the chiral amine product also represented a significant impact to conversion at reasonable productivity levels.

While more can be done to optimize the system, the reported work represents an encouraging first step toward continuous manufacturing of chiral amines with amine dehydrogenases.

CHAPTER 6. FUTURE PERSPECTIVES

6.1 Protein Engineering

6.1.1 Motivation for Protein Engineering Work

While it was not discussed in CHAPTER 2 or the published manuscript on protein engineering toward improving the L-AmDH,⁷⁹ the primary motivation for the protein engineering project was to gain activity toward 5-diethylamino-2-pentanone. The resulting (*R*)-2-amino-5-diethylaminopentane is a key intermediate toward the production an enantiopure form of the antimalarial drug chloroquine, as shown in the reaction scheme in Figure 6-1.

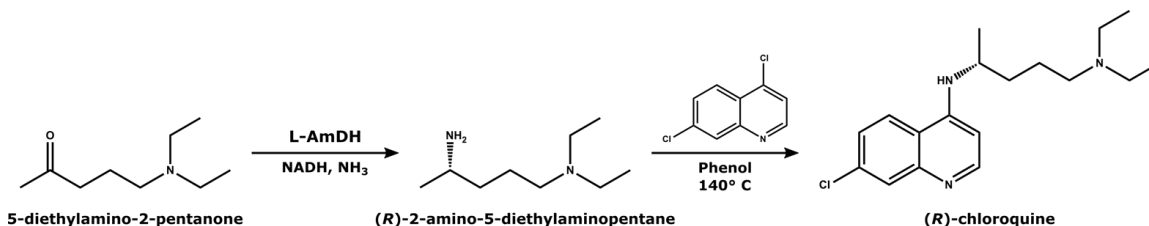


Figure 6-1 Obtaining (*R*)-chloroquine with the help of L-AmDH

Chloroquine is currently sold as a racemic mixture as a malaria prophylactic treatment, as well as a treatment for certain autoimmune diseases like lupus and rheumatoid arthritis. In February of 2020, interest in chloroquine and the structurally related hydroxychloroquine exploded for the potential treatment for and prophylaxis against COVID-19, the pandemic infections disease caused by severe acute respiratory syndrome coronavirus 2 (SARS-CoV-2).¹⁹⁵⁻¹⁹⁷ However, the work in this thesis was conducted and completed well before the start of the COVID-19 crisis. Chloroquine has been regarded as safe since the late 1940s, but there are still some serious side effects associated with the

drug including nausea, deafness, blindness, heart failure, anemia, etc. There has been some evidence that these side effects may be caused more by the (*S*)-enantiomer than the (*R*)-enantiomer of chloroquine.¹⁹⁸ As a result, it was desirable to develop a scalable synthesis for (*R*)-chloroquine.

The base case L-AmDH published by Abrahamson *et. al* in 2012² is only active on ketones the size of 2-hexanone or smaller, and also is not active on any methyl ketones with terminal tertiary amine groups. We employed a strategy of substrate walking³⁸ to attempt to achieve activity toward the target 5-diethylamino-2-pentanone (5DAP) by introducing mutations to the base case enzyme which would instill activity toward substrates which could be thought of as intermediate steps between 2-hexanone and 5DAP.

The series of intermediate substrates is shown in Figure 6-2.

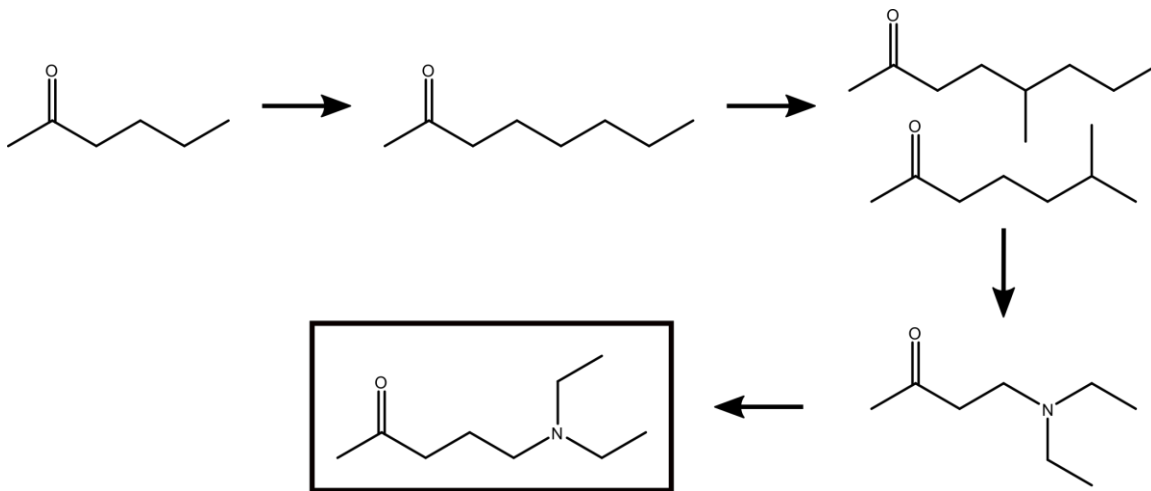


Figure 6-2 Steps in the substrate walk toward 5DAP

The first step was to increase the size of the binding pocket, which was accomplished with L39A and L39G mutations. Then activity toward longer branched ketones was enabled by A112G and T133G.⁷⁹ Finally, activity toward a number of tertiary amino ketones was tested with multiple enzyme variants including TV/L39A, TV/L39G, and

TV/A112G/T133G. These tertiary amino ketones included 3-dimethylamino-2-propanone, 3-diethylamino-2-propanone, 4-dimethylamino-2-butanone, 4-diethylamino-2-butanone, 5-dimethylamino-2-pentanone, and finally the target 5-diethylamino-2-pentanone. No activity was found for any of these ketones except for low but measurable activity for 4-diethylamino-2-butanone (23 mU/mg for TV/L39A, 21 mU/mg for TV/L39G, and 12 mU/mg for TV/A112G/T133G). The L39A/V293T mutation was attempted to provide a potential hydrogen bonding partner for the amine group on 5DAP, the resulting enzyme was not dead, but did not show improvement in activity for any substrate over the L39A variant on its own.

6.1.2 *Directed Evolution for AmDH Engineering*

6.1.2.1 The Need for Libraries

All the published mutations to the L-AmDH presented in this thesis were single point mutations, with one variant produced at a time. While there were some successful mutations, there were just as many, if not more unsuccessful ones. The amount of labor required to produce a single point mutation, especially one not based on previously reported in the literature for related enzymes, may not be worth the small probability of success. As such, a broader approach to mutations is necessary, where multiple mutants are created at once, and the resulting libraries are screened for desirable activity. Library generation and screening is ubiquitous for protein engineering projects, and more work in this area must be performed for further AmDH development.

6.1.2.2 Limitations to Library Size

The largest libraries found in protein engineering projects are generated by error-prone PCR, where DNA polymerase with a high error rate is used to generate one or more random mutations per copy of the gene. In this manner, libraries with thousands or millions of different individual colonies can be generated. However, the speed of the functional assay determines how large a library for a study can be. For antibody engineering or other systems with surface display, a high-throughput fluorescent assay can be developed which can allow for screening of millions of colonies with a FACS system.¹⁹⁹ There have also been some clever examples which used a fluorescent assay in a water-oil emulsion to sort and screen enzyme libraries with FACS.²⁰⁰

The current assay used for screening AmDH libraries is much slower than any of the cell sorting based assays. For library screening, the activity of L-AmDH is measured in the oxidative deamination direction by following the increase in absorbance at 340 nm due to the conversion of NAD⁺ to NADH. The reductive amination direction is not suitable, because endogenous NADH oxidases present in *E. coli* cells result in too many false-positive results. Because the activity assay is based on absorbance, it must be measured in free solution, after cell lysis and clarification. Colonies from agar plates containing the library to be screened are picked into 96 well plates filled with autoinduction media. After cell growth and expression overnight in an incubator, the cells are lysed using a chemical lysing agent like B-Per and centrifuged to remove cell debris. Afterward, the resulting clarified lysates are split into two separate 96-well plates and the activity in one plate is compared to the background absorbance increase in the other. This assay is quite tedious and limits feasible library sizes to the low thousands, which makes error prone PCR strategies less appealing.

6.1.2.3 Site-Directed Libraries

A compromise between random mutagenesis and single point mutations is the generation of libraries which contain multiple variants with mutations at the same site or handful of sites. Screening of larger libraries gives a greater chance of obtaining beneficial mutations. If a site-saturation library with an NNK codon at a potentially interesting site is generated, 96 colonies are required to be screened in order to achieve a theoretical 95% sequence coverage.²⁰¹ A single screening plate per site can be readily accomplished. If several variants at two individual sites are promising, a site-saturation library which contains both sites can be constructed. As the number of sites increases, however, so too does the number of colonies required to be screened for 95% coverage. 3066 colonies are needed for a 2-site library, while 98,163 are needed for a 3-site library.²⁰² In 2019, a plan was developed to try to achieve make the final step in the substrate walk toward 5-diethylamino-2-pentanone by creating several site saturation libraries at a handful of residues in the active site of the L-AmDH/TV/L39A. The sites were chosen based on homology modelling of the variant with a published crystal structure of the *Geobacillus stearothermophilus* LeuDH and rudimentary docking simulations with the target substrate using Audodock Vina. Residues were chosen based on their distance from the potential site of the tertiary amine group on the substrate. Residues considered for site saturation libraries are shown in FIGURE 6-3. Unfortunately, setbacks in generation of the libraries prevented significant progress. The chosen mutation sites may be a potential starting point for future work on L-AmDH, even if the future target substrate is not 5DAP.

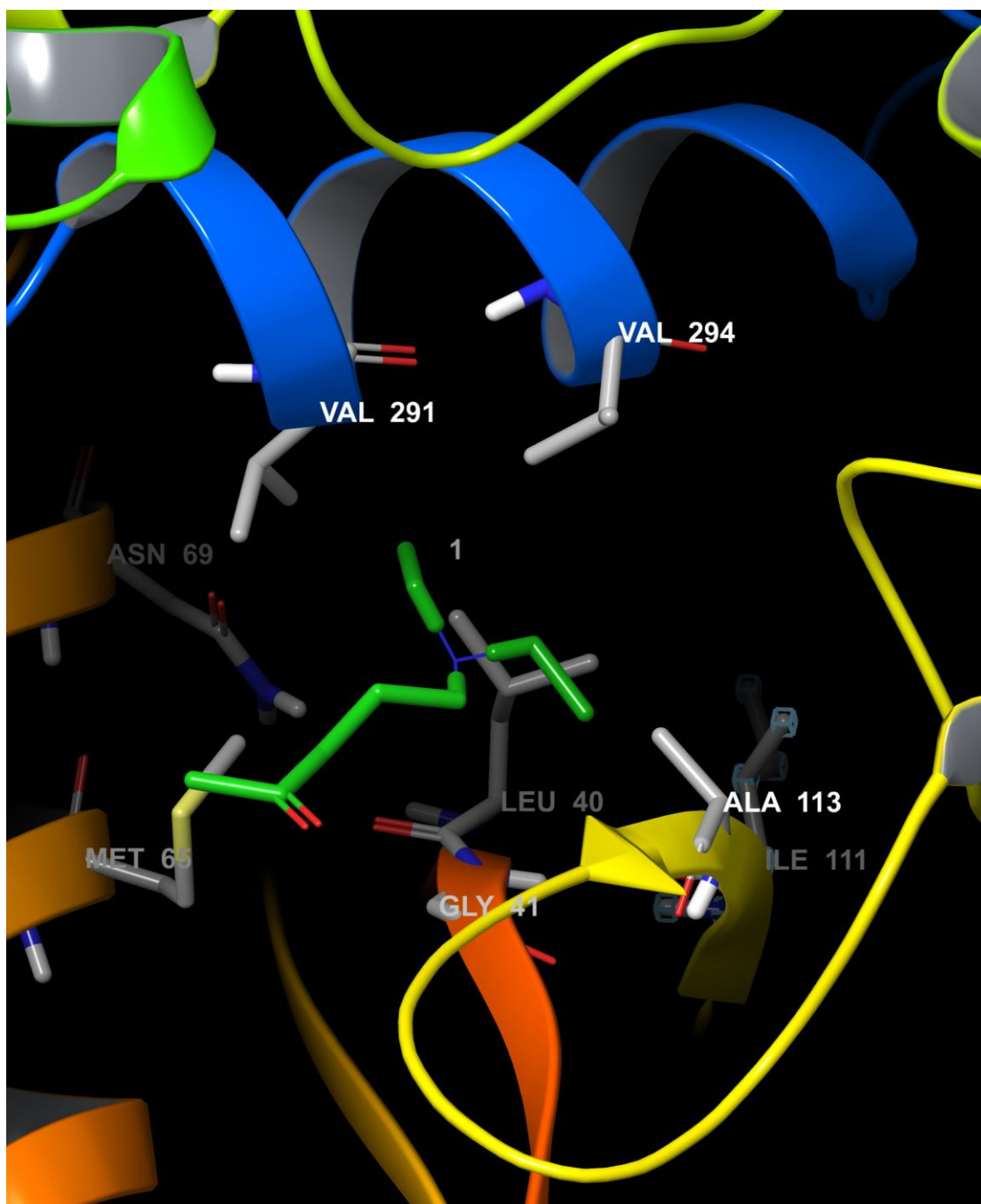


Figure 6-3 Potential sites for site-saturation libraries in L-AmDH/TV/L39A

6.1.2.4 The Future of Protein Engineering for AmDHs

While single-site saturation libraries, like the ones described in the previous section may produce successful variants, the selection of sites is still based largely on visual inspection of crystal structures. Such strategies employed in this reported thesis work cannot compete in the modern protein engineering landscape. Computational protein engineering and large-scale screening efforts such as those conducted by companies such as Codexis show a clear picture of where protein engineering for industrial biocatalysis is going. Any future effort toward engineering new or better activity in AmDHs by the Bommarius group should seek to leverage modern computational protein design tools. It is outside the scope of this thesis to provide a detailed discussion of these tools. However, a good starting point would be the recent work out of the Baker,²⁰³ Siegel,²⁰⁴ and Whitehead²⁰⁵ groups.

6.2 Understanding the Kinetics of Amine Dehydrogenases

6.2.1 Motivation: Binding of Ammonia

Initially, the goal of studying AmDH reaction kinetics in more detail than had been done previously was to solve the problem of ammonia binding. The AmDH reaction requires a very high concentration of an ammonium salt for significant turnover to be achieved. The standard reaction conditions in the continuous reactor calls for 2M ammonium formate at pH 8.5. This high ammonium salt concentration can potentially lead to undesirable side reactions, protein instability, and corrosion of reactor components. For Samantha Au, the PhD student who worked on this project from 2012 to 2016, a primary aim of her thesis project was to improve ammonia binding to AmDH through protein

engineering.¹²³ Her efforts toward this goal were ultimately not successful, and when the present thesis work was proposed, a similar goal was laid out to improve ammonia binding.

To start attacking the problem, we decided to take a step back and try to understand what (if any) fundamental differences existed between AmDH kinetics and the kinetics of their parent amino acid dehydrogenases. It was thought that the results of the mechanism study may guide future protein engineering efforts to improve ammonia binding. In the literature, the reported K_M values for ammonia for leucine dehydrogenases were all lower than 300 mM, while the K_M values for ammonia in L-AmDH was initially found to be between 1 and 2 M. We wanted to understand if the large difference in ammonia K_M between the engineered and parent enzymes was the result of some fundamental change in the reaction kinetics. The basic assumption made by our group had been that the AmDH and AADH had the same type of kinetics, but with different rates. One of the most surprising outcomes of the thesis project was disproving that assumption.

6.2.2 Ammonia Does Not Bind to the Enzyme

The results of the kinetic studies outlined in Table 3-1 show that the apparent K_M values for ammonium chloride are much higher than were previously reported for L-AmDH or LeuDHs.⁵⁵ For L-AmDH and LeuDH, the apparent K_M values were 7.8 M and 3.9 M, respectively. It was impossible to put enough ammonium chloride into solution to saturate either of the enzymes, and the K_M value of NH_4Cl estimated by for L-AmDH was higher than the solubility limit of NH_4Cl . This led us to believe that there is no true binding of ammonia to the enzyme, but rather ammonia interacts directly with the bound ketone to form an imine, which is then reduced to the product amine. As we proposed in the paper,⁵⁵

ammonia cannot “bind” to the enzyme without ketone already bound. Because there was no direct binding site of ammonia, further attempts to enhance ammonia binding through protein engineering were abandoned. It is possible that enzyme engineering work toward stabilizing the ketone-imine transition state may result in enhanced activity of AmDHs at lower ammonium salt loading, but that idea was not explored in the reported work.

6.2.3 *Further Exploration of AmDH Kinetics*

Beyond comparing an engineered enzyme to its parent, the techniques used in CHAPTER 3 could be employed to answer other lingering questions about the nature of AmDH kinetics. A few of those potential questions will be introduced in this section.

6.2.3.1 How Does the Kinetic Mechanism Depend on pH?

All assays in CHAPTER 3 were performed at pH 8.5 for the sake of experimental consistency. While this is not the pH value at which the AmDH shows maximum activity, it was the pH value chosen for reactor engineering studies due to stability concerns for AmDH and FDH. It may be interesting to compare the L-AmDH rate law at pH 9.9 to the rate law at pH 8.5. Both values are 0.7 pH units away from the pKa value of the ammonium ion, which is 9.26 and it is possible that the rate law for AmDH looks very different when operating above the ammonia pKa value. Care must be taken in sample preparation and storage, however, because the evaporation of ammonia from a buffer at pH 9.9 will be much more rapid than from a buffer at pH 8.5.

6.2.3.2 How do Other Enzymes Compare to LeuDH and L-AmDH?

In addition to L-AmDH, the Bommarius group has access to a wide variety of other enzymes in the AmDH family. It would be interesting to see if the relationship between F-AmDH and its parent PheDH is the same as the relationship reported between L-AmDH and its parent LeuDH. *Bacillus badius* PheDH and *Geobacillus stearothermophilus* LeuDH have strong structural and sequence similarity, but their substrate profile and activity levels are quite different from one another. Obtaining the rate law for F-AmDH will be much more difficult than L-AmDH, however. This is because the substrate, phenylpyruvate, absorbs light at 340 nm, which interferes with the rate assay, and it degrades in ammonia buffers over time. Great care must be taken to mitigate these challenges.

Additionally, comparisons could be drawn between the F-AmDH, cFL1-AmDH, and L-AmDH to determine what differences in the enzyme kinetics resulted from the domain shuffling required to create a chimeric enzyme. At the time of writing, work toward determining the kinetic mechanism for cFL1-AmDH for the reductive amination of 2-hexanone is ongoing, but with no concrete results to report.

6.2.3.3 What Kinetic Differences Exist for the Reactions of Different Substrates by the Same Enzyme?

A single AmDH may have activity towards dozens of different substrates, all with differing specific activities. The rate law fitting and kinetic solvent viscosity effect assays used to compare L-AmDH and LeuDH could be used to compare activity toward aromatic and aliphatic ketones by cFL1-AmDH. Because the structure of 2-hexanone and acetophenone, for example, are so different, the binding modes and rates of binding may be completely different between the enzymes. Additionally, the relative importance of

different steps in the kinetic mechanism could be explored by comparing the kinetics of two substrates which are structurally similar, but have very different specific activities, such as 2-butanone and 2-pentanone for the L-AmDH.¹²⁰

6.3 Reaction Engineering for the Production of Chiral Amines

The efforts in early 2020 to fully characterize and optimize the reaction platform described in CHAPTER 5 were severely hampered by the COVID-19 crisis. Several questions about the system remain which were unable to be explored by further experimentation in March, April, or May of that year. The following sections are mostly focused on the remaining questions, whether they need to be answered, and some ideas for experiments that would be useful to get started on answering them. If prediction of conversion and estimation of mass transfer limitations are desired, then more work needs to be done to test the validity of many of the assumptions made in the calculations found in CHAPTER 5.

6.3.1 Obtaining Improved Physical Parameters

6.3.1.1 Intrinsic Enzyme Kinetics

The steady state, free enzyme kinetics for cFL1-AmDH amination of 5-methyl-2-hexanone (5M2H) were never measured at 40 °C, but rather the rate constant at that temperature was estimated based on the apparent activation energy, 12.4 kcal/mol, calculated in 5.4.6 and the specific activity measured at room temperature, roughly 21 °C. The steady state kinetics for FDH were estimated purely based on literature sources.¹⁷²

Care should be taken to determine the true intrinsic kinetic constants for both enzymes under the desired process conditions.

Additionally, the full inhibition profile should be measured for cFL1-AmDH, similar to the experiments conducted to measure the inhibition patterns for L-AmDH and LeuDH in Franklin, 2019.⁵⁵ The results shown in Figure 5-12 were from a single experiment which was not repeated before the shutdown. More data at the process temperature will provide a much more reliable value for the inhibition constant for the amine product. The inhibition constant for NAD^+ is also necessary to fully describe the kinetics. Cross inhibition between enzymes should also be examined to determine if the ketone substrate or amine product of the AmDH have any inhibitory effect on the formate dehydrogenase.

It has been shown by the Bommarius group that the AmDH reaction rate is of the AmDH is dependent on the counterion chosen for the ammonium salt. AmDH shows a lower activity in ammonium formate compared to the same concentration of ammonium chloride. This effect is likely due in part to the increase in viscosity of ammonium formate solutions compared to ammonium chloride. However, high concentrations of chloride are often undesirable due to the corrosive effects of chloride ions on metal vessels. Because some amount of formate is needed for the FDH reaction to proceed, it may be useful to do a full exploration of potential mixtures of ammonium counterions and their effects on AmDH and FDH reaction rates.

Finally, it was assumed that the immobilization of the two dehydrogenases to the Nuvia IMAC resin had no impact on the intrinsic kinetics of the enzymes. This assumption

should be rigorously examined. While it is likely to be true, as high levels of activity retention were observed for similarly immobilized enzymes other processes,¹⁷⁰ each enzyme is different and must be individually validated. For each individual enzyme, a known small amount of enzyme should be immobilised onto the resin, and that resin should be added to a known volume of substrate solution at the process temperature (5M2H/NH₄COOH/NADH for AmDH and NH₄COOH/NAD⁺ for FDH) and the reaction rate followed by UV/VIS absorbance over time. After conducting these assays at multiple concentrations of substrates, the resulting specific activities should be compared to the free solution kinetics obtained under the same conditions to determine any impact of immobilization on intrinsic kinetics.

6.3.1.2 Fluid Properties

Reasonable estimates for the overall mass transfer coefficient and effective pore diffusivity are required for internal and external Damköhler number calculations, as well as the calculations for the Mears and Weisz-Prater criterions. Like the reaction rates in the previous section, the viscosity and density values needed to determine the Sherwood number and thus the mass transfer coefficient were measured at 25 °C and extrapolated to 40 °C. Measurements of the viscosity and density values of the actual process inlet solution at the process temperature are easy to perform and would be preferable to estimated values.

The diffusion coefficient of 5M2H was assumed to be close to the infinite dilution diffusion coefficient of 5M2H in water at 40 °C.¹⁸⁹ Better methods of measuring or estimating the free-solution diffusion behavior of 5M2H, as well as the other important small molecules in the system should be explored in more detail. Additionally, the effective

diffusivity of 5M2H was estimated based on the measured porosity of Nuvia IMAC beads, and an estimated value for tortuosity. The actual effective diffusion coefficient of each of the substrates and products inside the beads can be measured at the process conditions using the method outlined by Grunwald in 1989²⁰⁶ and utilized in support of a cephalixin synthesis study in 2012.²⁰⁷

6.3.2 *Other Assumptions That Need to be Tested*

6.3.2.1 Interplay Between AmDH and FDH

One of the largest simplifying assumptions which enabled the calculations in Section 5.5 was that the conversion of the NAD^+ in the feed to NADH by formate dehydrogenase is nearly complete and very fast. Additionally, the concentration of NADH was assumed to be constant over the length of the reactor. This assumption allowed the real system, which contains two co-immobilized enzymes operating simultaneously, to be modelled as a single enzyme system with single-substrate kinetics. While the assumption was very useful, it is necessary to determine to what extent it is valid. If the conversion of NAD^+ is not complete or fast, the resulting nonideality may have contributed to the prediction of much higher conversion values than were measured.

As a first step toward testing the constant $[\text{NADH}]$ assumption, the intrinsic k_{cat} values for FDH and AmDH should be determined at the process conditions as discussed in 6.3.1.1. A comparison of the more accurate rate constants will give a clearer picture of what is going on in the reactor. Additional experiments could be conducted by first generating a large batch of co-immobilized biocatalyst. Portions of the large batch of immobilized enzyme could be packed into the reactor at different bed heights and installed

into the continuous reactor setup described in 5.3.8. The conversion at the outlet can be measured by HPLC, and importantly the outlet NADH concentration can be measured by UV/VIS spectroscopy. If the constant [NADH] assumption is valid, then [NADH] in the outlet will be independent of bed height. Additionally, if the constant [NADH] assumption is valid, then the bed residence time vs. conversion plots at varied bed heights should overlay perfectly.

6.3.2.2 Stability of Inlet and Outlet Solutions

Another major assumption required to make the experimental methods for characterizing the system tractable was that the substrates in the inlet solution and amine in the outlet solution of the reactor are stable on the bench for at least a day. The inlet is stored in a glass bottle which is not airtight, but has a small opening in the cap. The outlet of the reactor is collected into open test tubes using an automated fraction collector. Additionally, it was assumed that the amine product in the outlet is stable for at least 5 days at 4 °C. This assumption was made so that the measurement of many outlet samples could be made at once, and so that only one bottle of the inlet solution needed to be made per day. The experiments to test the assumed stability of the inlet and outlet solutions are straightforward, but necessary to obtain a robust process.

6.3.3 *Is Predictive Modelling of the Reactor System Useful?*

The work described in 6.3.1 and 6.3.2 will certainly result in a more reliable model for predicting reactor performance than the one outlined in CHAPTER 5. However, it is prudent to ask if such a predictive model would be useful, or whether the complications introduced by the nonidealities in the system would render the model too difficult to fit, or

too specific to the tested conditions to be used for process optimization. For a process meant to run for multiple days, phenomena such as the relative deactivation rates of both enzymes and potential fouling of the enzyme support would also need to be included in a predictive model. Can such a model be developed with the tools, theory, time, and expertise available to the researchers? A serious evaluation of the limitations of any model produced should be made before significant resources are put into a task which may not produce useful results.

6.3.4 Repeatability of Reactor Characterization Measurements

The conversion and productivity values reported in Figure 5-10 were very promising, but they were only the result of a single batch of immobilized enzyme, packed into a single column, measured on a single day, with only a single trial for each flow rate. The validity of the experiment is not in question, but variability can happen in any system. Before a significant amount of time is spent developing a model to more accurately fit the results in Figure 5-10, the overall repeatability of the reaction system must be determined. If the error between reactor runs is greater than the uncertainty in the model, then time should be devoted to improving the experimental methods. Especially of interest is the repeatability of enzyme purification and immobilization from batch to batch, as well as the repeatability of column packing. The packing efficiency and any channelling effects or local disturbances due to bubbles or bead breakage has the potential to have a significant impact on reactor conversion. Thus, aliquots from the same batch of immobilized enzyme should be packed to the same bed height multiple times, and the relative conversion between the trials compared. Likewise, the repeatability of all other processes from enzyme expression to product quantification should be confirmed.

6.3.5 *Empirical Approach to Reactor Characterization*

Rather than developing a theoretical model for reactor performance which is fit based on measured physical properties of the enzyme and substrates, it may be more effective to develop an empirical model for the reactor system instead. Once the repeatability of all the processes used to set up the flow reactor is established, a multi-factorial design of experiments (DOE) approach could be used to design a set of experiments to optimize for conversion or productivity. Factors in the design might include enzyme loading, temperature, NAD⁺ concentration in the feed, flow rate, *etc.* The statistical theory behind DOE is well established and would provide a useful framework for future characterization of the reactor platform while minimizing the number of time-consuming experiments required.

6.3.6 *Scale-Up of Enzyme Production and Immobilization*

To carry out the experiments required for a theoretical or empirical model of the continuous packed bed reactor system, a large quantity of immobilized enzyme will be required. The Bommarius research group has a 10 L fed-batch fermenter which has the capability to produce much larger batches of enzyme at higher efficiency than fermentation in baffled shaking flasks with autoinduction media. The ability to produce an order of magnitude more enzyme than was possible in the reported work will change the types of experiments which can be run.

Additionally, the experiments I conducted at Merck during an internship in 2019 suggest that once immobilized onto the Nuvia IMAC resin, the biocatalysts could be easily lyophilized and would likely remain stable for months on the bench or longer in the freezer.

Immobilization of one large batch of enzymes which can be aliquoted for repeated experiments makes a big difference in the ease of future experiments and removes some of the potential repeatability issues related to variations between enzyme batches. An exploration of stabilization of immobilized AmDH and FDH for long-term storage should be explored, especially as the process moves from bench scale to a potential pilot scale.

APPENDIX A. LICENSES TO REPUBLISH COPYRIGHTED WORKS

A.1 Chemical Engineering Journal 2019 paper

Permission to reuse “Engineered amine dehydrogenase exhibits altered kinetic mechanism compared to parent with implications for industrial application”⁵⁵ in a dissertation by the author is granted without the need for a license by Elsevier Publishing.

A.2 ChemCatChem 2020 paper

JOHN WILEY AND SONS LICENSE

TERMS AND CONDITIONS

Apr 16, 2020

This Agreement between Robert Franklin ("You") and John Wiley and Sons ("John Wiley and Sons") consists of your license details and the terms and conditions provided by John Wiley and Sons and Copyright Clearance Center.

License Number	4810940804973
License date	Apr 16, 2020
Licensed Content Publisher	John Wiley and Sons
Licensed Content Publication	ChemCatChem
Licensed Content Title	Separate Sets of Mutations Enhance Activity and Substrate Scope of Amine Dehydrogenase

Licensed Content Author	Robert D. Franklin, Conner J. Mount, Bettina R. Bommarius, et al
Licensed Content Date	Apr 9, 2020
Licensed Content Volume	0
Licensed Content Issue	0
Licensed Content Pages	1
Type of Use	Dissertation/Thesis
Requestor type	Author of this Wiley article
Format	Print and electronic
Portion	Full article
Will you be translating?	No
Title	Expanding the utility of amine dehydrogenases through protein and reaction engineering for the biocatalytic production of chiral amines
Institution name	Georgia Institute of Technology
Expected presentation date	May 2020
Requestor Location	Robert Franklin 391 17TH ST NW Apartment 1053 ATLANTA, GA 30363 United States Attn: Robert Franklin
Publisher Tax ID	EU826007151
Total	0.00 USD
Terms and Conditions	

TERMS AND CONDITIONS

This copyrighted material is owned by or exclusively licensed to John Wiley & Sons, Inc. or one of its group companies (each a "Wiley Company") or handled on behalf of a society with which a Wiley Company has exclusive publishing rights in relation to a particular work (collectively "WILEY"). By clicking "accept" in connection with completing this licensing transaction, you agree that the following terms and conditions apply to this transaction (along with the billing and payment terms and conditions established by the Copyright Clearance Center Inc., ("CCC's Billing and Payment terms and conditions"), at the time that you opened your RightsLink account (these are available at any time at <http://myaccount.copyright.com>).

Terms and Conditions

- The materials you have requested permission to reproduce or reuse (the "Wiley Materials") are protected by copyright.
- You are hereby granted a personal, non-exclusive, non-sub licensable (on a stand-alone basis), non-transferable, worldwide, limited license to reproduce the Wiley Materials for the purpose specified in the licensing process. This license, **and any CONTENT (PDF or image file) purchased as part of your order**, is for a one-time use only and limited to any maximum distribution number specified in the license. The first instance of republication or reuse granted by this license must be completed within two years of the date of the grant of this license (although copies prepared before

the end date may be distributed thereafter). The Wiley Materials shall not be used in any other manner or for any other purpose, beyond what is granted in the license. Permission is granted subject to an appropriate acknowledgement given to the author, title of the material/book/journal and the publisher. You shall also duplicate the copyright notice that appears in the Wiley publication in your use of the Wiley Material. Permission is also granted on the understanding that nowhere in the text is a previously published source acknowledged for all or part of this Wiley Material. Any third party content is expressly excluded from this permission.

- With respect to the Wiley Materials, all rights are reserved. Except as expressly granted by the terms of the license, no part of the Wiley Materials may be copied, modified, adapted (except for minor reformatting required by the new Publication), translated, reproduced, transferred or distributed, in any form or by any means, and no derivative works may be made based on the Wiley Materials without the prior permission of the respective copyright owner. **For STM Signatory Publishers clearing permission under the terms of the [STM Permissions Guidelines](#) only, the terms of the license are extended to include subsequent editions and for editions in other languages, provided such editions are for the work as a whole in situ and does not involve the separate exploitation of the permitted figures or extracts**, You may not alter, remove or suppress in any manner any copyright, trademark or other notices displayed by the Wiley Materials. You may not license, rent, sell, loan, lease, pledge, offer as security, transfer or assign the Wiley Materials on a stand-alone basis, or any of the rights granted to you hereunder to any other person.
- The Wiley Materials and all of the intellectual property rights therein shall at all times remain the exclusive property of John Wiley & Sons Inc, the Wiley Companies, or their respective licensors, and your interest therein is only that of having possession of and the right to reproduce the Wiley Materials pursuant to Section 2 herein during the continuance of this Agreement. You agree that you own no right, title or interest in or to the Wiley Materials or any of the intellectual property rights therein. You shall have no rights hereunder other than the license as provided for above in Section 2. No right, license or interest to any trademark, trade name, service mark or other branding ("Marks") of WILEY or its licensors is granted hereunder, and you agree that you shall not assert any such right, license or interest with respect thereto
- NEITHER WILEY NOR ITS LICENSORS MAKES ANY WARRANTY OR REPRESENTATION OF ANY KIND TO YOU OR ANY THIRD PARTY, EXPRESS, IMPLIED OR STATUTORY, WITH RESPECT TO THE MATERIALS OR THE ACCURACY OF ANY INFORMATION CONTAINED IN THE MATERIALS, INCLUDING, WITHOUT LIMITATION, ANY IMPLIED WARRANTY OF MERCHANTABILITY, ACCURACY, SATISFACTORY QUALITY, FITNESS FOR A PARTICULAR PURPOSE, USABILITY, INTEGRATION OR NON-INFRINGEMENT AND ALL SUCH WARRANTIES ARE HEREBY EXCLUDED BY WILEY AND ITS LICENSORS AND WAIVED BY YOU.
- WILEY shall have the right to terminate this Agreement immediately upon breach of this Agreement by you.
- You shall indemnify, defend and hold harmless WILEY, its Licensors and their respective directors, officers, agents and employees, from and against any actual or threatened claims, demands, causes of action or proceedings arising from any breach of this Agreement by you.
- IN NO EVENT SHALL WILEY OR ITS LICENSORS BE LIABLE TO YOU OR ANY OTHER PARTY OR ANY OTHER PERSON OR ENTITY FOR ANY SPECIAL, CONSEQUENTIAL, INCIDENTAL, INDIRECT, EXEMPLARY OR PUNITIVE DAMAGES, HOWEVER CAUSED, ARISING OUT OF OR IN CONNECTION WITH THE DOWNLOADING, PROVISIONING, VIEWING OR USE OF THE MATERIALS REGARDLESS OF THE FORM OF ACTION, WHETHER FOR BREACH OF CONTRACT, BREACH OF WARRANTY, TORT, NEGLIGENCE, INFRINGEMENT OR OTHERWISE (INCLUDING, WITHOUT LIMITATION, DAMAGES BASED ON LOSS OF PROFITS, DATA, FILES, USE, BUSINESS OPPORTUNITY OR CLAIMS OF THIRD PARTIES), AND WHETHER OR NOT THE PARTY HAS BEEN ADVISED OF THE POSSIBILITY OF SUCH DAMAGES. THIS LIMITATION SHALL APPLY NOTWITHSTANDING ANY FAILURE OF ESSENTIAL PURPOSE OF ANY LIMITED REMEDY PROVIDED HEREIN.

- Should any provision of this Agreement be held by a court of competent jurisdiction to be illegal, invalid, or unenforceable, that provision shall be deemed amended to achieve as nearly as possible the same economic effect as the original provision, and the legality, validity and enforceability of the remaining provisions of this Agreement shall not be affected or impaired thereby.
- The failure of either party to enforce any term or condition of this Agreement shall not constitute a waiver of either party's right to enforce each and every term and condition of this Agreement. No breach under this agreement shall be deemed waived or excused by either party unless such waiver or consent is in writing signed by the party granting such waiver or consent. The waiver by or consent of a party to a breach of any provision of this Agreement shall not operate or be construed as a waiver of or consent to any other or subsequent breach by such other party.
- This Agreement may not be assigned (including by operation of law or otherwise) by you without WILEY's prior written consent.
- Any fee required for this permission shall be non-refundable after thirty (30) days from receipt by the CCC.
- These terms and conditions together with CCC's Billing and Payment terms and conditions (which are incorporated herein) form the entire agreement between you and WILEY concerning this licensing transaction and (in the absence of fraud) supersedes all prior agreements and representations of the parties, oral or written. This Agreement may not be amended except in writing signed by both parties. This Agreement shall be binding upon and inure to the benefit of the parties' successors, legal representatives, and authorized assigns.
- In the event of any conflict between your obligations established by these terms and conditions and those established by CCC's Billing and Payment terms and conditions, these terms and conditions shall prevail.
- WILEY expressly reserves all rights not specifically granted in the combination of (i) the license details provided by you and accepted in the course of this licensing transaction, (ii) these terms and conditions and (iii) CCC's Billing and Payment terms and conditions.
- This Agreement will be void if the Type of Use, Format, Circulation, or Requestor Type was misrepresented during the licensing process.
- This Agreement shall be governed by and construed in accordance with the laws of the State of New York, USA, without regards to such state's conflict of law rules. Any legal action, suit or proceeding arising out of or relating to these Terms and Conditions or the breach thereof shall be instituted in a court of competent jurisdiction in New York County in the State of New York in the United States of America and each party hereby consents and submits to the personal jurisdiction of such court, waives any objection to venue in such court and consents to service of process by registered or certified mail, return receipt requested, at the last known address of such party.

WILEY OPEN ACCESS TERMS AND CONDITIONS

Wiley Publishes Open Access Articles in fully Open Access Journals and in Subscription journals offering Online Open. Although most of the fully Open Access journals publish open access articles under the terms of the Creative Commons Attribution (CC BY) License only, the subscription journals and a few of the Open Access Journals offer a choice of Creative Commons Licenses. The license type is clearly identified on the article.

The Creative Commons Attribution License

The [Creative Commons Attribution License \(CC-BY\)](#) allows users to copy, distribute and transmit an article, adapt the article and make commercial use of the article. The CC-BY license permits commercial and non-

Creative Commons Attribution Non-Commercial License

The [Creative Commons Attribution Non-Commercial \(CC-BY-NC\) License](#) permits use, distribution and reproduction in any medium, provided the original work is properly cited and is not used for commercial purposes. (see below)

Creative Commons Attribution-Non-Commercial-NoDerivs License

The [Creative Commons Attribution Non-Commercial-NoDerivs License \(CC-BY-NC-ND\)](#) permits use, distribution and reproduction in any medium, provided the original work is properly cited, is not used for commercial purposes and no modifications or adaptations are made. (see below)

Use by commercial "for-profit" organizations

Use of Wiley Open Access articles for commercial, promotional, or marketing purposes requires further explicit permission from Wiley and will be subject to a fee.

Further details can be found on Wiley Online Library <http://olabout.wiley.com/WileyCDA/Section/id-410895.html>

Other Terms and Conditions:

v1.10 Last updated September 2015

REFERENCES

1. Newton, I., Isaac Newton letter to Robert Hooke. 1675.
2. Abrahamson, M. J.; Vazquez-Figueroa, E.; Woodall, N. B.; Moore, J. C.; Bommarius, A. S., Development of an amine dehydrogenase for synthesis of chiral amines. *Angew Chem Int Ed Engl* **2012**, *51* (16), 3969-72.
3. Young, B. D., Smelling matter. *Philosophical Psychology* **2016**, *29* (4), 520-534.
4. Evans, A. M., Comparative Pharmacology of S(+)-Ibuprofen and (RS)-Ibuprofen. *Clinical Rheumatology* **2001**, *20* (1), 9-14.
5. Melchert, M.; List, A., The thalidomide saga. *The International Journal of Biochemistry & Cell Biology* **2007**, *39* (7), 1489-1499.
6. Tokunaga, E.; Yamamoto, T.; Ito, E.; Shibata, N., Understanding the Thalidomide Chirality in Biological Processes by the Self-disproportionation of Enantiomers. *Scientific Reports* **2018**, *8* (1), 17131.
7. McGrath, N. A.; Brichacek, M.; Njardarson, J. T., A Graphical Journey of Innovative Organic Architectures That Have Improved Our Lives. *Journal of Chemical Education* **2010**, *87* (12), 1348-1349.
8. Tian, S.; Tang, B.; Zhang, M.; Gao, Q.; Chen, B.; Zhang, Q.; Xu, G., An Improved Synthesis of Rivaroxaban. *Organic Preparations and Procedures International* **2017**, *49* (2), 169-177.
9. Lam, H. Y.; Zhang, Y.; Liu, H.; Xu, J.; Wong, C. T. T.; Xu, C.; Li, X., Total Synthesis of Daptomycin by Cyclization via a Chemoselective Serine Ligation. *Journal of the American Chemical Society* **2013**, *135* (16), 6272-6279.
10. Taylor, J. G.; Zipfel, S.; Ramey, K.; Vivian, R.; Schrier, A.; Karki, K. K.; Katana, A.; Kato, D.; Kobayashi, T.; Martinez, R.; Sangi, M.; Siegel, D.; Tran, C. V.; Yang, Z.-Y.; Zablocki, J.; Yang, C. Y.; Wang, Y.; Wang, K.; Chan, K.; Barauskas, O.; Cheng, G.; Jin, D.; Schultz, B. E.; Appleby, T.; Villaseñor, A. G.; Link, J. O., Discovery of the pan-genotypic hepatitis C virus NS3/4A protease inhibitor voxilaprevir (GS-9857): A component of Vosevi®. *Bioorganic & Medicinal Chemistry Letters* **2019**, *29* (16), 2428-2436.
11. Fan, X.; Song, Y.-L.; Long, Y.-Q., An Efficient and Practical Synthesis of the HIV Protease Inhibitor Atazanavir via a Highly Diastereoselective Reduction Approach. *Organic Process Research & Development* **2008**, *12* (1), 69-75.

12. Chen, X.; Ni, F.; Liu, Y.; Fu, L.; Li, J., A New and Practical Synthesis of Cariprazine through the Facile Construction of 2-[trans-4-(3,3-Dimethylureido)cyclohexyl]acetic Acid. *Synthesis* **2016**, *48* (18), 3120-3126.
13. Daniels, B. E.; Stivala, C. E., A solid-phase approach for the synthesis of α -aminoboronic acid peptides. *RSC Advances* **2018**, *8* (6), 3343-3347.
14. Williams, J. M.; Brands, K. M. J.; Skerlj, R. T.; Jobson, R. B.; Marchesini, G.; Conrad, K. M.; Pipik, B.; Savary, K. A.; Tsay, F.-R.; Houghton, P. G.; Sidler, D. R.; Dolling, U.-H.; DiMichele, L. M.; Novak, T. J., Practical Synthesis of the New Carbapenem Antibiotic Ertapenem Sodium. *The Journal of Organic Chemistry* **2005**, *70* (19), 7479-7487.
15. Michida, M.; Ishikawa, H.; Kaneda, T.; Tatekabe, S.; Nakamura, Y., Development of an Efficient Manufacturing Process for a Key Intermediate in the Synthesis of Edoxaban. *Organic Process Research & Development* **2019**, *23* (4), 524-534.
16. Trinadhachari, G. N.; Kamat, A. G.; Venkata Balaji, B.; Prabahar, K. J.; Naidu, K. M.; Babu, K. R.; Sanasi, P. D., An Improved Process for the Preparation of Highly Pure Solifenacin Succinate via Resolution through Diastereomeric Crystallisation. *Organic Process Research & Development* **2014**, *18* (8), 934-940.
17. Hsiao, T. Y.; Lee, S. W. Process for the preparation of leuprolide and its pharmaceutically acceptable salts. US9150615B2, 2015.
18. Ghosh, S.; Kumar, A. S.; Mehta, G. N., A short and efficient synthesis of valsartan via a Negishi reaction. *Beilstein J. Org. Chem.* **2010**, *6*, 27-27.
19. Kim, K. B.; Crews, C. M., From epoxomicin to carfilzomib: chemistry, biology, and medical outcomes. *Nat Prod Rep* **2013**, *30* (5), 600-604.
20. Lau, S.-H.; Bourne, S. L.; Martin, B.; Schenkel, B.; Penn, G.; Ley, S. V., Synthesis of a Precursor to Sacubitril Using Enabling Technologies. *Organic Letters* **2015**, *17* (21), 5436-5439.
21. Bin, Y.; Hongmeng, X.; Kerui, R.; Yongjun, G., Efficient Synthesis and Resolution of Tenofovir Alafenamide. *Letters in Organic Chemistry* **2018**, *15* (1), 10-14.
22. Stecko, S., Total Synthesis of Lacosamide. *The Journal of Organic Chemistry* **2014**, *79* (13), 6342-6346.
23. Mylavarapu, R.; Anand, R. V.; Kondaiah, G. C. M.; Reddy, L. A.; Reddy, G. S.; Roy, A.; Bhattacharya, A.; Mukkanti, K.; Bandichhor, R., An alternate synthesis of levetiracetam. *Green Chemistry Letters and Reviews* **2010**, *3* (3), 225-230.
24. Śnieżek, M.; Stecko, S.; Panfil, I.; Furman, B.; Chmielewski, M., Total Synthesis of Ezetimibe, a Cholesterol Absorption Inhibitor. *The Journal of Organic Chemistry* **2013**, *78* (14), 7048-7057.

25. Castaldi, M.; Baratella, M.; Menegotto, I. G.; Castaldi, G.; Giovenzana, G. B., A concise and efficient synthesis of vildagliptin. *Tetrahedron Letters* **2017**, *58* (35), 3426-3428.
26. Chapman, H.; Kernan, M.; Prisbe, E.; Rohloff, J.; Sparacino, M.; Terhorst, T.; Yu, R., PRACTICAL SYNTHESIS, SEPARATION, AND STEREOCHEMICAL ASSIGNMENT OF THE PMPA PRO-DRUG GS-7340. *Nucleosides, Nucleotides & Nucleic Acids* **2001**, *20* (4-7), 621-628.
27. Ruchelman, A. L.; Connolly, T. J., Enantioselective synthesis of the apremilast aminosulfone using catalytic asymmetric hydrogenation. *Tetrahedron: Asymmetry* **2015**, *26* (10), 553-559.
28. Ireland, R. E.; Gleason, J. L.; Gegnas, L. D.; Highsmith, T. K., A Total Synthesis of FK-5061. *The Journal of Organic Chemistry* **1996**, *61* (20), 6856-6872.
29. Gouda, M. A., Overview of the synthetic routes to tadalafil and its analogues. *Synthetic Communications* **2017**, *47* (24), 2269-2304.
30. Vadali, L. R.; Konda, R.; Dandala, R. Preparation of cobicistat intermediates. US9975864B2, 2018.
31. Qi, H.; Wen, J.; Li, L.; Bai, R.; Chen, L.; Wang, D., An Efficient Synthesis of Pemetrexed Disodium. *Journal of Heterocyclic Chemistry* **2015**, *52* (5), 1565-1569.
32. Ivanov, A. S.; Zhalnina, A. A.; Shishkov, S. V., A convergent approach to synthesis of bortezomib: the use of TBTU suppresses racemization in the fragment condensation. *Tetrahedron* **2009**, *65* (34), 7105-7108.
33. Nugent, T. C., *Chiral Amine Synthesis: Methods, Developments and Applications*. WILEY-VCH Verlag GmbH & Co. KGaA: Weinheim, Germany, 2010.
34. Bommarius, A. S., Biocatalysis: A Status Report. In *Annual Review of Chemical and Biomolecular Engineering, Vol 6*, Prausnitz, J. M., Ed. Annual Reviews: Palo Alto, 2015; Vol. 6, pp 319-345.
35. Huisman, G. W.; Collier, S. J., On the development of new biocatalytic processes for practical pharmaceutical synthesis. *Current Opinion in Chemical Biology* **2013**, *17* (2), 284-292.
36. Patil, M. D.; Grogan, G.; Bommarius, A.; Yun, H., Oxidoreductase-Catalyzed Synthesis of Chiral Amines. *Acs Catalysis* **2018**, *8* (12), 10985-11015.
37. Shin, J.-S.; Kim, B.-G., Transaminase-catalyzed asymmetric synthesis of 1-2-aminobutyric acid from achiral reactants. *Biotechnology Letters* **2009**, *31* (10), 1595-1599.
38. Savile, C. K.; Janey, J. M.; Mundorff, E. C.; Moore, J. C.; Tam, S.; Jarvis, W. R.; Colbeck, J. C.; Krebber, A.; Fleitz, F. J.; Brands, J.; Devine, P. N.; Huisman, G. W.;

Hughes, G. J., Biocatalytic asymmetric synthesis of chiral amines from ketones applied to sitagliptin manufacture. *Science* **2010**, 329 (5989), 305-9.

39. Janey, J. M., Development of A Sitagliptin Transaminase. In *Sustainable Catalysis*, John Wiley & Sons, Inc.: 2013; pp 75-87.

40. Mathew, S.; Deepankumar, K.; Shin, G.; Hong, E. Y.; Kim, B.-G.; Chung, T.; Yun, H., Identification of novel thermostable ω -transaminase and its application for enzymatic synthesis of chiral amines at high temperature. *RSC Advances* **2016**, 6 (73), 69257-69260.

41. Mangion, I. K.; Sherry, B. D.; Yin, J.; Fleitz, F. J., Enantioselective Synthesis of a Dual Orexin Receptor Antagonist. *Organic Letters* **2012**, 14 (13), 3458-3461.

42. Green, A. P.; Turner, N. J.; O'Reilly, E., Chiral Amine Synthesis Using ω -Transaminases: An Amine Donor that Displaces Equilibria and Enables High-Throughput Screening. *Angewandte Chemie International Edition* **2014**, 53 (40), 10714-10717.

43. Dourado, D. F. A. R.; Pohle, S.; Carvalho, A. T. P.; Dheeman, D. S.; Caswell, J. M.; Skvortsov, T.; Miskelly, I.; Brown, R. T.; Quinn, D. J.; Allen, C. C. R.; Kulakov, L.; Huang, M.; Moody, T. S., Rational Design of a (S)-Selective-Transaminase for Asymmetric Synthesis of (1S)-1-(1,1'-biphenyl-2-yl)ethanamine. *ACS Catalysis* **2016**, 6 (11), 7749-7759.

44. Hou, A. W.; Deng, Z. X.; Ma, H. M.; Liu, T. G., Substrate screening of amino transaminase for the synthesis of a sitagliptin intermediate. *Tetrahedron* **2016**, 72 (31), 4660-4664.

45. D. Patil, M.; Grogan, G.; Bommarius, A.; Yun, H., Recent Advances in ω -Transaminase-Mediated Biocatalysis for the Enantioselective Synthesis of Chiral Amines. *Catalysts* **2018**, 8 (7), 254.

46. Seo, J.-H.; Kyung, D.; Joo, K.; Lee, J.; Kim, B.-G., Necessary and sufficient conditions for the asymmetric synthesis of chiral amines using ω -aminotransferases. *Biotechnology and Bioengineering* **2011**, 108 (2), 253-263.

47. Shin, J.-S.; Kim, B.-G., Asymmetric synthesis of chiral amines with ω -transaminase. *Biotechnology and Bioengineering* **1999**, 65 (2), 206-211.

48. Gand, M.; Thole, C.; Muller, H.; Brundiek, H.; Bashiri, G.; Hohne, M., A NADH-accepting imine reductase variant: Immobilization and cofactor regeneration by oxidative deamination. *J Biotechnol* **2016**, 230, 11-8.

49. Borlinghaus, N.; Nestl, B. M., Switching the Cofactor Specificity of an Imine Reductase. *ChemCatChem* **2018**, 10 (1), 183-187.

50. Huber, T.; Schneider, L.; Präg, A.; Gerhardt, S.; Einsle, O.; Müller, M., Direct Reductive Amination of Ketones: Structure and Activity of S-Selective Imine Reductases from *Streptomyces*. *ChemCatChem* **2014**, 6 (8), 2248-2252.

51. Grogan, G.; Turner, N. J., Inspired by Nature: NADPH-Dependent Imine Reductases (IREDs) as Catalysts for the Preparation of Chiral Amines. *Chemistry* **2016**, *22* (6), 1900-1907.
52. Aleku, G. A.; France, S. P.; Man, H.; Mangas-Sanchez, J.; Montgomery, S. L.; Sharma, M.; Leipold, F.; Hussain, S.; Grogan, G.; Turner, N. J., A reductive aminase from *Aspergillus oryzae*. *Nat Chem* **2017**, *9* (10), 961-969.
53. Sharma, M.; Mangas-Sanchez, J.; France, S. P.; Aleku, G. A.; Montgomery, S. L.; Ramsden, J. I.; Turner, N. J.; Grogan, G., A Mechanism for Reductive Amination Catalyzed by Fungal Reductive Aminases. *ACS Catalysis* **2018**, *8* (12), 11534-11541.
54. Knaus, T.; Bohmer, W.; Mutti, F. G., Amine dehydrogenases: efficient biocatalysts for the reductive amination of carbonyl compounds. *Green Chem* **2017**, *19* (2), 453-463.
55. Franklin, R. D.; Whitley, J. A.; Robbins, J. M.; Bommarius, A. S., Engineered amine dehydrogenase exhibits altered kinetic mechanism compared to parent with implications for industrial application. *Chemical Engineering Journal* **2019**, *369*, 634-640.
56. Kinbara, K.; Sakai, K.; Hashimoto, Y.; Nohira, H.; Saigo, K., Design of resolving reagents: p-substituted mandelic acids as resolving reagents for 1-arylalkylamines. *Tetrahedron: Asymmetry* **1996**, *7* (6), 1539-1542.
57. Saigo, K.; Kobayashi, Y., The role of CH/ π interaction in the stabilization of less-soluble diastereomeric salt crystals. *The Chemical Record* **2007**, *7* (1), 47-56.
58. Kinbara, K.; Sakai, K.; Hashimoto, Y.; Nohira, H.; Saigo, K., Chiral discrimination upon crystallisation of the diastereomeric salts of 1-arylethylamines with mandelic acid or p-methoxymandelic acid: interpretation of the resolution efficiencies on the basis of the crystal structures. *Journal of the Chemical Society, Perkin Transactions 2* **1996**, (12), 2615-2622.
59. Tseliou, V.; Knaus, T.; Vilím, J.; Masman, M. F.; Mutti, F., Kinetic Resolution of Racemic Primary Amines using *Geobacillus stearothermophilus* Amine Dehydrogenase variant. *ChemCatChem* **2020**, *n/a* (n/a).
60. Jeon, H.; Yoon, S.; Ahsan, M. M.; Sung, S.; Kim, G. H.; Sundaramoorthy, U.; Rhee, S. K.; Yun, H., The Kinetic Resolution of Racemic Amines Using a Whole-Cell Biocatalyst Co-Expressing Amine Dehydrogenase and NADH Oxidase. *Catalysts* **2017**, *7* (9), 251.
61. Dias Gomes, M.; Bommarius, B. R.; Anderson, S. R.; Feske, B. D.; Woodley, J. M.; Bommarius, A. S., Bubble Column Enables Higher Reaction Rate for Deracemization of (R,S)-1-Phenylethanol with Coupled Alcohol Dehydrogenase/NADH Oxidase System. *Advanced Synthesis & Catalysis* **2019**, *361* (11), 2574-2581.
62. Kim, Y.; Park, J.; Kim, M.-J., Dynamic Kinetic Resolution of Amines and Amino Acids by Enzyme–Metal Cocatalysis. *ChemCatChem* **2011**, *3* (2), 271-277.

63. Paetzold, J.; Bäckvall, J. E., Chemoenzymatic Dynamic Kinetic Resolution of Primary Amines. *Journal of the American Chemical Society* **2005**, *127* (50), 17620-17621.
64. Kadyrov, R., Reduction of Amides to Amines under Mild Conditions via Catalytic Hydrogenation of Amide Acetals and Imidates. *Advanced Synthesis & Catalysis* **2019**, *361* (1), 185-191.
65. Bürger, M.; Chory, J., Structural and chemical biology of deacetylases for carbohydrates, proteins, small molecules and histones. *Communications Biology* **2018**, *1* (1), 217.
66. De, C. K.; Klauber, E. G.; Seidel, D., Merging Nucleophilic and Hydrogen Bonding Catalysis: An Anion Binding Approach to the Kinetic Resolution of Amines. *Journal of the American Chemical Society* **2009**, *131* (47), 17060-17061.
67. Brunhuber, N. M. W.; Thoden, J. B.; Blanchard, J. S.; Vanhooke, J. L., Rhodococcus L-phenylalanine dehydrogenase: Kinetics, mechanism, and structural basis for catalytic specificity. *Biochemistry* **2000**, *39* (31), 9174-9187.
68. Reetz, M. T.; Bocola, M.; Carballeira, J. D.; Zha, D. X.; Vogel, A., Expanding the range of substrate acceptance of enzymes: Combinatorial active-site saturation test. *Angewandte Chemie-International Edition* **2005**, *44* (27), 4192-4196.
69. Abrahamson, M. J.; Wong, J. W.; Bommarius, A. S., The Evolution of an Amine Dehydrogenase Biocatalyst for the Asymmetric Production of Chiral Amines. *Advanced Synthesis & Catalysis* **2013**, *355* (9), 1780-1786.
70. Ye, L. J.; Toh, H. H.; Yang, Y.; Adams, J. P.; Snajdrova, R.; Li, Z., Engineering of Amine Dehydrogenase for Asymmetric Reductive Amination of Ketone by Evolving Rhodococcus Phenylalanine Dehydrogenase. *Acs Catalysis* **2015**, *5* (2), 1119-1122.
71. Pushpanath, A.; Sirola, E.; Bornadel, A.; Woodlock, D.; Schell, U., Understanding and Overcoming the Limitations of Bacillus badius and Caldalkalibacillus thermarum Amine Dehydrogenases for Biocatalytic Reductive Amination. *ACS Catalysis* **2017**, 3204-3209.
72. Abrahamson, M. J.; Vazquez-Figueroa, E.; Woodall, N. B.; Moore, J. C.; Bommarius, A. S., Development of an Amine Dehydrogenase for Synthesis of Chiral Amines. *Angewandte Chemie-International Edition* **2012**, *51* (16), 3969-3972.
73. Lowe, J.; Ingram, A. A.; Groger, H., Enantioselective synthesis of amines via reductive amination with a dehydrogenase mutant from Exigobacterium sibiricum: Substrate scope, co-solvent tolerance and biocatalyst immobilization. *Bioorg Med Chem* **2018**, *26* (7), 1387-1392.
74. Chen, F. F.; Liu, Y. Y.; Zheng, G. W.; Xu, J. H., Asymmetric Amination of Secondary Alcohols by using a Redox-Neutral Two-Enzyme Cascade. *Chemcatchem* **2015**, *7* (23), 3838-3841.

75. Bommarius, B. R.; Schurmann, M.; Bommarius, A. S., A novel chimeric amine dehydrogenase shows altered substrate specificity compared to its parent enzymes. *Chemical Communications* **2014**, 50 (95), 14953-14955.
76. Tseliou, V.; Knaus, T.; Masman, M. F.; Corrado, M. L.; Mutti, F. G., Generation of amine dehydrogenases with increased catalytic performance and substrate scope from epsilon-deaminating L-Lysine dehydrogenase. *Nat Commun* **2019**, 10 (1), 3717.
77. Mayol, O.; Bastard, K.; Beloti, L.; Frese, A.; Turkenburg, J. P.; Petit, J. L.; Mariage, A.; Debard, A.; Pellouin, V.; Perret, A.; de Berardinis, V.; Zapparucha, A.; Grogan, G.; Vergne-Vaxelaire, C., A family of native amine dehydrogenases for the asymmetric reductive amination of ketones. *Nature Catalysis* **2019**, 2 (4), 324-333.
78. Caparco, A.; Pelletier, E.; Petit, J.-L.; Fossey, A.; Bommarius, B.; de Berardinis, V.; Zapparucha, A.; Champion, J.; Bommarius, A.; Vergne-Vaxelaire, C., Metagenomic Mining for Amine Dehydrogenase Discovery. *Advanced Synthesis & Catalysis* **2020**, DOI: 10.1002/adsc.202000094 (n/a).
79. Franklin, R. D.; Mount, C. J.; Bommarius, B. R.; Bommarius, A. S., Separate sets of mutations enhance activity and substrate scope of amine dehydrogenase. *ChemCatChem* **2020**, 12, 2436-2439.
80. Chen, F. F.; Zheng, G. W.; Liu, L.; Li, H.; Chen, Q.; Li, F. L.; Li, C. X.; Xu, J. H., Reshaping the Active Pocket of Amine Dehydrogenases for Asymmetric Synthesis of Bulky Aliphatic Amines. *Acs Catalysis* **2018**, 8 (3), 2622-2628.
81. Tishkov, V. I.; Popov, V. O., Catalytic mechanism and application of formate dehydrogenase. *Biochemistry (Moscow)* **2004**, 69 (11), 1252.
82. Grogan, G., Synthesis of chiral amines using redox biocatalysis. *Curr Opin Chem Biol* **2018**, 43, 15-22.
83. Hartley, C. J.; Williams, C. C.; Scoble, J. A.; Churches, Q. I.; North, A.; French, N. G.; Nebl, T.; Coia, G.; Warden, A. C.; Simpson, G.; Frazer, A. R.; Jensen, C. N.; Turner, N. J.; Scott, C., Engineered enzymes that retain and regenerate their cofactors enable continuous-flow biocatalysis. *Nature Catalysis* **2019**, 2 (11), 1006-1015.
84. Ozbakir, H. F.; Garcia, K. E.; Banta, S., Creation of a formate: malate oxidoreductase by fusion of dehydrogenase enzymes with PEGylated cofactor swing arms. *Protein Engineering, Design and Selection* **2018**, 31 (4), 103-108.
85. Aalbers, F. S.; Fraaije, M. W., Enzyme Fusions in Biocatalysis: Coupling Reactions by Pairing Enzymes. *Chembiochem : a European journal of chemical biology* **2019**, 20 (1), 20-28.
86. Mutti, F. G.; Knaus, T.; Scrutton, N. S.; Breuer, M.; Turner, N. J., Conversion of alcohols to enantiopure amines through dual-enzyme hydrogen-borrowing cascades. *Science* **2015**, 349 (6255), 1525-9.

87. Knaus, T.; Cariati, L.; Masman, M. F.; Mutti, F. G., In vitro biocatalytic pathway design: orthogonal network for the quantitative and stereospecific amination of alcohols. *Org Biomol Chem* **2017**, *15* (39), 8313-8325.
88. Bohmer, W.; Knaus, T.; Mutti, F. G., Hydrogen-Borrowing Alcohol Bioamination with Coimmobilized Dehydrogenases. *ChemCatChem* **2018**, *10* (4), 731-735.
89. Liu, J.; Li, Z., Enhancing cofactor recycling in the bioconversion of racemic alcohols to chiral amines with alcohol dehydrogenase and amine dehydrogenase by coupling cells and cell-free system. *Biotechnol Bioeng* **2019**, *116* (3), 536-542.
90. Wang, H.; Zheng, Y.-C.; Chen, F.-F.; Xu, J.-H.; Yu, H.-L., Enantioselective Bioamination of Aromatic Alkanes Using Ammonia: A Multienzymatic Cascade Approach. *ChemCatChem* **2020**, *n/a* (n/a).
91. Chen, F.-F.; Zhang, Y.-H.; Zhang, Z.-J.; Liu, L.; Wu, J.-P.; Xu, J.-H.; Zheng, G.-W., An Ammonium-Formate-Driven Trienzymatic Cascade for ω -Transaminase-Catalyzed (R)-Selective Amination. *The Journal of Organic Chemistry* **2019**, *84* (22), 14987-14993.
92. Lin, B.; Tao, Y., Whole-cell biocatalysts by design. *Microbial Cell Factories* **2017**, *16* (1), 106.
93. Lowe, J.; Siewert, A.; Scholpp, A. C.; Wobbe, L.; Groger, H., Providing reducing power by microalgal photosynthesis: a novel perspective towards sustainable biocatalytic production of bulk chemicals exemplified for aliphatic amines. *Sci Rep* **2018**, *8* (1), 10436.
94. Brena, B.; González-Pombo, P.; Batista-Viera, F., Immobilization of Enzymes: A Literature Survey. In *Immobilization of Enzymes and Cells: Third Edition*, Guisan, J. M., Ed. Humana Press: Totowa, NJ, 2013; pp 15-31.
95. Homaei, A. A.; Sariri, R.; Vianello, F.; Stevanato, R., Enzyme immobilization: an update. *Journal of Chemical Biology* **2013**, *6* (4), 185-205.
96. Thompson, M. P.; Derrington, S. R.; Heath, R. S.; Porter, J. L.; Mangas-Sanchez, J.; Devine, P. N.; Truppo, M. D.; Turner, N. J., A generic platform for the immobilisation of engineered biocatalysts. *Tetrahedron* **2019**, *75* (3), 327-334.
97. Ren, H.; Zhang, Y.; Su, J.; Lin, P.; Wang, B.; Fang, B.; Wang, S., Encapsulation of amine dehydrogenase in hybrid titania nanoparticles by polyethylenimine coating and templated biomineralization. *J Biotechnol* **2017**, *241*, 33-41.
98. Caparco, A. A.; Bommarius, B. R.; Bommarius, A. S.; Champion, J. A., Protein-Inorganic Calcium-Phosphate Supraparticles as a Robust Platform for Enzyme Co-Immobilization. *Biotechnology and Bioengineering* **2020**, DOI: 10.1002/bit.27348 (n/a).

99. Caparco, A. A.; Bommarius, A. S.; Champion, J. A., Effect of Peptide Linker Length and Composition on Immobilization and Catalysis of Leucine Zipper-Enzyme Fusion Proteins. *Aiche Journal* **2018**, *64* (8), 2934-2946.
100. Ghislieri, D.; Turner, N. J., Biocatalytic Approaches to the Synthesis of Enantiomerically Pure Chiral Amines. *Topics in Catalysis* **2014**, *57* (5), 284-300.
101. Mangas-Sanchez, J.; France, S. P.; Montgomery, S. L.; Aleku, G. A.; Man, H.; Sharma, M.; Ramsden, J. I.; Grogan, G.; Turner, N. J., Imine reductases (IREDs). *Curr Opin Chem Biol* **2017**, *37*, 19-25.
102. Aleku, G. A.; Mangas-Sanchez, J.; Citoler, J.; France, S. P.; Montgomery, S. L.; Heath, R. S.; Thompson, M. P.; Turner, N. J., Kinetic Resolution and Deracemization of Racemic Amines Using a Reductive Aminase. *Chemcatchem* **2018**, *10* (3), 515-519.
103. Bommarius, B. R.; Schurmann, M.; Bommarius, A. S., A novel chimeric amine dehydrogenase shows altered substrate specificity compared to its parent enzymes. *Chem Commun (Camb)* **2014**, *50* (95), 14953-5.
104. Pushpanath, A.; Siirola, E.; Bornadel, A.; Woodlock, D.; Schell, U., Understanding and Overcoming the Limitations of *Bacillus badius* and *Caldalkalibacillus thermarum* Amine Dehydrogenases for Biocatalytic Reductive Amination. *Acs Catalysis* **2017**, *7* (5), 3204-3209.
105. Au, S. K.; Bommarius, B. R.; Bommarius, A. S., Biphasic Reaction System Allows for Conversion of Hydrophobic Substrates by Amine Dehydrogenases. *Acs Catalysis* **2014**, *4* (11), 4021-4026.
106. Mayol, O.; David, S.; Darii, E.; Debard, A.; Mariage, A.; Pellouin, V.; Petit, J. L.; Salanoubat, M.; de Berardinis, V.; Zapparucha, A.; Vergne-Vaxelaire, C., Asymmetric reductive amination by a wild-type amine dehydrogenase from the thermophilic bacteria *Petrotoxa mobilis*. *Catal. Sci. Technol.* **2016**, *6* (20), 7421-7428.
107. Liu, J.; Pang, B. Q. W.; Adams, J. P.; Snajdrova, R.; Li, Z., Coupled Immobilized Amine Dehydrogenase and Glucose Dehydrogenase for Asymmetric Synthesis of Amines by Reductive Amination with Cofactor Recycling. *Chemcatchem* **2017**, *9* (3), 425-431.
108. Yoon, S.; Patil, M. D.; Sarak, S.; Jeon, H.; Kim, G. H.; Khobragade, T. P.; Sung, S.; Yun, H., Deracemization of Racemic Amines to Enantiopure (R)- and (S)-amines by Biocatalytic Cascade Employing ω -Transaminase and Amine Dehydrogenase. *ChemCatChem* **2019**, *11* (7), 1898-1902.
109. Kataoka, K.; Tanizawa, K., Alteration of substrate specificity of leucine dehydrogenase by site-directed mutagenesis. *Journal of Molecular Catalysis B-Enzymatic* **2003**, *23* (2-6), 299-309.
110. Rozzell, J.; Hua, L.; Mayhew, M.; Novick, S. Mutants of enzymes and methods for their use. US20040115691 A1, 2004.

111. Bienert, S.; Waterhouse, A.; de Beer, T. A.; Tauriello, G.; Studer, G.; Bordoli, L.; Schwede, T., The SWISS-MODEL Repository-new features and functionality. *Nucleic Acids Res* **2017**, *45* (D1), D313-D319.
112. Waterhouse, A.; Bertoni, M.; Bienert, S.; Studer, G.; Tauriello, G.; Gumienny, R.; Heer, F. T.; de Beer, T. A. P.; Rempfer, C.; Bordoli, L.; Lepore, R.; Schwede, T., SWISS-MODEL: homology modelling of protein structures and complexes. *Nucleic Acids Res* **2018**, *46* (W1), W296-W303.
113. Yamaguchi, H.; Kamegawa, A.; Nakata, K.; Kashiwagi, T.; Mizukoshi, T.; Fujiyoshi, Y.; Tani, K., Structural insights into thermostabilization of leucine dehydrogenase from its atomic structure by cryo-electron microscopy. *J Struct Biol* **2019**, *205* (1), 11-21.
114. Brunhuber, N. M.; Thoden, J. B.; Blanchard, J. S.; Vanhooke, J. L., Rhodococcus L-phenylalanine dehydrogenase: kinetics, mechanism, and structural basis for catalytic specificity. *Biochemistry* **2000**, *39* (31), 9174-87.
115. Bradford, M. M., A rapid and sensitive method for the quantitation of microgram quantities of protein utilizing the principle of protein-dye binding. *Anal Biochem* **1976**, *72* (1-2), 248-54.
116. Mayol, O.; David, S.; Darii, E.; Debard, A.; Mariage, A.; Pellouin, V.; Petit, J.-L.; Salanoubat, M.; de Berardinis, V.; Zapparucha, A.; Vergne-Vaxelaire, C., Asymmetric reductive amination by a wild-type amine dehydrogenase from the thermophilic bacteria *Petrotoga mobilis*. *Catal. Sci. Technol.* **2016**, *6* (20), 7421-7428.
117. Turner, N. J.; Truppo, M. D., Biocatalytic Routes to Nonracemic Chiral Amines. In *Chiral Amine Synthesis*, Wiley-VCH Verlag GmbH & Co. KGaA: 2010; pp 431-459.
118. Sheldon, R. A.; Brady, D., The limits to biocatalysis: pushing the envelope. *Chem Commun (Camb)* **2018**, *54* (48), 6088-6104.
119. Esparza-Isunza, T.; González-Brambila, M.; Gani, R.; Woodley, J. M.; López-Isunza, F., The coupling of ω -transaminase and Oppenauer oxidation reactions via intra-membrane multicomponent diffusion – A process model for the synthesis of chiral amines. *Chemical Engineering Journal* **2015**, *259*, 221-231.
120. Cook, P. F.; Cleland, W. W., *Enzyme Kinetics and Mechanism*. Garland Science: 2007.
121. Gadda, G.; Sobrado, P., Kinetic Solvent Viscosity Effects as Probes for Studying the Mechanisms of Enzyme Action. *Biochemistry* **2018**, *57* (25), 3445-3453.
122. Wolfram Research, I. *Mathematica*, 11.3; Wolfram Research, Inc.: Champaign, Illinois, 2018.

123. Au, S. K. Development of Amine Dehydrogenases Toward Production of Chiral Amines. Georgia Institute of Technology, Atlanta, Georgia, 2016.
124. Ohshima, T.; Misono, H.; Soda, K., Properties of crystalline leucine dehydrogenase from *Bacillus sphaericus*. *The Journal of biological chemistry* **1978**, 253 (16), 5719-25.
125. Katoh, R.; Ngata, S.; Ozawa, A.; Ohshima, T.; Kamekura, M.; Misono, H., Purification and characterization of leucine dehydrogenase from an alkaliphilic halophile, *Natronobacterium magadii* MS-3. *Journal of Molecular Catalysis B-Enzymatic* **2003**, 23 (2-6), 231-238.
126. Misono, H.; Sugihara, K.; Kuwamoto, Y.; Nagata, S.; Nagasaki, S., Leucine dehydrogenase from *Corynebacterium pseudodiphtheriticum*: purification and characterization. *Agric Biol Chem* **1990**, 54 (6), 1491-8.
127. Vanhooke, J. L.; Thoden, J. B.; Brunhuber, N. M.; Blanchard, J. S.; Holden, H. M., Phenylalanine dehydrogenase from *Rhodococcus* sp. M4: high-resolution X-ray analyses of inhibitory ternary complexes reveal key features in the oxidative deamination mechanism. *Biochemistry* **1999**, 38 (8), 2326-39.
128. Rife, J. E.; Cleland, W. W., Determination of the chemical mechanism of glutamate dehydrogenase from pH studies. *Biochemistry* **1980**, 19 (11), 2328-33.
129. Labrou, N. E.; Rigden, D. J., Active-site characterization of *Candida boidinii* formate dehydrogenase. *Biochem J* **2001**, 354 (Pt 2), 455-63.
130. Hilt, W.; Pfeleiderer, G.; Fortnagel, P., Glucose dehydrogenase from *Bacillus subtilis* expressed in *Escherichia coli*. I: Purification, characterization and comparison with glucose dehydrogenase from *Bacillus megaterium*. *Biochim Biophys Acta* **1991**, 1076 (2), 298-304.
131. Ohshima, T.; Nagata, S.; Soda, K., Purification and Characterization of Thermostable Leucine Dehydrogenase from *Bacillus-Stearothermophilus*. *Arch. Microbiol.* **1985**, 141 (4), 407-411.
132. Maeda, M.; Furuhashi, H.; Ikami, J., Evaluation of Dissociation-Constants of Ammonium-Ions in Aqueous Ammonium-Chloride and Potassium-Chloride Solutions and of Pertinent Higher-Order Parameters According to the Pitzer Approach. *J Chem Soc Faraday T* **1993**, 89 (18), 3371-3374.
133. Maeda, M.; Kato, K., Dissociation-Constants of Ammonium Ion and Activity-Coefficients of Ammonia in Ammonium-Nitrate Solutions. *J Chem Eng Data* **1995**, 40 (1), 253-256.
134. Nagata, S.; Bakthavatsalam, S.; Galkin, A. G.; Asada, H.; Sakai, S.; Esaki, N.; Soda, K.; Ohshima, T.; Nagasaki, S.; Misono, H., Gene cloning, purification, and characterization of thermostable and halophilic leucine dehydrogenase from a halophilic

thermophile, *Bacillus licheniformis* TSN9. *Appl. Microbiol. Biotechnol.* **1995**, *44* (3-4), 432-8.

135. Ohashima, T.; Soda, K., Purification and properties of alanine dehydrogenase from *Bacillus sphaericus*. *Eur J Biochem* **1979**, *100* (1), 29-30.

136. Grimshaw, C. E.; Cleland, W. W., Kinetic mechanism of *Bacillus subtilis* L-alanine dehydrogenase. *Biochemistry* **1981**, *20* (20), 5650-5.

137. Ohshima, T.; Takada, H.; Yoshimura, T.; Esaki, N.; Soda, K., Distribution, purification, and characterization of thermostable phenylalanine dehydrogenase from thermophilic actinomycetes. *J Bacteriol* **1991**, *173* (13), 3943-8.

138. Misono, H.; Yonezawa, J.; Nagata, S.; Nagasaki, S., Purification and characterization of a dimeric phenylalanine dehydrogenase from *Rhodococcus maris* K-18. *J Bacteriol* **1989**, *171* (1), 30-6.

139. Garland, W. J.; Dennis, D. T., Steady-state kinetics of glutamate dehydrogenase from *Pisum sativum* L. mitochondria. *Arch Biochem Biophys* **1977**, *182* (2), 614-25.

140. Leskovac, V., *Comprehensive Enzyme Kinetics*. Kluwer Academic Publishers: Secaucus, UNITED STATES, 2003.

141. Yuan, H.; Xin, Y.; Hamelberg, D.; Gadda, G., Insights on the mechanism of amine oxidation catalyzed by D-arginine dehydrogenase through pH and kinetic isotope effects. *J Am Chem Soc* **2011**, *133* (46), 18957-65.

142. Yuan, H.; Fu, G.; Brooks, P. T.; Weber, I.; Gadda, G., Steady-state kinetic mechanism and reductive half-reaction of D-arginine dehydrogenase from *Pseudomonas aeruginosa*. *Biochemistry* **2010**, *49* (44), 9542-50.

143. Prakash, P.; Punekar, N. S.; Bhaumik, P., Structural basis for the catalytic mechanism and alpha-ketoglutarate cooperativity of glutamate dehydrogenase. *The Journal of biological chemistry* **2018**, *293* (17), 6241-6258.

144. Robbins, J. M.; Bommarius, A. S.; Gadda, G., Mechanistic studies of formate oxidase from *Aspergillus oryzae*: A novel member of the glucose-Methanol-choline oxidoreductase enzyme superfamily that oxidizes carbon acids. *Arch Biochem Biophys* **2018**, *643*, 24-31.

145. Smitherman, C.; Gadda, G., Evidence for a transient peroxy-nitro acid in the reaction catalyzed by nitronate monooxygenase with propionate 3-nitronate. *Biochemistry* **2013**, *52* (15), 2694-704.

146. Shrestha, R.; Huang, G.; Meekins, D. A.; Geisbrecht, B. V.; Li, P., Mechanistic Insights into Dye-Decolorizing Peroxidase Revealed by Solvent Isotope and Viscosity Effects. *ACS Catal.* **2017**, *7* (9), 6352-6364.

147. Wang, G. P.; Lundegaard, C.; Jensen, K. F.; Grubmeyer, C., Kinetic mechanism of OMP synthase: a slow physical step following group transfer limits catalytic rate. *Biochemistry* **1999**, *38* (1), 275-83.
148. D'Cunha, G. B.; Satyanarayan, V.; Madhusudanan Nair, P., Stabilization of phenylalanine ammonia lyase containing *Rhodotorula glutinis* cells for the continuous synthesis of l-phenylalanine methyl ester/96. *Enzyme Microb. Technol.* **1996**, *19* (6), 421-427.
149. Jones, G.; Dole, M., The viscosity of aqueous solutions of strong electrolytes with special reference to barium chloride. *Journal of the American Chemical Society* **1929**, *51* (10), 2950-2964.
150. Jenkins, H. D. B.; Marcus, Y., Viscosity B-coefficients of ions in solution. *Chemical Reviews* **1995**, *95* (8), 2695-2724.
151. Abrahamson, M. J. Development of an amine dehydrogenase. Ph.D., Georgia Institute of Technology, Atlanta, GA, 2012.
152. Bommarius, A. S.; Abrahamson, M. J.; Bommarius, B., Engineered amine dehydrogenases and methods of use thereof. In *Google Patents*, Office, U. S. P., Ed. Georgia Tech Research Corp: United States of America, 2014.
153. Rogers, T. A.; Daniel, R. M.; Bommarius, A. S., Deactivation of TEM-1 beta-Lactamase Investigated by Isothermal Batch and Non-Isothermal Continuous Enzyme Membrane Reactor Methods. *ChemCatChem* **2009**, *1* (1), 131-137.
154. McDonald, M. A.; Bromig, L.; Grover, M. A.; Rousseau, R. W.; Bommarius, A. S., Kinetic model discrimination of penicillin G acylase thermal deactivation by non-isothermal continuous activity assay. *Chemical Engineering Science* **2018**, *187*, 79-86.
155. Ozdural, A. R.; Tanyolac, D.; Boyaci, I. H.; Mutlu, M.; Webb, C., Determination of apparent kinetic parameters for competitive product inhibition in packed-bed immobilized enzyme reactors. *Biochem. Eng. J.* **2003**, *14* (1), 27-36.
156. Hwang, J. S.; Chang, H. N., Biotransformation of acrylonitrile to acrylamide using immobilized whole cells of *Brevibacterium* CH1 in a recycle fed-batch reactor. *Biotechnology and Bioengineering* **1989**, *34* (3), 380-386.
157. Rajan, A.; Nair, G. R., Production of soya milk containing low flatulence-causing oligosaccharides in a packed bed reactor using immobilised α -galactosidase. *International Journal of Food Science & Technology* **2010**, *45* (10), 2023-2031.
158. Veny, H.; Aroua, M. K.; Sulaiman, N. M. N., Kinetic study of lipase catalyzed transesterification of jatropha oil in circulated batch packed bed reactor. *Chemical Engineering Journal* **2014**, *237*, 123-130.

159. Rippin, D. W. T., Recycle Reactor as a Model of Incomplete Mixing. *Industrial & Engineering Chemistry Fundamentals* **1967**, 6 (4), 488-&.
160. Fogler, H. S., *Elements of Chemical Reaction Engineering*. fifth ed.; Prentice Hall Upper Saddle River, New York, 2016.
161. Sanroman, A.; Chamy, R.; Nunez, M. J.; Lema, J. M., Enzymatic-Hydrolysis of Starch in a Fixed-Bed Pulsed-Flow Reactor. *Applied Biochemistry and Biotechnology* **1991**, 28-9 (1), 527-538.
162. Allegro, C. S.; Malcata, F. X., How performance of a recycle plug flow reactor is optimized for protease-driven autocatalytic reactions. *Bioprocess Engineering* **1998**, 19 (5), 331-335.
163. Nguyen, L. A.; He, H.; Pham-Huy, C., Chiral drugs: an overview. *Int J Biomed Sci* **2006**, 2 (2), 85-100.
164. Kohls, H.; Steffen-Munsberg, F.; Hohne, M., Recent achievements in developing the biocatalytic toolbox for chiral amine synthesis. *Curr Opin Chem Biol* **2014**, 19, 180-92.
165. Truppo, M. D., Biocatalysis in the Pharmaceutical Industry: The Need for Speed. *ACS Medicinal Chemistry Letters* **2017**, 8 (5), 476-480.
166. Thompson, M. P.; Penafiel, I.; Cosgrove, S. C.; Turner, N. J., Biocatalysis Using Immobilized Enzymes in Continuous Flow for the Synthesis of Fine Chemicals. *Organic Process Research & Development* **2019**, 23 (1), 9-18.
167. Poehlauer, P.; Colberg, J.; Fisher, E.; Jansen, M.; Johnson, M. D.; Koenig, S. G.; Lawler, M.; Laporte, T.; Manley, J.; Martin, B.; O’Kearney-McMullan, A., Pharmaceutical Roundtable Study Demonstrates the Value of Continuous Manufacturing in the Design of Greener Processes. *Organic Process Research & Development* **2013**, 17 (12), 1472-1478.
168. Lee, S. L.; O’Connor, T. F.; Yang, X. C.; Cruz, C. N.; Chatterjee, S.; Madurawe, R. D.; Moore, C. M. V.; Yu, L. X.; Woodcock, J., Modernizing Pharmaceutical Manufacturing: from Batch to Continuous Production. *Journal of Pharmaceutical Innovation* **2015**, 10 (3), 191-199.
169. Gaberc-Porekar, V.; Menart, V., Perspectives of immobilized-metal affinity chromatography. *J Biochem Biophys Methods* **2001**, 49 (1-3), 335-60.
170. Huffman, M. A.; Fryszkowska, A.; Alvizo, O.; Borra-Garske, M.; Campos, K. R.; Canada, K. A.; Devine, P. N.; Duan, D.; Forstater, J. H.; Grosser, S. T.; Halsey, H. M.; Hughes, G. J.; Jo, J.; Joyce, L. A.; Kolev, J. N.; Liang, J.; Maloney, K. M.; Mann, B. F.; Marshall, N. M.; McLaughlin, M.; Moore, J. C.; Murphy, G. S.; Nawrat, C. C.; Nazor, J.; Novick, S.; Patel, N. R.; Rodriguez-Granillo, A.; Robaire, S. A.; Sherer, E. C.; Truppo, M. D.; Whittaker, A. M.; Verma, D.; Xiao, L.; Xu, Y.; Yang, H., Design of an in vitro

biocatalytic cascade for the manufacture of islatravir. *Science* **2019**, 366 (6470), 1255-1259.

171. Zhu, M.; Carta, G., Protein adsorption equilibrium and kinetics in multimodal cation exchange resins. *Adsorption* **2016**, 22 (2), 165-179.

172. Slusarczyk, H.; Felber, S.; Kula, M.-R.; Pohl, M., Stabilization of NAD-dependent formate dehydrogenase from *Candida boidinii* by site-directed mutagenesis of cysteine residues. *European Journal of Biochemistry* **2000**, 267 (5), 1280-1289.

173. Damköhler, G., Einflüsse der Strömung, Diffusion und des Wärmeüberganges auf die Leistung von Reaktionsöfen.: I. Allgemeine Gesichtspunkte für die Übertragung eines chemischen Prozesses aus dem Kleinen ins Große. *Zeitschrift für Elektrochemie und angewandte physikalische Chemie* **1936**, 42 (12), 846-862.

174. Inger, G. R., Scaling Nonequilibrium-Reacting Flows: The Legacy of Gerhard Damköhler. *Journal of Spacecraft and Rockets* **2001**, 38 (2), 185-190.

175. Lortie, R.; Pelletier, D., Comparison between dispersion and plug-flow models for fixed-bed enzyme reactors. *AIChE Journal* **1992**, 38 (9), 1477-1480.

176. dos Santos, P.; Meireles, M. A. A.; Martínez, J., Production of isoamyl acetate by enzymatic reactions in batch and packed bed reactors with supercritical CO₂. *The Journal of Supercritical Fluids* **2017**, 127, 71-80.

177. Lortie, R., Evaluation of the performance of immobilized enzyme reactors with michaelis—menten kinetics. *Journal of Chemical Technology & Biotechnology* **1994**, 60 (2), 189-193.

178. Sadana, A., Enzyme Deactivation in Reactors. *Biocatalysis* **1989**, 2 (3), 175-216.

179. Parker, J. W.; Schwartz, C. S., Modeling the kinetics of immobilized glucose oxidase. *Biotechnol Bioeng* **1987**, 30 (6), 724-35.

180. Al-Muftah, A. E.; Abu-Reesh, I. M., Effects of internal mass transfer and product inhibition on a simulated immobilized enzyme-catalyzed reactor for lactose hydrolysis. *Biochem. Eng. J.* **2005**, 23 (2), 139-153.

181. Abu-Reesh, I. M.; Abu-Sharkh, B. F., Comparison of Axial Dispersion and Tanks-in-Series Models for Simulating the Performance of Enzyme Reactors. *Industrial & Engineering Chemistry Research* **2003**, 42 (22), 5495-5505.

182. Horvath, C.; Engasser, J.-M., External and internal diffusion in heterogeneous enzymes systems. *Biotechnology and Bioengineering* **1974**, 16 (7), 909-923.

183. Romas, B.; Juozas, K.; Linas, P., Modelling the enzyme catalysed substrate conversion in a microbioreactor acting in continuous flow mode. *Nonlinear Analysis: Modelling and Control* **2018**, 23 (3).

184. Khalilpour, R.; Roostaazad, R., Development and verification of a model to describe an immobilized glucose isomerase packed bed bioreactor. *Biochem. Eng. J.* **2008**, *40* (2), 328-336.
185. Murty, V. R.; Bhat, J.; Muniswaran, P. K. A.; Sivasankaran, S., Dispersion and Mass Transfer Effects on the Performance of an Immobilized Lipase Packed Bed Reactor During the Hydrolysis of Rice Bran Oil. *The Canadian Journal of Chemical Engineering* **2005**, *83* (4), 780-783.
186. Cha, S., Kinetic Behavior at High Enzyme Concentrations: MAGNITUDE OF ERRORS OF MICHAELIS-MENTEN AND OTHER APPROXIMATIONS. *J. Biol. Chem.* **1970**, *245* (18), 4814-4818.
187. Tzafiriri, A. R., Michaelis-Menten kinetics at high enzyme concentrations. *Bulletin of Mathematical Biology* **2003**, *65* (6), 1111-1129.
188. Thiele, E. W., Relation between Catalytic Activity and Size of Particle. *Industrial & Engineering Chemistry* **1939**, *31* (7), 916-920.
189. Yaws, C. L., Diffusion Coefficient at infinite dilution in Water – Organic Compounds. In *Transport Properties of Chemicals and Hydrocarbons*, Yaws, C. L., Ed. Gulf Publishing Company: Oxford, 2014; pp 614-703.
190. Weisz, P. B.; Prater, C. D., Interpretation of Measurements in Experimental Catalysis. In *Advances in Catalysis*, Frankenburg, W. G.; Komarewsky, V. I.; Rideal, E. K., Eds. Academic Press: Cambridge, Massachusetts, 1954; Vol. 6, pp 143-196.
191. Bird, R. B.; Lightfoot, E. N.; Stewart, W. E., Interphase Transport in Nonisothermal Mixtures. In *Transport Phenomena*, second ed.; J. Wiley: Hoboken, New Jersey, 2002.
192. Korson, L.; Drost-Hansen, W.; Millero, F. J., Viscosity of water at various temperatures. *The Journal of Physical Chemistry* **1969**, *73* (1), 34-39.
193. Mears, D. E., Tests for Transport Limitations in Experimental Catalytic Reactors. *Industrial & Engineering Chemistry Process Design and Development* **1971**, *10* (4), 541-547.
194. Lee, G. K.; Lesch, R. A.; Reilly, P. J., Estimation of intrinsic kinetic constants for pore diffusion-limited immobilized enzyme reactions. *Biotechnology and Bioengineering* **1981**, *23* (3), 487-497.
195. Sahraei, Z.; Shabani, M.; Shokouhi, S.; Saffaei, A., Aminoquinolines against coronavirus disease 2019 (COVID-19): chloroquine or hydroxychloroquine. *International Journal of Antimicrobial Agents* **2020**, *55* (4), 105945.
196. Devaux, C. A.; Rolain, J.-M.; Colson, P.; Raoult, D., New insights on the antiviral effects of chloroquine against coronavirus: what to expect for COVID-19? *International Journal of Antimicrobial Agents* **2020**, 105938.

197. Cortegiani, A.; Ingoglia, G.; Ippolito, M.; Giarratano, A.; Einav, S., A systematic review on the efficacy and safety of chloroquine for the treatment of COVID-19. *Journal of Critical Care* **2020**.
198. Brocks, D. R.; Mehvar, R., Stereoselectivity in the Pharmacodynamics and Pharmacokinetics of the Chiral Antimalarial Drugs. *Clinical Pharmacokinetics* **2003**, *42* (15), 1359-1382.
199. Yim, S. S.; Bang, H. B.; Kim, Y. H.; Lee, Y. J.; Jeong, G. M.; Jeong, K. J., Rapid Isolation of Antibody from a Synthetic Human Antibody Library by Repeated Fluorescence-Activated Cell Sorting (FACS). *PLOS ONE* **2014**, *9* (10), e108225.
200. Mastrobattista, E.; Taly, V.; Chanudet, E.; Treacy, P.; Kelly, B. T.; Griffiths, A. D., High-Throughput Screening of Enzyme Libraries: In Vitro Evolution of a β -Galactosidase by Fluorescence-Activated Sorting of Double Emulsions. *Chemistry & Biology* **2005**, *12* (12), 1291-1300.
201. Li, A.; Acevedo-Rocha, C. G.; Reetz, M. T., Boosting the efficiency of site-saturation mutagenesis for a difficult-to-randomize gene by a two-step PCR strategy. *Applied microbiology and biotechnology* **2018**, *102* (14), 6095-6103.
202. Reetz, M. T.; Kahakeaw, D.; Lohmer, R., Addressing the Numbers Problem in Directed Evolution. *ChemBioChem* **2008**, *9* (11), 1797-1804.
203. Siegel, J. B.; Zanghellini, A.; Lovick, H. M.; Kiss, G.; Lambert, A. R.; St Clair, J. L.; Gallaher, J. L.; Hilvert, D.; Gelb, M. H.; Stoddard, B. L.; Houk, K. N.; Michael, F. E.; Baker, D., Computational design of an enzyme catalyst for a stereoselective bimolecular Diels-Alder reaction. *Science* **2010**, *329* (5989), 309-13.
204. Mak, W. S.; Siegel, J. B., Computational enzyme design: Transitioning from catalytic proteins to enzymes. *Current Opinion in Structural Biology* **2014**, *27*, 87-94.
205. Wrenbeck, E. E.; Faber, M. S.; Whitehead, T. A., Deep sequencing methods for protein engineering and design. *Current Opinion in Structural Biology* **2017**, *45*, 36-44.
206. Grunwald, P., Determination of effective diffusion coefficients — an important parameters for the efficiency of immobilized biocatalysts. *Biochemical Education* **1989**, *17* (2), 99-102.
207. Valencia, P.; Flores, S.; Wilson, L.; Illanes, A., Batch reactor performance for the enzymatic synthesis of cephalixin: influence of catalyst enzyme loading and particle size. *N Biotechnol* **2012**, *29* (2), 218-226.

VITA

Robert D. Franklin was born in Columbus, Ohio to Ladd and Jean Franklin in 1992. After completing an International Baccalaureate Diploma at Southeast High School in Bradenton, Florida in 2010, Robert attended The Florida State University in Tallahassee, Florida. At Florida State Robert completed two bachelor's degrees, one in Chemical Engineering with a focus on Biomedical engineering, and another in Biochemistry. During his time in Tallahassee, Robert was also president of FAMU/FSU College of Engineering chapter of the Tau Beta Pi engineering honors society and completed an undergraduate honors thesis under the direction of Dr. Anant Paravastu focused on an educational application to demonstrate protein folding using simplified Monte-Carlo simulations.

After graduating from Florida State in 2015, Robert attended the Georgia Institute of Technology in Atlanta, Georgia to pursue a PhD in Chemical Engineering. Over the course of his graduate work, Robert earned the departmental award for outstanding performance on the oral qualifying examination in 2016 and the AIChE Outstanding Teaching Assistant Award in 2017. His thesis work produced three first author publications, and six external presentations. After returning in 2019 from a summer internship with Merck Co. Inc. Chemical Engineering R&D, Robert completed and defended his PhD thesis in May 2020.